(NASA-CR-162072) EXTENDED RANGE X-RAY TELESCOPE: X-RAY MICROSCOPE DESIGN Final Report, 29 Jan. - 28 Jun. 1982 (Alabama Univ., Birmingham.) 118 p HC A06/MF A01 CSCL 03A G3/89

N82-32208

Unclas 32381

Extended Range X-Ray Telescope:

X-Ray Microscope Design

PRINCIPAL INVESTIGATOR: D.L.Shealy

CONTRACT NO: NAS8-34728

FINAL REPORT

TITLE: Extended Range X-Ray Telescope: X-Ray Microscope Design

AUTHORS: D.L.Shealy, A.Kassim, S.Chao

NO: Contract NAS8-34728

PERIOD: January 29 - June 28, 1982

DATE OF PUBLICATION: July 30, 1982

PRINCIPAL INVESTIGATOR: David L. Shealy
Physics Department, UC#2
Univ. of Alabama in Birmingham
Birmingham, Alabama 35294
205-934-2182

PREPARED FOR: George C. Marshall Space Flight Center
Marshall Space Flight, Alabama 35812

DISTRIBUTION: 5/AS24D
10/ES52, ATTN: R.B.Hoover
1/AS24D
1/E12B-15

ORIGINAL PAGE IS
OF POOR QUALITY

ABSTRACT

A glancing incidence x-ray microscope using a confocal hyperboloid-ellipsoid mirror has been designed to couple optically a Wolter I telescope (SKYLAB, ATM experiment S-056 optics) to a CCD focal plane detector. Both the RMS spot size and the point spread function calculations have been used to evaluate the resolution, defocusing and vignetting effects of the system for microscope focal lengths of 1, 1.5 and 2 meters and for magnifications varying from 2 to 10x. For the specific application with the S-056 telescope, a 2 meter, 8x microscope with a fabrication ratio of the microscope mirror length to the inner diameter at hyperboloid-ellipsoid intersection of 2.5 has been designed to be used with a thinned, back illuminated CCD detector array with 320 x 512, 30 micron pixels. The system provides sub-arc second resolution over a field of view of $\pm$ 2 arc minutes. By optimizing the microscope mirror lengths, the vignetting effects have been reduced such that the energy transfer from the entrance pupil to the image plane exceeds 20% at 2 arc minutes off axis and 40% at 1 arc minute off axis.

TABLE OF CONTENTS

I. INTRODUCTION

There has been considerable progress in glancing incidence x-ray optics during the past two decades, since the first flight of a Wolter I telescope[3], used to photograph the sun in x-ray, aboard an Aerobee rocket.[17] An interesting summary of activities in the field thru 1978 is given in Ref.18. Subsequent work consisted of putting into orbit the Einstein X-Ray Observatory with a resolution of approximately 4 arc-seconds,[19] which was configured with four nested Wolter I telescopes. Study plans are under way to construct an Advanced X-Ray Astrophysics Facility (AXAF) consisting of six nested Wolter I telescopes with a resolution goal of 0.5 arc-seconds.[20] There have been other quests for high resolution (sub-arc second) in glancing incidence x-ray optics.[11] One such proposal consists of locating a glancing incidence microscope near the focal plane of a Wolter I telescope in order to magnify the image to a CCD array.[11,21,22,23] To date, there has been no such system made. However, the technological capabilities for building glancing incidence x-ray microscopes are available.[4,8,9,10] Thus, as part of a proposal to develop an extended range x-ray telescope (ERXRT) funds have been allocated by Marshall Space Flight Center (MSFC) for the

design, analysis, fabrication, and testing of a glancing incidence x-ray microscope to couple the radiation from a Wolter I telescope (S056 optics) to CCD array in order to yield sub-arc second resolution over a field of view of $\pm$ 2 arc mins.

The present report gives (1) the mathematical equations required to ray trace a coupled Wolter I telescope-microscope system; (2) a summary of the intrinsic microscope variables; (3) RMS and point spread function analyses; (4) optimization of the microscope system for coupling the S056 to the CCD array; and (5) the design of the aperture stops. Also, specific conclusions and recommendations of this study are given.

II. MATHEMATICAL ANALYSIS OF ERXRT SYSTEM

A. Ray Trace Equations for ERXRT

In this section, a summary of the mathematical equations used for the ray trace analysis of the ERXRT will be given. Figure 1* presents a schematic view of the ERXRT system. The mirror surfaces P and H are the paraboloid and hyperboloid surfaces of the S056, Wolter I telescope[1-3] of the ERXRT system, and H' and E represent the hyperboloid and ellipsoid mirror surfaces of the converging microscope located in the focal plane of the Wolter I telescope. Using the coordinate system set forth in Ref.1 for the Wolter I telescope it follows that the surface equations for P and H are given by

$$x^2 = p\,(2z + p) \qquad z = \frac{x^2}{2p} - \frac{p}{2} \tag{1}$$

for the paraboloid, and

$$\frac{(z-c)^2}{a^2} - \frac{x^2}{b^2} = 1 \qquad z = c + a\sqrt{1 + \frac{x^2}{b^2}} \tag{2}$$

*All Figures (1-41) are grouped together in pages 69 thru 113 .

for the hyperboloid. When Eqs.1-2 are used for 3-dimensional applications, X is replaced by $R = [x^2 + y^2]^{1/2}$. The mirror surface parameters for the S056 Wolter I telescope were specified in the "Scope of Work" for this contract and summarized below:

$$
\begin{aligned}
&\text{glancing angle, } \theta m = 0.916^\circ \\
&X_p \text{ min} = 4.792\ 896\ 48 \\
&Z_p \text{ min} = 149.846\ 697 \\
&X_p \text{ max} = 4.868\ 790\ 7 \\
&Z_p \text{ max} = 154.631\ 134\ 5 \\
&L_p = 4.784\ 437\ 7 \\
&X_h \text{ min} = 4.576\ 677\ 6 \\
&X_h \text{ max} = 4.792\ 896\ 48 \\
&Z_h \text{ min} = 145.353\ 53 \\
&Z_h \text{ max} = 149.846\ 697 \\
&L_h = 4.493\ 167 \\
&a = 37.461\ 664\ 4 \\
&b = 1.695\ 198\ 8 \\
&c = 37.500\ 000 \\
&p = 0.076\ 631\ 56
\end{aligned}
\tag{3}
$$

where all linear dimensions are in inches.

The microscope surface equations for H' and E in the Wolter I coordinate system are for the hyperboloid,

$$\frac{(z - z_{oH})^2}{A_H^{\,2}} - \frac{x^2}{B_H^{\,2}} = 1 \tag{4}$$

where $Z_{OH} = F_W + C_H$ (4a)

$$C_H = \frac{F_m}{2M} \frac{\sin(4\theta_m)}{\sin(4\theta_m')} \frac{\sin(2\theta_m')}{\sin(4\theta_m - 2\theta_m')} \tag{4b}$$

$$A_H = \frac{F_m}{2M} \frac{\sin(4\theta_m)}{\sin(4\theta_m')} \left[\frac{\sin(4\theta_m)}{\sin(4\theta_m - 2\theta_m')} - 1 \right] \tag{4c}$$

$$B_H^{\,2} = C_H^{\,2} - A_H^{\,2} \tag{4d}$$

$$\theta_m' = \theta_m + \frac{1}{4} \sin^{-1} \left[\frac{\sin(4\theta_m)}{M} \right] \tag{4e}$$

and for the ellipsoid

$$\frac{(z - z_{oE})^2}{A_E^{2}} + \frac{x^2}{B_E^{2}} = 1 \tag{5}$$

where

$$z_{oE} = F_w - F_m + C_E \tag{5a}$$

$$A_E = \frac{F_m}{2} \frac{\sin(4\theta_m)}{\sin(4\theta_m')} \left[1 + \frac{\sin(4\theta_m)}{M \sin(4\theta_m - 2\theta_m')} \right] \tag{5b}$$

$$C_E = \frac{F_m}{2} \frac{\sin(4\theta_m)}{\sin(4\theta_m')} \frac{\sin(2\theta_m')}{\sin(4\theta_m - 2\theta_m')} \tag{5c}$$

$$B_E^2 = A_E^2 - C_E^2 \ . \tag{5d}$$

Referring to Fig.2 and Appendix A, one has the following interpretations for variables appearing in Eqs.4-5:

F_W = 2C, focal length of S056, Wolter I telescope,

F_m = distance along the optical axis from the object point to the image point of the microscope,

M = magnification of the microscope,

$\theta m'$ = glancing angle t the intersection point of H' and E surfaces.

The relationships given by Eqs.4a-e and 5a-d are based on the assumptions that

(1) F_1 is the focus of H' and E surfaces;

(2) F_2 is the second focus of H' surface, and F_2 is also the primary focus of the Wolter I telescope;

ORIGINAL PAGE IS
OF POOR QUALITY

(3) F_3 is the second focus of the E surface;

(4) the glancing angle of ray with H' and E surfaces at the intersection point are equal.

Details of the derivation of Eqs.4-e and 5a-d are given in Appendix A.

The coordinates of the intersection point of the H' and E surfaces are also of interest and are given by

$$X^* = \frac{F_m}{M} \frac{\sin^2(4\theta_m)}{\sin(4\theta_m')} \qquad Z^* = F_w - \frac{F_m}{2M} \frac{\sin(8\theta_m)}{\sin(4\theta_m')} \quad . \tag{6}$$

It is interesting to note that under the constraints given above, the microscope surfaces are completely specified in terms of F_m, M, and θm.

Knowing the equations of each surface of the ERXRT system, a ray trace can be done following established methods.[5] A summary of the ray trace equations which have been developed for ERXRT are given below. Assume the incident ray with direction cosines

$$\vec{A}_o = - \sin\alpha\, \hat{i} - \cos\alpha\, \hat{k} \quad , \tag{7}$$

ORIGINAL PAGE IS
OF POOR QUALITY

strikes the entrance pupil (plane at $z_o = z_{p,max}$) at the point (x_o, y_o, z_o) of radius $R_o = \left[x_o + y_o\right]^{1/2}$, where $R_{pmin} \leq R_o \leq R_{pmax}$. Then the ray strikes the paraboloid at point (x_1, y_1, z_1), which are obtained from the ray trace equations

$$\frac{x_1 - x_o}{z_1(x_1, y_1) - z_o} = \tan \alpha \tag{8a}$$

$$y_1 = y_o \tag{8b}$$

where

$$z_1(x_1, y_1) = \frac{(x_1^2 + y_1^2)}{2p} - \frac{p}{2}, \tag{8c}$$

$$\frac{\partial z_1}{\partial R_1} = \frac{R_1}{P}. \tag{8d}$$

Solving Eqs.8a-c simultaneously for x_1 gives

$$_1 = \frac{1 - [1 - \frac{2 \tan \alpha}{p} (x_o - z_o \tan \alpha - \frac{p}{2} \tan \alpha + \frac{\tan \alpha}{2p} y_o)^2]^{1/2}}{(\tan \alpha)/p} \tag{8e}$$

The direction cosines of the reflected ray from (x_1, y_1, z_1) is given by[6]

$$\vec{A}_1 = \vec{A}_o - 2 \vec{N}_1 (\vec{A}_o - \vec{N}_1) \tag{9}$$

where $\vec{N}_1$ is the unit surface normal to P and is given by

$$\vec{N}_1 = \frac{-\cos \phi_1 \frac{\partial z_1}{\partial R_1} \hat{i} - \sin \phi_1 \frac{\partial z_1}{\partial R_1} \hat{j} + \hat{k}}{\left[1 + \left(\frac{\partial z_1}{\partial R_1}\right)^2\right]^{1/2}} \tag{10}$$

where $\tan\phi_1 = y_1/x_1$. The ray trace equations from $P(x_1,y_1,z_1)$ to $H(x_2,y_2,z_2)$ surface are given by

$$\frac{x_2 - x_1}{z_2(x_2,y_2) - z_1(x_1,y_1)} = \frac{A_{1x}}{A_{1z}} \tag{11a}$$

$$\frac{y_2 - y_1}{x_2 - x_1} = \frac{A_{1y}}{A_{1x}} \tag{11b}$$

where A_{1x}, A_{1y}, A_{1z} = direction cosines of $\vec{A}_1$,

$$z_2\ (x_2,y_2) = C + a \left[1 + \frac{(x_2^{\ 2} + y_2^{\ 2})}{b^2}\right]^{1/2} \tag{11c}$$

Solving Eqs.11a-c simultaneously for x_2 yields the quadratic equation

$$x_2^{\ 2}\ [A_{1z}^{\ 2} - (\tfrac{a}{b})^2\ (A_{1x}^{\ 2} + A_{1y}^{\ 2})] + x_2\ [-2x_1A_{1z}^2$$
$$+ 2\ A_{1x}\ A_{1z}\ (z_1 - C) - 2(\tfrac{a}{b})^2\ A_{1x}\ A_{1y}\ y_1 + 2(\tfrac{a}{b})^2\ x_1A_{1y}^{\ 2}\ ]$$
$$+ [-x_1\ A_{1z} + (z_1 - c)\,A_{1x}]^2 - (\tfrac{a}{b})^2\ [b^2A_{1x}^{\ 2} + (x_1\ A_{1y} - y_1A_{1x})^2] = 0. \tag{12}$$

The appropriate solution of Eq.12 for a Wolter I telescope has a minimum distance from (x_1,y_1,z_1) to (x_2,y_2,z_2) where

$$y_2 = y_1 + \frac{(x_2 - x_1)\ A_{1y}}{A_{1x}} \tag{12a}$$

$$z_2 = C + a\sqrt{1 + \frac{(x_2^{\,2} + y_2^{\,2})}{b^2}},\ \frac{\partial z_2}{\partial R_2} = \frac{aR_2}{b\sqrt{b^2 + R_2^{\,2}}}\ . \tag{12b}$$

The direction cosines of the ray reflected from H are given

ORIGINAL PAGE IS
OF POOR QUALITY

by

$$\vec{A}_2 = \vec{A}_1 - 2\vec{N}_2\ (\vec{A}_1 \cdot \vec{N}_2) \tag{13}$$

where $\vec{N}_2$ is the unit surface normal to H and is given by

$$\vec{N}_2 = \frac{-\cos\phi_2\ (\partial z_2/\partial R_2)\ \hat{i} - \sin\phi_2\ (\partial z_2/\partial R_2)\ \hat{j} + \hat{k}}{[\ 1 + (\partial z_2/\partial R_2)^2]} \tag{14}$$

where $\tan\phi_2 = y_2/x_2$.

The ray intercepts (x_3, y_3, z_3) on H' of the microscope associated with the reflected ray with direction cosines $\vec{A}_2$ from $H(x_2, y_2, z_2)$ of the Wolter I telescope are obtained by solving the ray trace equations

$$\frac{x_3 - x_2}{z_3(x_3,y_3) - z_2(x_2,y_2)} = \frac{A_{2x}}{A_{2Z}} \tag{15a}$$

$$\frac{y_3 - y_2}{x_3 - x_2} = \frac{A_{2y}}{A_{2x}} \tag{15b}$$

where from Eq. 4 the surface equation of H' can be written as

$$z_3 = Z_{oH} - A_H \left[1 + \frac{x_3^{\ 2} + y_3^{\ 2}}{B_H^{\ 2}}\right]^{1/2} \tag{15c}$$

where the minus sign is used since $Z_3 < Z_{OH}$. Solving Eqs.15a-c for x_3 yields the quadratic equation

$$x_3^{\ 2}\ [\ A_{2z}^2 - (\frac{A_H}{B_H})^2\ (A_{2x}^2 + A_{2y}^2\ )] + x_3\ [-2\ X_2 A_{2z}^2$$

$$+ 2A_{2x}A_{2z}(z_2 - z_{oH}) - 2\ (\frac{A_H}{B_H})^2\quad (A_{2x}A_{2y}y_2 - x_2 A_{2y}^2)\ ]$$

(Eq. Con'td)

ORIGINAL PAGE IS
OF POOR QUALITY

$$+ [-x_2A_{2z} + (z_2 - z_{oH})A_{2x}]^2 - \left(\frac{A_H}{B_H}\right)^2 [B_H{}^2 A_{2x}{}^2 + (x_2A_{2y} - y_2A_{2x})^2 = 0. \tag{16}$$

The valid solution of Eq.16 has the larger distance from (x_2, y_2, z_2) to (x_3, y_3, z_3) where y_3, z_3 are computed from Eqs.15b-c. The direction cosines of the reflected ray from H' are given by

$$\vec{A}_3 = \vec{A}_2 - 2\vec{N}_3(\vec{A}_2 \cdot \vec{N}_3) \tag{17}$$

where

$$\vec{N}_3 = \frac{-\cos\phi_3 \frac{\partial z_3}{\partial R_3}\hat{i} - \sin\phi_3 \frac{\partial z_3}{\partial R_3}\hat{j} + \hat{k}}{[1 + (\frac{\partial z_3}{\partial R_3})^2]^{1/2}} \tag{17a}$$

$$\frac{\partial z_3}{\partial R_3} = \frac{-A_H R_3}{B_H\sqrt{B_H{}^2 + R_3{}^2}} \tag{17b}$$

$$\tan\phi_3 = \frac{y_3}{x_3} \tag{17c}$$

In similar manner, the ray intercepts (x_4, y_4, z_4) on E of the microscope follow from the ray trace equations

$$\frac{x_4 - x_3}{z_4(x_4, y_4) - z_3(x_3, y_3} = \frac{A_{3x}}{A_{3z}} \tag{18a}$$

$$\frac{y_4 - y_3}{x_4 - x_3} = \frac{A_{3y}}{A_{3x}} \tag{18b}$$

where from Eq.5 the surface equation of E can be written as

$$z_4 = z_{oE} \pm A_E \left[1 - \frac{x_4^2 + y_4^2}{B_E^2}\right]^{1/2}. \tag{18c}$$

ORIGINAL PAGE IS
OF POOR QUALITY

The plus(+) sign is used in Eq.18c when the left half of the ellipsoid corresponds to the mirror surface E, and the minus(-) sign is used in Eq.18c when the right half of the ellipsoid corresponds to the mirror surface E. That is, if

$$z^* < z_{oE}\ , \quad \text{Then} \quad z_4 = z_{oE} - A_E \, [1 - (x_4^2)/B_E^2]^{1/2} \ , \qquad (19a)$$

$$z^* > z_{oE}, \quad \text{Then} \quad z_4 = z_{oE} + A_E \, [1 - (x_4^2)/B_E^2]^{1/2} \ . \qquad (19b)$$

It is also possible that if z^* is slightly larger than z_{OE}, then it would be necessary to change signs in Eq.18c as one traced rays over the entrance pupil. Therefore, it is interesting to know for what physical conditions

$$z^* = z_{oE}. \qquad (20a)$$

Simplifying Eq.20a from Eqs.5a, 5c, and 6 yields an equation for M(θm) when Eq.20a holds:

$$\sin(8\theta m)\sin(4\theta m - 2\theta m') - 2M\sin(4\theta m')\sin(4\theta m - 2\theta m') + M\sin(4\theta m)\sin(2\theta m') = 0 \qquad (20b)$$

where $\theta m'$ is given by Eq.4e. A solution of Eq.20b is given

by

$$M = \frac{\sin\,(4\theta m)}{\sin\,(\frac{4\theta m}{3})} = \overline{M}\ . \tag{20}$$

It is also interesting to note that the angle the tangent to E makes with respect to the Z-axis is given by

$$\gamma_E = 4\theta m - 3\theta m' \tag{20c}$$

and $\gamma_E = 0$ implies that M is given by Eq.20. For the S056, Wolter I telescope $\theta m = 0.916^\circ$ and

$$\overline{M} = 2.998. \tag{20d}$$

to summarize these results:

(1) For $M < \overline{M}$, $z_{oE} > z^*$, and

$$z_4 = z_{oE} - A_E\,[1 - (x_4^2)/B_E^2]^{1/2}\ ; \tag{21a}$$

(2) For $M > \overline{M}$, $z_{oE} < z^*$, and

$$z_4 = z_{oE} + A_E\,[1 - (x_4^2)/B_E^2]^{1/2}\ . \tag{21b}$$

Now return to the ray trace equations of the ERXRT.

Solving Eqs.18a-c for x_4 yields the quadratic equation

$$x_4^2 \, [\, A_{3z}^2 + (A_E \,/\, B_E)^2 \; (A_{3x}^2 + A_{3y}^2)\,] + x_4 \, [-2x_3 \, A_{3z}^2$$

$$+ 2 \, A_{3x} \, A_{3z} \, (z_3 - z_{oE}) + 2 \, (A_E \,/\, B_E)^2 \, A_{3x} \, A_{3y} \, y_3$$

$$- 2 \, (A_E \,/\, B_E)^2 \; x_3 \, A_{3y}^2 \,] + [-x_3 \, A_{3z} + (z_3 - z_{oE}) \, A_{3x}]^2$$

$$+ (A_E \,/\, B_E)^2 \, [-B_E^2 \, A_{3x}^2 + (x_3 \, A_{3y} - y_3 \, A_{3x})^2] = 0 \, . \tag{22}$$

where y_4, z_4 are obtained from Eqs.18b-c. The direction cosines of the reflected ray from E are given by

$$\vec{A}_4 = \vec{A}_3 - 2 \, \vec{N}_4 \, (\vec{A}_3 \cdot \vec{N}_4) \tag{23}$$

where

$$\vec{N}_4 = \frac{-\cos\phi_4 \dfrac{\partial z_4}{\partial R_4} \, \hat{i} - \sin\phi_4 \dfrac{\partial z_4}{\partial R_4} \, \hat{j} + \hat{k}}{[1 + (\dfrac{\partial z_4}{R_4})^2]^{1/2}} \tag{23a}$$

$$\frac{\partial z_4}{\partial R_4} = \mp A_E \, R_4 \,/\, (B_E \cdot (B_E^2 - R_4^2)^{1/2}) \; , \text{ for } z_4 \gtrless z_{oE} \, . \tag{23b}$$

$$\tan\phi_4 = \frac{y_4}{x_4} \tag{23c}$$

Then the ray intercepts with the focal plane are given by

$$z_5 = F_w - F_m + \Delta Z$$

$$x_5 = x_4 + (z_5 - z_4) \, A_{4x} \,/\, A_{4z}$$

$$y_5 = y_4 + (z_5 - z_4) \, A_{4y} \,/\, A_{4z} \tag{24}$$

where ΔZ corresponds to the displacement of the image plane from the axial focal point.

B. RMS Blur Circle Equations

Since the ray intercepts with the image plane result from a complicated, aberrated emerging wavefront for off-axis incident radiation, it is conventional to consider that the ray intercepts are randomly distributed over the image plane and to use statistical methods for analyzing the ray intercepts with the image plane, or spot diagram.

The ray trace equation is used to calculate the root mean square deviation around the average image point that represents the ray intercepts over the image plane for all rays passing through the ERXRT over the whole aperture, i.e., the RMS blur radius or RMS of the spot diagram.[7]

Since the spot diagram for non-zero, off-axis angles has no rotational symmetry about any axis parallel to the optical axis, it is necessary to define in some way how to compute the radius of the spot diagram.

ORIGINAL PAGE IS
OF POOR QUALITY

Suppose (X', Y') represents the coordinates of the intersection point of an arbitrary ray striking the nominal focal plane, $Z' = 0$. Then the ray coordinates on the optimum image plane are given by

$$X_I = X'_{(i)} + Z_{min} A_{(i)} \tag{25a}$$

$$Y_I = Y'_{(i)} + Z_{min} B_{(i)} \tag{25b}$$

where $A_{(i)} = A_{4x}/A_{4z}$, $B_{(i)} = A_{4y}/A_{4z}$, and $\vec{A}_4$ is the unit vector of the direction of the reflected ray toward the focal plane. Z_{min} is the distance from the nominal image plane to the optimum plane.

The average over N rays of Eqs.25a-b is given as

$$\overline{X}_I = X' + Z_{min} \overline{A}$$

$$\overline{Y}_I = \overline{Y}' + Z_{min} \overline{B} \tag{26}$$

where

$$\overline{X}_I = \frac{1}{N} \sum_{i=1}^{N} X_I (i) \quad , \quad \overline{Y}_I = \frac{1}{N} \sum_{i=1}^{N} \overline{Y} (i) \quad ,$$

$$\overline{X}' = \frac{1}{N} \sum_{i=1}^{N} X' (i) \quad , \quad \overline{Y}' = \frac{1}{N} \sum_{i=1}^{N} Y'(i) \quad ,$$

$$\overline{A} = \frac{1}{N} \sum_{i=1}^{N} A_{3x}(i)/A_{3z}(i) \quad , \quad \text{and}$$

ORIGINAL PAGE IS OF POOR QUALITY

$$\overline{B} = \frac{1}{N} \sum_{i=1}^{N} A_{3y}(i)/A_{3z}(i) .$$

If one defines the least square errors, e^2, as

$$e^2(Z_{min}) = \frac{1}{N} \sum_{i=1}^{N} [(X_I(i) - \overline{X}_I)^2 + (Y_I(i) - \overline{Y}_I{}^2)^2] , \tag{27}$$

Eq.27 can be rearranged as

$$e^2(Z_{min}) = a\, Z_{min}^2 + b\, Z_{min} + c , \tag{28}$$

where

$$a = \frac{1}{N} \sum_{i=1}^{N} (A_{(i)}{}^2 + B_{(i)}{}^2) - \overline{A}^2 - \overline{B}^2$$

$$b = \frac{2}{N} \sum_{i=1}^{N} (X'_{(i)} A_{(i)} + Y'_{(i)} B_{(i)}) - 2(\overline{X}'\overline{A} + \overline{Y}'\overline{B})$$

$$c = \frac{1}{N} \sum_{i=1}^{N} (X'^2_{(i)} + Y'^2_{(i)}) - \overline{X}'^2 - \overline{Y}'^2$$

(e^2) has a minimum with respect to Z_{min} when

$$\frac{\partial(e^2)}{\partial Z_{min}} = 0 = 2\, Z_{min}\, a + b \tag{29}$$

or

$$Z_{min} = -b/a.$$

Thus, the RMS of the spot radius on Z_{min} is given by

$$(RMS)_{Zmin} = \sqrt{e^2\ (Z_{min})} \tag{30}$$

and on $Z' = 0$, $RMS = \sqrt{c}$. (31)

C. Ray Trace Code

In sections II.A-B, the mathematical equations to be used in the ray trace analysis of the ERXRT system have been presented. A brief discussion of the ray trace code used in this study is given in this section. The computer ray trace program can be broken down into the following parts:

1. Define input constants for ERXRT system. For Wolter I telescope (Eq.3):

   a, b, c, p, θm, L_p, L_H, $X_{pmin}=X_{Hmax}$,

   $Z_{pmin}=Z_{Hmax}$, X_{pmax}, Z_{pmax}, X_{Hmin}, Z_{Hmin}.

   For converging microscope:

   F_m (= 1, 1.5, 2 m.)

   M (= 2, 3, 4, 5, 6, 6.5, 7, 8)

   L_H', L_E (varied from minimum to maximum values)

   where L_p, L_H, L_H', L_E are the axial lengths of the respective surfaces and are measured from the intersection point of each subscription.

ORIGINAL PAGE IS
OF POOR QUALITY

2. Assign direction cosines to an incident ray. It has been assumed that the incident ray is in the X-Z plane and makes an angle α with respect to the Z axis. The angle α assumes values 0, 0.25, 0.50, ..., 2.5 arc-min.

3. Set up a grid on the entrance pupil, which is an imaginary plane perpendicular to the optical axis located at Z_{pmax}, such that each ray will pass thru equal areas on the entrance pupil. For RMS calculations, a rectilinear grid is used where 3,844 rays pass thru the ERXRT system for $\alpha = 0$. For point spread function (PSF) calculations, polar coordinates R_o, ϕ_o on the entrance pupil are used where

$$\phi_o = o,\ \Delta\phi,\ 2\Delta\phi,\ \ldots\ 180^0 - \Delta\phi$$

$$\Delta\phi = 180^o \ /\ (NPHO-1)$$

$$R_o = R_{o1}\ (\equiv X_{pmin}),\ R_{o2}\ (\equiv [R_{o1}^2 + \Delta]^{1/2}),$$

$$\ldots,\ R_{oN}\ (\equiv [R_{o1}^2 + (NRO-1)\,\Delta\,]^{1/2} \equiv X_{pmax})$$

$$\Delta = (X_{pmax}^2 - X_{pmin}^2)\ /\ (NRO-1)$$

$$NPHO = 3000$$

$$NRO = 100\ .$$

The reflection symmetry of the ERXRT system about the X-Z plane is used to obtain the intercepts of the rays, which would have passed thru the entrance pupil for $\phi_o = 180^o$ to 360^o. Thus, 600,000 rays have been used to compute the PSF of the ERXRT system.

4. For each field angle α, a ray is traced thru each grid point on the entrance pupil, using the equations outlined in Section II.A. For a given ray, it is necessary that this ray intercepts each mirror surface of the ERXRT system of the specified lengths before arriving at the image plane and being used in RMS and PSF calculations. For each field angle, the rays which actually intercept the image plane are counted for the vignetting study.

5. After completing the ray trace for all grid points at a given field angle, the RMS blur circle radius is evaluated from the equations in Section II.B for a series of image planes, such that defocusing effects can be studied. Also, the optimum image surface, i.e., the loci of image points with minimum RMS blur circle radius, is computed.

6. The PSF is evaluated by setting up a NXG by NYG grid on the image surface. For each field angle, the ray intercepts with the image plane are sorted into different image grid locations. The number of rays per image plane cell time the element of area ΔA (=collecting area divided by the total number of rays incident upon the telescope) is a measure of the PSF. The size of the image plane grid is chosen such that all rays will be incident within the image grid. Generally, NXG = NYG = 41 has been used for the number of grid points.

III. RESULTS

In this chapter the results of the ray trace analysis of the ERXRT system are presented. Results have been obtained for the microscope focal lengths, F_m, to have values of 1, 1.5, and 2 meters and for the microscope magnification, M, to have values of 2, 3, 4, 5, 6, 6.5, 7, 8x. The field angle, α, has assumed values of 0, .25, .5, •••, 2.5 arc-mins where it has been recognized that the measured resolution of the S056, Wolter I optics varies from 0.75 arc-sec on-axis to approximately 1 arc-sec over a field of view of $\pm$ 2.5 arc-mins.

The overriding objective in developing this chapter is to present the performance data on a wide range of coupled Wolter I (S056) - microscope systems such that a microscope configuration can be identified for optimum coupling between the S056 telescope and the CCD detecter array located in the focal plane of the microscope. Input and analysis of interim data by the MSFC ERXRT design team and the MSFC principal investigator have been instrumental in restricting the range of F_m and M variables such that recommendations on a finalized mirror design to be used in the fabrication effort can be made.

Specific data presented in this chapter will

include: (1) in Section A, a discussion of intrinsic microscope variables, such as the mirror surface parameters, the glancing angle, θ_m', and the intersection diameter as a function of M; (2) in Section B, an evaluation of the RMS spot radius versus the field angle for different values of M, F_m, and image plane displacements, ΔZ, from the nominal location; (3) in Section C, an analysis of vignetting effects thru plots of the percent energy loss versus the lengths of the microscope hyperboloid and ellipsoid mirror surfaces for selected field angles; and a comparison of the percent energy loss and RMS spot radius; (4) in Section D, a study of the point spread function in the meridional and sagittal plane versus image plane coordinates for selected field angle, magnification, focal length of the microscope and hyperboloid and ellipsoid lengths; (5) in Section E, optimization of the microscope mirror lengths for coupling the S056 telescope to the CCD detector array for the ERXRT system; and (6) in Section E, a design of appropriate aperture stops for the selected mirror design to vignette unwanted radiation and prevent it from striking the detector. In Chapter IV, conclusions and recommendations based on the data given in this chapter will be presented.

A. Intrinsic Microscope Variables

As indicated in Chapter II, the microscope surface parameters (A_H, B_H, C_H, Z_{OH}, A_E, B_E, C_E, Z_{OE}), which are given by Eqs.4a-d, 5a-d, are functions of F_m and M, when the Wolter I telescope configuration is fixed. For microscope systems of interest for use in the ERXRT system (F_m=1, 1.5, 2 meters and M=5,6,6.5,7,8x), Tables 1,2,3 present the surface parameters, minimum hyperboloid and ellipsoid lengths, and the X-Z plane intersection coordinates. It should be noted that L_H' and L_E given in Tables 1-3 are the minimum axial lengths of the hyperboloid and ellipsoid microscope mirror surfaces such that all the radiation incident upon the S056, Wolter I telescope, which is parallel to the optical axis, will be reflected by the microscope to the ERXRT focal point. Furthermore, it is interesting to note, that the K value for the microscopes defined by Tables 1-3 are given by

M	K
5	0.808
6	0.831
6.5	0.840
7	0.848
8	0.864

where these results are independent of the value of F_m

TABLE 1: MICROSCOPE SURFACE PARAMETERS

FOR F_m = 1 meter

MAGNIFICATION (x)

CM.	5	6	6.5	7	8
A_H	12.489775	9.991479	9.083044	8.326030	7.136467
B_H	0.505495	0.412722	0.378073	0.348807	0.302071
C_H	12.50	10.0	9.090909	8.333333	7.142857
Z_{OH}	203.03	200.50	199.590909	198.833333	197.642857
$L_H'^{+}$	0.842359	0.741581	0.699430	0.661688	0.597003
A_E	62.510220	60.008516	59.098770	58.340633	57.149244
B_E	1.130320	1.010959	0.96390	0.922855	0.854385
C_E	62.50	60.0	59.090909	58.333333	57.142857
Z_{OE}	153.03	150.50	149.590909	148.833333	147.642857
L_E^{+}	0.878679	0.775851	0.732619	0.693805	0.627062
X*	1.065524	0.913244	0.852338	0.799049	0.710240
Z*	173.860599	176.238628	177.189735	178.021907	179.408767

+Minimum axial lengths of microscope mirror surfaces required to reflect on axis radiation incident upon the Wolter I telescope towards the focal point of the ERXRT system. L_H' and L_E are measured from the microscope intersection point (X*, Z*).

TABLE 2: MICROSCOPE SURFACE PARAMETERS

FOR F_m = 1.5 meter.

MAGNIFICATION (x)

cm.	5	6	6.5	7	8
A_H	18.734662	14.987219	13.624566	12.489045	10.704701
B_H	0.758242	0.619083	0.567109	0.523210	0.453106
C_H	18.750	15.0	13.636363	12.50	10.714286
Z_{OH}	209.250	205.50	204.136363	203.0	201.214286
$L_H'^{+}$	1.263538	1.112371	1.049145	0.992532	0.895504
A_E	93.765330	90.012775	88.648155	87.510949	85.723866
B_E	1.695481	1.516438	1.445850	1.384283	1.281577
C_E	93.750	90.0	88.636363	87.50	85.714286
Z_{OE}	134.250	130.50	129.126363	128.0	126.214286
L_E +	1.318018	1.163777	1.098929	1.040707	0.940592
X*	1.598285	1.369866	1.278508	1.198574	1.065360
Z*	165.540899	169.107943	170.534603	171.782861	173.863150

+Minimum axial lengths of microscope mirror surfaces required to reflect on axis radiation incident upon the Wolter I telescope towards the focal point of the ERXRT system. L_H' and L_E are measured from the microscope intersection point (X*,Z*).

ORIGINAL PAGE IS OF POOR QUALITY

TABLE 3. MICROSCOPE SURFACE PARAMETERS

FOR F_m = 2 meter.

MAGNIFICATION (x)

cm.	5	6	6.5	7	8
A_H	24.979550	19.982959	18.166088	16.652060	14.272934
B_H	1.010989	0.825444	0.756146	0.697613	0.604141
C_H	25.0	20.0	18.181818	16.666667	14.285714
Z_{OH}	215.50	210.50	208.681818	207.166667	204.785714
$L_H'^{+}$	1.684717	1.4831618	1.3988602	1.323375	1.194006
A_E	125.020440	120.017033	118.197540	116.681266	114.298488
B_E	2.260641	2.021917	1.927801	1.845711	1.703770
C_E	125.0	120.0	118.181818	116.666667	114.285714
Z_{OE}	115.50	110.50	108.681818	107.166667	104.785714
L_E^{+}	1.75736	1.551702	1.46524	1.387609	1.254123
X*	2.131047	1.826487	1.704677	1.598099	1.420480
Z*	157.221199	161.977257	163.879471	165.543814	168.317533

+Minimum axial lengths of microscope mirror surfaces required to reflect on axis radiation incident upon the Wolter I telescope towards the focal point of the ERXRT system. L_H' and L_E are measured from the microscope intersection point (X*, Z*).

within the range of consideration and K is defined by

$$K = \frac{L_H' + L_E}{2X^*} .$$

Previous x-ray microscope systems, which have been fabricated, have had K values ranging from 0.98(ref.8) to 1.87(ref.9). Current manufacturing techniques have suggested that typical midplane diameters for x-ray microscopes are in the range of 10 to 40 mm and the element lengths can be up to double these dimensions.[10] For the ERXRT system a goal of K=2.5 has been set. The effects of increasing the hyperboloid and ellipsoid length over the minimum lengths given in Table 1-3 will be reported in Section C.

In Fig.3, the midplane diameters of the ERXRT microscope system are displayed as a function of the magnification for F_m = 1, 1.5, 2 meters, where Eq.6 was used to compute these results. It should be noted that for F_m = 2 meters and M = 5 and 8x, the midplane diameter varied from 42mm to 28mm, respectively, which are well within the range of manufactorable systems. Figure 4 presents the glancing angle at the intersection point of the microscope system versus the magnification for an axis radiation incident upon the S056, Wolter I telescope. Note from Eq.4e that θ_m' is only a function of the glancing

angle, θ_m, at the intersection point of the Wolter I telescope and the magnification, M, of the microscope. For magnifications in the range of 5 to 8x, θ_m' varies from 1.10 to 1.03 degrees, respectively. Figures 5 and 6 give the glancing angles θ_H' and θ_E as a function of the Wolter I entrance pupil radius R_o for the magnifications M = 5, 6, 6.5, 7, 8 and for on axis radiation incident upon ERXRT system. The results presented in Figs.5 and 6 have been obtained from the ray trace analysis by computing the angle between the ray vectors $\vec{A}_2$, $\vec{A}_3$ and the surface tangent vectors to H' and E, respectively. Although θ_H' is a stronger function of R_o than θ_E; both θ_H' and θ_E are within an acceptable range to achieve high reflectivities from the microscope mirror surfaces for the wavelengths under consideration for the ERXRT system.

B. <u>RMS Spot Radius Analysis</u>

In this section, the RMS spot radius data versus the field angle for different values of M, F_m, the displacement ΔZ of a flat image plane from the nominal position will be presented and discussed. The purpose of this analysis is to establish an upper bound on resolution of ERXRT as measured by RMS as a function of F_m and M of the microscope

subsystem. Also, defocusing effects will be analyzed.

Figures 7-9 give the RMS spot radius as a function of the field angle for the ERXRT system with the microscope image to object distance F_m equal to 1, 1.5, 2m and the magnification M varying from 2 to 8x. The general trends are that the RMS for a given field angle decreases with increasing values of F_m for constant M and that the RMS for a given field angle increases with increasing M for a constant F_m. For the calculations given in Figs. 7-8, the image plane has the nominal location at F_3 (see Fig.2), and the microscope mirror lengths L_H', L_E have the minimum lengths given in Tables 1-3. Figure 10 plots the RMS versus magnification for F_m = 1,2m at a field angle of 2.5 arc-mins. It follows that the RMS at the full field is a linear function of the magnification. Also, for F_m = 1m, the RMS is a stronger function of the magnification than for F_m = 2m.

By removing the constraints that the microscope mirror surfaces have, the minimum lengths, the RMS versus field angle over the nominal image plane for F_m = 1.5m were calculated for maximum mirror lengths and are presented in Fig.11. The actual lengths of the microscope mirror surfaces used in Fig.11 are given in Table 4.

ORIGINAL PAGE IS
OF POOR QUALITY

TABLE 4: Lengths of H', E Mirror Surfaces of Microscope for F_m = 150 cm used in Fig.10.

M	$L_{H'}$ (cm)	L_E (cm)	K
5	9.22529	5.71551	4.67
6	9.35261	4.95065	5.22
7	9.46021	4.33431	5.75
8	9.69431	3.87089	6.37

It is clear after comparing the RMS for a given field angle and magnification between Figs.8 and 11 that there are significant losses in resolution by increasing the mirror lengths. However, there is a compensating effect of an increased through put of energy from the entrance pupil to the image plane, which will be discussed more fully in Section C. For an additional comparison of the RMS with minimum and maximum mirror length systems, Fig.12 gives the RMS versus the field angle for F_m = 1m and M = 6x. From Fig.12, it follows that for field angles greater than 0.5 arc-mins the microscope mirror lengths have a significant influence on the RMS of the system. Optimization of the microscope mirror lengths for the S056 telescope and CCD detector array to be used in the ERXRT system will be discussed in Section E.

It is generally known that resolution of an optical system can be improved by defocusing the image surface from the nominal location. As a lower limit for the RMS, Figures 13-15 present the RMS versus the field angle on the optimum curved image surface for F_m = 1, 1.5, 2m using the minimum microscope mirror lengths. The optimum image surface is a concave surface facing the ERXRT system where the displacement ΔZ from the nominal image plane as a function of the field angle is given by Figs.16-18, corresponding to Figs.13-15. It is recognized that it is not practical to make a curved image surface for the ERXRT system, but the information given in Figs.13-18 is useful in evaluating the depth of field and defocusing tolerances of the ERXRT system.

For specific defocusing results, Figure 19 gives the RMS versus the field angle over different image planes. Each image plane has been displaced toward the microscope from the nominal focal point F_3 (see Fig.2) by an amount ΔZ. The information presented in Fig.19 is used by setting an upper limit for an axis ($\alpha = 0^{\circ}$) RMS, such as, one (1) arc-sec. Then, by using the image plane which has been defocused 6mm towards the microscope, an RMS of less than one (1) arc-sec will be maintained up to 1.5 arc-mins of

field. By normalizing the RMS by the RMS at $\alpha = 2$ arc-mins on the nominal image plane ($\Delta Z = 0$), the RMS data given in Fig.19 has been replotted in Fig.20 as a function of ΔZ for $\alpha = 0, 1, 1.75, 2$ arc-mins. Figure 20 is useful in extrapolating the defocusing information presented in Fig.19 to ERXRT systems with different values of F_m, M, or K. This will be considered in more detail in Section E.

As a closing comment on defocusing, a limited evaluation of the effect on the RMS over the image plane has been carried out when the microscope is shifted along the symmetry axis towards the S056 telescope by a small amount ΔZ_m. In these calculations, the image plane remained at original location F_3. For the system F_m = 1m, M = 5x, K = 2, the RMS increased by 2% at the field angle of 1.5 arc-mins when ΔZ_m = 2mm. This suggests the microscope should be positioned at the design location to within an axial accuracy of 2mm. The effects of lateral displacements or tilts of the microscope from the design position have not been considered in this study.

C. Vignetting Effects

In this section vignetting effects of the ERXRT system will be considered. As indicated in Fig.12, there are large increases in the RMS at field angles greater than 0.5 arc-mins when the microscope mirror lengths are increased from their minimum lengths. However, there is a compensating effect of an increased transmission of energy for the ERXRT system when the mirror lengths are increased. Figure 21 gives the percent energy loss due to vignetting versus the field angle for F_m = 1m and for minimum and maximum microscope mirror lengths. In order to more carefully evaluate the effect of increasing the microscope mirror lengths on the percent energy loss, Figures 22a-c give the percent energy loss versus the microscope hyperboloid length for F_m = 1, 1.5m and α = 1 arc-min. Figures 23a-c give the percent energy loss versus the ellipsoid length. Comparing Figs.22-23, one concludes that the percent energy loss is a stronger function of the hyperboloid length than of the ellipsoid length. In order to compare the two effects of percent of energy loss and increase in RMS, that is, the loss of resolution when the mirror surfaces are made longer, refer to Figs.24-25 for the ERXRT system F_m = 1m, M = 5x at α = 1 arc-min. Figures

24-25 show that the percent energy loss and the gain in resolution, that is, reduction in RMS, are reciprocal effects and that the hyperboloid length has a stronger effect on both the energy loss and resolution than the ellipsoid length. The mirror lengths for the crossing point of the energy loss and RMS curves in Figs.24-25 may be considered to a first approximation as optimum mirror lengths for the purpose of balancing the competing energy loss - RMS effects. However, matching of the S056/ERXRT system imaging characteristics with the detector capabilities and the K values of the microscope system must be considered before suitable optimization of the mirror lengths can be effective.

After matching the ERXRT system imaging capabilities with the CCD detector resolution and considering the mission objectives for the field of view, the MSFC ERXRT Design Team selected the microscope parameters F_m = 2m and M = 8x for fabrication. Therefore, more detailed vignetting information for the selected microscope will be given at the field angles of 1 and 2 arc-mins. Figures 26-27 present the RMS and percent energy loss versus L_H' and L_E for K = 1.5. Similar results for K = 2.5 are given in Figs.28-29. It follows from Figs.26-27 that maximum

transmittance (energy transmitted thru the ERXRT system = 1 - energy loss) and maximum RMS occurs for $L_H' = L_E = 2.1$cm at $\alpha = 1$, 2 arc-min for $K = 1.5$, $F_m = 2$m, $M = 8$x. Also, from Figs.28-29 it follows that the maximum transmittance and RMS occurs when $L_H' = 3.7$cm, $L_E = 3.30$ for $\alpha = 1$ arc-min and $L_H' = 3.8$cm, $L_E = 3.2$cm when $\alpha = 2$ arc-min for $K = 2.5$, $F_m = 2$m, $M = 8$x. Further consideration of the optimization of the mirror lengths will be presented in Section E.

In concluding the present discussion on vignetting effects, it is interesting to note the dependence of the RMS and transmittance on K for a given field angle. Figure 30 gives the RMS versus K for $\alpha = 2$ arc-mins, $F_m = 2$m, $M = 8$x. Figure 30 further illustrates that there can be large variations in the RMS for a given K as a result of varying the microscope mirror lengths. Figure 31 presents the transmittance versus K for $\alpha = 2$ arc-mins, $F_m = 2$m, $M = 8$x. The percentage variations in the transmittance resulting from changing the mirror lengths at a constant K are not as great as those presented in Fig.30. Before an effectively optimizing the mirror lengths, it is necessary to analyze the behavior of the point spread function (PSF) and compare the full width half maximum (FWHM) of the PSF in the

meridional and sagittal directions with the RMS spot radius.

D. Point Spread Function

It is generally recognized in glancing incidence x-ray optics[11] that the RMS spot radius does not provide a quantitative measure of resolution. Experience has shown that the full width half maximum (FWHM) of the point spread function (PSF) is more in keeping with the measured resolution of glancing incidence x-ray optical systems.[12-13] Using conventional ray tracing techniques, PSF calculations require several orders of magnitude more rays to be traced than RMS calculations. There is a need for new theoretical developments in glancing incidence x-ray optics such that the PSF can readily be evaluated. Interesting prospects are in progress for applying the analytical flux flow equation[14] to glancing incidence systems and for developing a general aberration theory for glancing incidence systems which would not be limited to the intersection zone of such optical systems.[15-16] However, in this study only conventional ray tracing methods have been used.

In this section the results for the PSF of the ERXRT system defined by F_m = 2m, M = 8x, K = 2.5, L_H' = 3.3cm, L_E = 3.7cm will be presented. Then, by comparing the RMS data to the PSF data for this ERXRT system a resolution scaling

factor is obtained. Using these results, optimization of the microscope lengths for the fabrication effort will be presented in Section E.

Tables 5, 6, 7 give the ray distribution (number of rays per image plane cell) over half of the X-Y image plane ($Y \geq 0$) for the field angles $\alpha = 0.5, 1, 2$ arc-minutes off axis. Also, the number of rays with constant X and Y coordinates, partial sums of rays, and percent of total rays at given distance from the axis are given. The point spread function (PSF) is computed by multiplying the number of rays per image plane cell times the area per ray at the entrance pupil, $\Delta A = 2.50203 \times 10^{-5} cm^2$, and the incident x-ray flux density at the system.

The meridional line spread function has been evaluated from data in Tables 5-7 and is plotted in Figs.32, 33, 34 for the field angles $\alpha = 0.5, 1, 2$ arc-minutes. It should be noted that Figs.32-34 are in fact a plot of the " IYG" data in Tables 5-7 versus XG. Since the image plane ray distributions are strongly aberrated, it is not useful to plot analogous graphs to Figs.32-34 in the sagittal direction. Rather, Figures 35, 36, 37 represents slices of the point spread function at constant X. The wedges in the center of the sagittal line

TABLE 5

Ray distribution over half xy image plane (y>/0) for α = 0.5 arc-min, F_m = 2m, M = 8x, L_H' = 3.3cm, L_E = 3.7 cm. Also, the image plane grid is ΔXG = 0.013534 arc-secs and ΔYG = 0.01015 arc-secs. The entrance pupil area for each ray is $\Delta A = 2.50203 \times 10^{-5}$ cm^2.

XG (cm) \ YG (μm)	0	0.75	1.5	2.25	3.0	3.75	4.5	5.25	6.0	6.75	7.5	8.25	9.0	9.75	10.5	11.25	12.0	12.75	13.5	14.25	15	ΣIYG	Partial Sum	%
.2238	173	180	171	162	136	105	66	15	–	–	–	–	–	–	–	–	–	–	–	–	–	1008	190670	100
.2237	242	250	237	236	237	235	231	234	188	120	39	–	–	–	–	–	–	–	–	–	–	2249	189662	99.5
.2236	252	260	246	246	248	248	245	241	244	237	237	185	80	2	–	–	–	–	–	–	–	2971	187413	98.3
.2235	261	269	259	259	258	256	257	255	250	253	250	243	246	177	67	–	–	–	–	–	–	3582	184442	96.7
.2234	267	275	276	273	272	272	266	264	267	261	256	257	249	252	245	156	13	–	–	–	–	4121	180860	94.9
.2233	279	287	291	286	286	283	281	283	273	274	273	268	265	261	256	254	219	32	–	–	–	4652	176739	92.7
.2232	294	302	305	302	300	298	297	291	296	285	286	280	277	272	268	264	259	234	50	–	–	5160	172087	90.3
.2231	310	318	321	320	318	317	310	312	325	301	296	298	288	285	278	277	270	263	238	34	–	5660	166927	87.6
.2230	328	336	339	337	337	334	332	328	322	319	317	309	304	298	293	286	284	275	269	215	7	6169	161267	84.6
.2229	381	390	357	358	358	354	353	346	341	337	332	324	317	317	307	299	292	287	282	274	131	6739	155098	81.3
.2228	385	393	383	387	379	381	374	367	364	359	357	343	337	338	321	317	307	299	294	285	315	7269	148359	77.8
.2227	398	406	417	414	409	401	400	394	385	378	372	359	355	350	337	326	322	311	304	297	553	7288	141090	74.0
.2226	52	53	85	156	272	413	426	420	414	403	392	387	377	365	353	350	333	329	318	310	772	6962	133802	69.9
.2225	–	–	–	–	–	23	223	437	441	432	422	407	294	325	375	360	354	337	331	317	945	6186	126820	66.2
.2224	–	–	–	–	–	–	–	70	458	461	447	434	423	459	394	383	368	354	346	333	1066	5936	120634	63.0
.2223	–	–	–	–	–	–	–	–	88	478	480	453	446	430	415	396	392	366	361	339	1131	5785	114698	59.8
.2222	–	–	–	–	–	–	–	–	–	264	514	476	476	457	440	414	385	394	387	338	1144	5709	108313	56.8
.2221	–	–	–	–	–	–	–	–	–	61	551	532	491	471	473	448	417	403	385	375	1088	5695	102204	53.8
.2220	–	–	–	–	–	–	–	–	–	–	546	584	512	514	484	457	441	420	403	389	957	5702	96909	50.8
.2219	–	–	–	–	–	–	–	–	–	–	590	605	562	540	504	481	459	435	412	397	735	5227	91307	47.8
.2218	–	–	–	–	–	–	–	–	–	99	689	637	597	563	530	505	472	447	428	409	438	5818	85480	44.8
.2217	–	–	–	–	–	–	–	–	–	435	731	682	634	573	553	521	489	461	437	414	189	6139	79662	41.8
.2216	–	–	–	–	–	–	–	–	214	836	781	714	662	612	574	535	505	475	449	319	6	6682	73523	38.6
.2215	–	–	–	–	–	–	–	278	941	906	818	747	687	635	590	547	575	484	374	29	–	7555	66841	35.1
.2214	–	–	–	–	–	134	793	1203	1066	947	842	774	701	649	603	557	533	361	30	–	–	9186	57286	31.1
.2213	1305	1305	1137	1276	1554	1758	1494	1267	1096	966	866	780	716	655	605	543	255	–	–	–	–	17578	50100	26.3
.2212	908	908	4489	3137	2297	1817	1492	1262	1094	966	862	783	714	626	355	64	–	–	–	–	–	21776	32522	17.1
.2211	0	0	192	1104	1465	1535	1372	1199	1064	931	727	497	256	36	–	–	–	–	–	–	–	10404	10746	5.6
.2210	–	–	–	–	–	–	82	144	92	18	–	–	–	–	–	–	–	–	–	–	–	342	342	0.2
ΣIXG	5835	5932	9505	9255	9128	9164	9326	9630	10174	11377	13373	13390	11378	10502	9620	8740	7869	6977	6032	5069	4472			
PARTIAL SUM	5835	11767	21272	30527	39655	48819	58145	67775	77949	89326	102699	116089	126317	136819	146439	155179	163048	170025	176123	181192	190673			
%	3.1	6.2	11.2	16.0	20.8	25.6	30.5	35.6	40.9	46.8	53.8	60.3	66.3	71.8	76.8	81.7	85.5	89.2	92.4	95.0	100			

TABLE 6

Ray distribution over half xy image plane (y>/0) for α = 1 arc-minute, F_m = 2m, M = 8x, L_H' = 3.3cm, L_E = 3.7 cm. Also, the image plane grid is ΔXG = 0.05075 arc-secs and ΔYG = 0.05955 arc-secs. The entrance pupil area for each ray is ΔA = 2.50203x10-5 cm^2.

XG (cm)	YG (μm) 0	4.4	8.8	13.2	17.6	22	26.4	30.8	35.2	39.6	44	48.4	52.8	57.2	61.6	66	70.4	74.8	79.2	83.6	88	HALF PLANE (Y>0) ΣIYG	PARTIAL SUM	%
.4531	–	–	–	–	–	–	–	–	24	100	21	–	–	–	–	–	–	–	–	–	–	145	107505	100
.4527	–	–	–	–	–	–	–	–	–	108	220	196	82	2	–	–	–	–	–	–	–	652	107360	[illegible]
.4524	–	–	–	–	–	–	–	–	–	–	169	291	285	237	100	4	–	–	–	–	–	1036	106692	[illegible]
.4520	–	–	–	–	–	–	–	–	–	–	10	256	296	287	220	228	71	–	–	–	–	1428	105606	98.2
.4516	–	–	–	–	–	–	–	–	–	–	–	103	306	297	293	257	375	171	18	–	–	1752	104172	[illegible]
.4512	–	–	–	–	–	–	–	–	–	–	–	1	266	310	249	292	270	276	239	60	–	2033	102426	95.3
.4509	–	–	–	–	–	–	–	–	–	–	–	–	146	319	312	301	295	289	277	267	106	2312	100393	93.4
.4505	–	–	–	–	–	–	–	–	–	–	–	–	49	331	322	314	305	294	291	272	519	2694	98081	91.2
.4501	–	–	–	–	–	–	–	–	–	–	–	–	–	270	334	322	311	308	284	292	663	2804	95387	88.7
.4497	–	–	–	–	–	–	–	–	–	–	–	–	–	229	341	333	330	298	311	294	665	2801	92583	86.1
.4494	–	–	–	–	–	–	–	–	–	–	–	–	–	179	354	343	322	324	314	304	634	2774	89782	83.5
.4490	–	–	–	–	–	–	–	–	–	–	–	–	–	156	366	348	356	332	317	304	606	2755	87008	80.9
.4486	–	–	–	–	–	–	–	–	–	–	–	–	–	155	360	375	342	339	331	317	531	2756	84253	78.3
.4482	–	–	–	–	–	–	–	–	–	–	–	–	–	154	391	376	365	349	335	321	436	2727	81467	75.8
.4479	–	–	–	–	–	–	–	–	–	–	–	–	–	181	410	390	372	360	342	333	323	2711	78740	73.2
.4475	–	–	–	–	–	–	–	–	–	–	–	–	–	242	421	404	386	369	356	335	239	2752	76029	70.7
.4471	–	–	–	–	–	–	–	–	–	–	–	–	–	331	435	416	397	377	360	347	147	2810	73277	68.2
.4467	–	–	–	–	–	–	–	–	–	–	–	–	7	446	450	427	402	387	370	349	35	2873	70467	65.6
.4464	–	–	–	–	–	–	–	–	–	–	–	–	143	491	465	436	420	396	380	251	–	2782	67594	62.9
.4460	–	–	–	–	–	–	–	–	–	–	–	–	355	508	480	459	428	406	384	95	–	3115	64812	60.1
.4456	–	–	–	–	–	–	–	–	–	–	–	65	550	522	491	463	439	411	299	–	–	3240	61497	57.2
.4452	–	–	–	–	–	–	–	–	–	–	–	362	577	542	502	477	445	419	78	–	–	3402	58257	54.2
.4449	–	–	–	–	–	–	–	–	–	–	134	636	577	553	518	482	455	235	–	–	–	3612	54855	51.0
.4445	–	–	–	–	–	–	–	–	–	36	605	664	609	566	528	497	370	11	–	–	–	3886	51243	47.7
.4441	–	–	–	–	–	–	–	–	17	572	753	679	627	582	539	446	51	–	–	–	–	4266	47357	44.1
.4437	–	–	–	–	–	–	–	41	654	853	766	699	637	589	490	76	–	–	–	–	–	4805	43091	40.1
.4434	–	–	–	–	–	–	234	923	986	877	785	711	649	480	62	–	–	–	–	–	–	5707	38286	35.6
.4430	–	–	–	–	343	999	1341	1152	1007	886	793	706	354	18	–	–	–	–	–	–	–	7605	32579	30.3
.4426	2048	2048	2979	2485	2160	1692	1375	1169	1002	862	495	110	–	–	–	–	–	–	–	–	–	18425	24974	23.2
.4422	6	6	893	1329	1290	1146	893	620	321	45	–	–	–	–	–	–	–	–	–	–	–	5549	6549	6.1
ΣIXG	2054	2054	3872	3814	3793	3837	3843	3711	4011	4339	4813	5477	6526	8799	9573	8496	7433	6351	5286	4147	4909			
PARTIAL SUM	2054	4108	7980	11794	15587	19424	23267	27178	31189	35528	40341	45820	52346	61345	70888	79384	86817	93168	98454	102601	107505			
%	1.9	3.8	7.4	11.0	14.5	18.1	21.6	25.3	29.0	33.1	37.5	42.6	48.7	57.1	65.9	73.8	80.8	86.7	91.6	95.4	100			

ORIGINAL PAGE IS OF POOR QUALITY

TABLE 7

Ray distribution over half xy image plane (y>/0) for $\alpha = 2$ arc-minutes, $F_m = 2m$, $M = 8x$, $L_H' = 3.3$ cm, $L_E = 3.7$ cm. Also, the image plane grid is $\Delta XG = 0.1015$ arc-secs and $\Delta YG = 0.29775$ arc-secs. The entrance pupil area for each ray is $\Delta A = 2.50203 \times 10^{-5}$ cm^2.

XG (μm)	YG (μm)																				FOR HALF PLANE (Y>0)		
	0	22	44	66	88	110	132	154	176	198	220	242	264	286	308	330	352	374	396	418	Σ I YG	PARTIAL SUM	%
.9070	–	–	–	–	–	–	–	–	–	–	–	–	–	–	–	–	1	52	–	–	53	46199	100
.9062	–	–	–	–	–	–	–	–	–	–	–	–	–	–	–	–	32	146	1	–	179	46146	99.9
.9055	–	–	–	–	–	–	–	–	–	–	–	–	–	–	–	–	78	175	49	–	302	45967	99.5
.9047	–	–	–	–	–	–	–	–	–	–	–	–	–	–	–	–	126	179	123	–	428	45665	98.8
.9040	–	–	–	–	–	–	–	–	–	–	–	–	–	–	–	4	178	178	169	21	550	45237	97.9
.9032	–	–	–	–	–	–	–	–	–	–	–	–	–	–	–	46	188	193	166	87	670	44687	96.7
.9025	–	–	–	–	–	–	–	–	–	–	–	–	–	–	–	103	194	185	182	145	809	44017	95.3
.9017	–	–	–	–	–	–	–	–	–	–	–	–	–	–	–	168	192	176	172	167	875	43208	93.5
.9010	–	–	–	–	–	–	–	–	–	–	–	–	–	–	29	204	197	189	179	152	950	42333	91.6
.9002	–	–	–	–	–	–	–	–	–	–	–	–	–	–	99	211	192	191	175	98	966	41383	89.6
.8995	–	–	–	–	–	–	–	–	–	–	–	–	–	–	174	210	210	188	181	37	1000	40417	87.5
.8987	–	–	–	–	–	–	–	–	–	–	–	–	–	34	226	207	196	192	151	–	1006	39417	85.3
.8980	–	–	–	–	–	–	–	–	–	–	–	–	–	119	229	214	205	191	87	–	1045	38411	83.1
.8972	–	–	–	–	–	–	–	–	–	–	–	–	2	214	230	217	204	190	17	–	1074	37366	80.9
.8965	–	–	–	–	–	–	–	–	–	–	–	–	72	247	230	223	205	129	–	–	1106	36292	78.6
.8957	–	–	–	–	–	–	–	–	–	–	–	–	184	250	235	221	207	48	–	–	1145	35186	76.2
.8950	–	–	–	–	–	–	–	–	–	–	–	48	270	255	235	222	164	–	–	–	1194	34041	73.7
.8942	–	–	–	–	–	–	–	–	–	–	–	124	273	250	240	221	71	–	–	–	1239	32847	71.1
.8935	–	–	–	–	–	–	–	–	–	–	40	293	275	252	232	182	1	–	–	–	1293	31608	68.4
.8927	–	–	–	–	–	–	–	–	–	–	199	297	278	259	239	75	–	–	–	–	1347	30315	65.6
.8920	–	–	–	–	–	–	–	–	–	59	326	308	278	261	191	–	–	–	–	–	1423	28968	62.7
.8912	–	–	–	–	–	–	–	–	1	268	335	305	282	261	53	–	–	–	–	–	1505	27545	59.6
.8905	–	–	–	–	–	–	–	–	144	371	334	308	286	158	–	–	–	–	–	–	1601	26040	56.4
.8897	–	–	–	–	–	–	–	45	383	370	338	309	253	16	–	–	–	–	–	–	1714	24439	52.9
.8890	–	–	–	–	–	–	8	352	417	375	341	308	72	–	–	–	–	–	–	–	1873	22725	49.2
.8882	–	–	–	–	–	–	314	473	422	379	342	146	–	–	–	–	–	–	–	–	2076	20852	45.1
.8875	–	–	–	–	1	336	550	477	425	379	207	1	–	–	–	–	–	–	–	–	2376	18776	40.6
.8867	–	–	–	31	474	646	553	482	425	235	4	–	–	–	–	–	–	–	–	–	2850	16400	35.5
.8860	–	3	368	826	792	648	556	475	196	1	–	–	–	–	–	–	–	–	–	–	3865	13550	29.3
.8852	1384	1762	1357	995	787	656	403	88	–	–	–	–	–	–	–	–	–	–	–	–	7432	9685	21.0
.8845	89	625	637	502	313	87	–	–	–	–	–	–	–	–	–	–	–	–	–	–	4506	4506	4.9
Σ I XG	1473	2350	2362	2354	2367	2373	2384	2392	2413	2437	2466	2507	2525	2582	2642	2734	2841	2572	1652	707			
PARTIAL SUM	1473	3863	6225	8579	10946	13319	15703	18095	20508	22945	25411	27918	30443	33025	35673	38407	41242	43840	45492	46199			
% OF TOTAL	3.2	8.4	13.5	18.5	23.3	28.8	34.0	39.2	44.4	49.7	55.0	60.4	65.9	71.5	77.2	83.1	89.3	94.5	98.5	100			

spread functions in Figs.35-37 result from the strong aberrations and the vignetting effects. (For on axis radiation, all ray are incident into a single cell, as designed.)

Tables 5-7 and Figs.32-37 contain significant information about the performance of the ERXRT system. The results can be summarized, in part, by Fig.38, which plots different measures of resolution (RMS, FWHM, 50% enclosed energy) versus the field angle. Laboratory experience has suggested that the average of the meridional and sagittal FWHM provides a reasonable measure of resolution for glancing incidence x-ray systems. Table 8 details these results.

TABLE 8

Field angle Arc-minutes	RMS(arc-sec)	Average FWHM(arc-secs)	Scale Factor RMS/Av.FWHM
0.5	0.17197	0.059553	2.8876
1.0	0.86073	0.378115	2.276
2.0	3.4377	1.1615	2.9597

Also, given in Table 8 is a scaling factor which is defined as the ratio of the RMS to the average FWHM value. In

order to transform the RMS data for different microscope mirror lengths into resolution data, it is proposed to divide the RMS data by the scaling factors given in Table 8. This will be considered in more detail in Section E. Before closing the present discussion of the point spread function, it is useful to note the percent of energy contained under the central peak of the line spread functions in Figs.32-37.

Table 9 gives the transmittance of the ERXRT system under consideration and the percent energy under peaks of line spread function.

TABLE 9

Field Angle (arc-mins)	Transmittance (%)	Energy at FWHM (%) Meridional	Sagittal
0.5	62.15	10.0	13.4
1.0	35.6	5.5	6.5
2.0	16.0	2.3	3.7

A practical consideration in determining the resolution over the field of view for the ERXRT system is the threshold power for operation of the CCD detectors. This point should be analyzed more carefully than was possible with CCD data available for this study.

E. Optimization of the Microscope

The microscope variables available for optimization are the focal length, F_m, the magnification, and the mirror lengths L_H' and L_E. As a result, the overall length consideration, the MSFC ERXRT design teams have selected F_m = 2m for the fabrication effort. In terms of the magnification, the plate factor (PF) for the ERXRT is

$$PF = \frac{180 \quad 3600 \text{ arc-secs} \quad 1}{190.5\text{cm} \qquad\qquad M}$$

$$= \frac{1082.754888}{M} \frac{\text{arc-secs}}{\text{cm}}. \tag{32a}$$

By matching the limit of resolution of the S056 telescope (0.8 arc-secs) to two adjacent 30 micron pixels on the image plane, the desired plate factor for the ERXRT system is

$$PF = \frac{0.8 \text{ arc-secs}}{0.0060\text{cm}} = 133\ 1/3 \ \frac{\text{arc-secs}}{\text{cm}}. \tag{32b}$$

Equating Eqs.32a-b and solving for M gives

$$M = 8.12. \tag{32c}$$

Taking these calculations into consideration the MSFC ERXRT design team has selected for the fabrication M = 8x, which

has the plate factor

$$PF = 135.3443610 \frac{\text{arc-secs}}{\text{cm}} . \qquad (33)$$

Using the plate factor given by Eq.33, the half field of view for the 320X 512-30 micron CCD array is

$$1/2 \text{ field of view} = 65 \times 104 \text{ arc-secs}$$

$$1/2 \text{ diagonal view} = 122 \text{ arc-secs}. \qquad (34)$$

In view of Eq. 34, a practical half field of view of ERXRT will be considered to be 1.75 arc-minutes. It now remains to optimize the mirror lengths of the ERXRT.

As established in Sections B-D, the RMS and transmittance increase with increasing L_H', L_E. However, it is desirable to select L_H', L_E for maximum transmittance. Then select the fabrication constant K such that the resolution at 1.75 arc-min field angle corresponds to the limit of resolution of the S056 telescope. Figure 39 gives the RMS versus K at $\alpha = 1.75$ arc-min for L_H', L_E which give the maximum transmittance. Using the scaling factor 2.9597 from Table 8, it follows that an RMS = 2.37 arc-secs at full field will translate to sub-arc second resolution. Thus, K = 2.02 is optimum. Figure 40 displays (L_H'/L_E) versus K for maximum transmittance at $\alpha = 1.75$

arc-minutes, which indicates $(L_H'/L_E) = 1.055$ for $K = 2$, or

$$L_H' = 2.9160 \text{ cm}$$

$$L_E = 2.7640 \text{ cm.} \tag{35}$$

In view of the resolution improvements resulting from defocusing the image plane, discussed in Section B, which were not considered in Table 8, and from laboratory experience with the S056 optics, one may expect the potential resolution to be a little better than 0.8 arc-secs for the microscope defined by Eq.35, which suggest building the microscope with maximum K (=2.5) for maximum transmittance

$$L_H' = 3.82 \text{ cm} \qquad (K=2.5)$$

$$L_E = 3.2951 \text{ cm.} \tag{36}$$

The RMS and transmittance for the microscope defined by Eqs.36 is given in Table 10.

TABLE 10

(arc-min)	RMS (arc-secs)	Transmittance (%)
0.5	.17197	62.15
0.75	.46634	57.90
1.0	.54292	45.70
1.25	1.51317	31.89
1.50	2.2303	25.70
1.75	3.0472	21.59
2.0	3.9754	18.6

Using the scaling factor from Table 9 and defocusing the image plane by approximately 4mm (see Fig.20) gives resolution for the ERXRT system of approximately 0.8 arc-sec.

F. Aperture Stops

The purpose of aperture stops or baffles is to block unwanted radiation from striking the image plane CCD detector array. There are two types of unwanted radiation leaving the S056 telescope which require different types of baffles. First, for large field angles, there are some highly distorted rays leaving the S056 telescope which will strike the entrance plane of the microscope at radii greater than the radius of H', $R_H'(min)$, at $Z_H'(max)$ (=172.0978cm). These exterior, unwanted rays will miss the microscope altogether and can be blocked from striking the image plane by use of a large exterior baffle mounted in front of the microscope at $Z_H'(max)$, with a hole of diameter $2R_H'(min)$ ($R_H'(min)$=1.226955 cm) centered with respect to and perpendicular to the optical axis.

The second type of unwanted rays pass into the interior of the microscope thru the plane at $Z_H'(max)$ with radii less than $R_H'(min)$, but either hit H' and miss E or hit E without reflecting from H'. Figure 41 displays the maximum and minimum aperture radii as a function of the field angle. R_{1S} refers to radii on the front aperture plane at $Z_H'(max)$ and R_{2S}, the back aperture plane at $Z_E(min)$. For field angles greater than 0.5 arc-mins

R_{1S}(max) is greater than R_H'(min) resulting in exterior unwanted rays. These rays can not be used for the present microscope imaging and must be blocked from striking the image plane. It is interesting to note from Eq.6 that as F_m/M increase, the microscope intersection diameter increases which is one way to increase R_H'(min), and thus, to minimize the exterior unwanted rays. Also, from Fig.41, R_{2S}(max) is greater than R_E(min) (=1.4353703 cm) at Z_E(min) which indicates the presence of interior, unwanted rays for field angles greater than 0.25 arc-mins. Since R_{2S}(min) is constant as a function of the field angle, it would appear that the second aperture stop does not have a strong influence on rays which strike both H' and E. It is also interesting to note that for $\alpha=0$ the value R_{S1}(min) = 1.7784 from Fig.41 is consistent with the following:

$$R_{S1} = (F_W - Z_H'(\text{max})) \tan 4\theta m$$

$$= (190.5 - 172.0978) \tan(4 * .916^{\circ}) \text{cm}$$

$$= 1.1784 \text{ cm}$$

where the fact that the microscope intersection rays are adjacent to front aperture stop for an axis incident light and make an angle of 4θm with the Z axis have been used.

The data presented in Fig.41 was based on the ray intercepts with the aperture planes of both the wanted and

unwanted rays. Table 11 presents the minimum values of R_{S1} and R_{S2} for the wanted rays, ie, rays which intercept H' for R_{S1} and both H' and E for R_{S2}.

TABLE 11

α (arc-min)	$R_{S1,min}$ (cm)	$R_{S2,min}$ (cm)
0	1.1784	1.3967
.5	1.1755	1.3967
.75	1.1758	1.3975
1.0	1.1757	1.3975
1.5	1.1762	1.3975
2.0	1.1762	1.3975

In order to select radii for the aperture stops to be used in the ERXRT system, both RMS and transmittance calculations have been done for field angles 0, .5, 1, 1.5, 1.75, 2 arc-mins and for R_{S1} = 1.16, 1.17, 1.175, 1.1764, 1.1779, 1.18 cm and R_{S2} = 1.35, 1.36, ···, 1.40 cm. The results were independent of R_{S2} in the range of 1.35 to 1.39 cm. When R_{S2} = 1.40 cm, the microscope intersection rays are blocked, resulting in large RMS values. Therefore,

$$R_{S2} = 1.35 \text{ to } 1.3975 \text{ cm}$$

is the recommended value for radius of the back aperture stop. Table 12 presents the RMS, transmittance, and number of unwanted rays for R_{S2} = 1.39 cm. It follows from the

TABLE 12: R_{S2} = 1.39 cm

R_{S1}(cm)	α(arc-mins)	RMS(arc-secs)	TRANSMITTANCE %	TRANSMITTANCE #Wanted	#UNWANTED RAYS ALL	#UNWANTED RAYS INTERIOR
1.16	0	0	100	3844	0	0
	0.5	.1719	62.1	2389	959	959
	1.0	.9499	45.7	1757	755	393
	1.5	2.230	25.7	988	1331	238
	1.75	3.050	21.6	830	1433	179
	2.0	3.975	19.8	760	1505	170
1.17	0	0	100	3844	0	0
	.5	.1719	62.1	2389	310	310
	1.0	.9499	45.7	1757	540	178
	1.5	2.230	25.7	988	1195	102
	1.75	3.050	21.6	830	1330	76
	2.0	3.975	18.4	716	1403	68
1.175	0	0	100	3844	0	0
	.5	.1719	62.1	2389	74	74
	1.0	.9499	45.7	1757	438	76
	1.5	2.230	25.7	988	1121	28
	1.75	3.050	21.6	830	1270	16
	2.0	3.975	18.4	716	1347	12
1.1764	0	0	100	3844	0	0
	.5	.172	61.9	2379	18	18
	1.0	.9504	45.6	1753	410	48
	1.5	2.232	25.7	986	1107	14
	1.75	3.05	21.4	823	1258	4
	2.0	3.98	18.4	714	1337	2
1.17797	0	0	100	3844	0	0
	.5	.1724	60.6	2331	0	0
	1.0	.9521	45.2	1239	400	38
	1.5	2.242	25.4	976	1103	10
	1.75	3.063	21.3	820	1256	2
	2.0	3.991	18.2	710	1335	0

ORIGINAL PAGE IS
OF POOR QUALITY

TABLE 12 - Continued

R_{S1} (cm)	α(arc-mins)	RMS (arc-secs)	TRANSMITTANCE %	#Wanted	#UNWANTED RAYS ALL	INTERIOR
1.18	0	0	91.4	3512	0	0
	.5	.1733	58.0	2229	0	0
	1.0	.9593	43.7	1679	400	38
	1.5	2.283	24.3	934	1103	10
	1.75	3.121	20.4	786	1256	2
	2.0	4.075	17.6	678	1335	0
1.19	0	0	37.7	1448	0	0
	.5	.1718	47.5	1827	0	0
	1.0	.9772	38.6	1485	0	0
	1.5	2.244	20.9	802	1103	10
	1.75	3.343	17.3	666	1256	2
	2.0	4.379	14.9	574	1335	0

data in Table 12 that the RMS and transmittance are not affected by increasing R_{S1} = 1.16, 1.17, 1.175, 1.1764, 1.17797 cm, but there are large reductions in the number of unwanted interior rays. However, when R_{S1} is further increased to 1.18 or 1.19 cm, there are increases in RMS, resulting from blockage of good imaging rays near the microscope intersection point, and there is some reduction in the number of unwanted, interior rays. From this data,

$$1.175 \text{ cm} \leq R_{S1} \leq 1.17797 \text{ cm}$$

is the recommended radius of the front aperture stop. It should be noted that for the aperature stops defined by Eqs.38a-b there are some unwanted, interior rays which pass thru the same aperture space as good imaging rays, and thus, can not be blocked from striking the image plane.

IV. RECOMMENDATIONS AND CONCLUSIONS

The mathematical equations and computer programs have been developed for ray tracing a coupled Wolter I telescope (S-056 optics) and a glancing incidence hyperboloid-ellipsoid x-ray microscope. The intrinsic microscope variables (glancing angle $\theta m'$, intersection diameter $2x^*$, and surface parameters) have been evaluated and analyzed for the microscope focal lengths F_m = 1, 1.5, 2m and magnifications M = 5, 6, 6.5, 7, 8. The RMS spot radius as a function of the field angles 0, .25, •••, 2.5 arc-mins on a flat image plane have been computed in order to evaluate the effect of magnification variations, varying microscope focal lengths, defocusing the image plane and vignetting effects. The point spread function has also been analyzed for F_m = 2m, M = 8x, and microscope mirror lengths L_H' = 3.3 cm and L_E = 3.7 cm. Taking this data into account, the microscope has been optimized to couple the S056 optics to the proposed CCD detector array such that the ERXRT system provides sub-arc seconds resolution over a field of view of ± 2 arc-mins with a energy transmittance of 20% at 2 arc-minutes off axis and 40% at 1 arc-minute off axis. The recommended microscope to achieve these goals is defined by

$F_m = 2m$, $M = 8x$, $K = 2.5$

$L_H' = 3.82$ cm, $L_E = 3.2951$ cm

where the flat image plane is defocused by 4mm towards the microscope.

Three aperture stops have also been designed to block unwanted radiation from striking the image plane. First, in the plane at the front of the microscope hyperboloid surface $Z_H'(max) = 172.0978$ cm, there should be two baffles. One stop should have a large hole of radius $R_H'(min) = 1.22696$ cm. The second stop should be a disk of radius $R_{S1} = 1.17797$ cm. Both of the stops in the front aperture plane should be centered with respect to the optical axis. The second aperture plane should be at the rear of the microscope ellipsoid surface $Z_E(min) = 164.9827$ cm. Within the second aperture plane, a disk of radius $R_{S2} = 1.3975$ cm. should be centered with respect to the optical axis. Depending upon microscope fabrication techniques used, it may be necessary to redesign the aperture stops for the manufactured system.

APPENDIX A: X-Ray Microscope System Parameters

The x-ray microscope system parameters will be derived by using the same coordinate system as used in the design of the S056 x-ray telescope. From Fig.A-1, F_1 is the focus of H- and E-mirror, F_2 is the second focus of H-mirror, and F_3 is the second focus of the E-mirror. It is assumed that F_2 is also the focus of the Wolter Type I (S056) x-ray telescope. It also follows F_w is the focal length of the S056 telescope, and F_m $(=\overline{F_2F_3})$ is the axial focal length of the x-ray microscope. Then the center coordinates of H- and E-mirror, O_H, O_E, will be given by $(O \cdot Z_{oH})$, $(O \cdot Z_{oE})$ where

$$Z_{oH} = F_w + C_H$$

$$Z_{oE} = F_w - F_m + C_E .$$

The equations for x-ray microscope surfaces in S056 coordinate system are for the ellipsoid

$$\frac{\left(Z - Z_{oE}\right)^2}{A_E^2} + \frac{X^2}{B_E^2} = 1 \qquad \text{(A-1)}$$

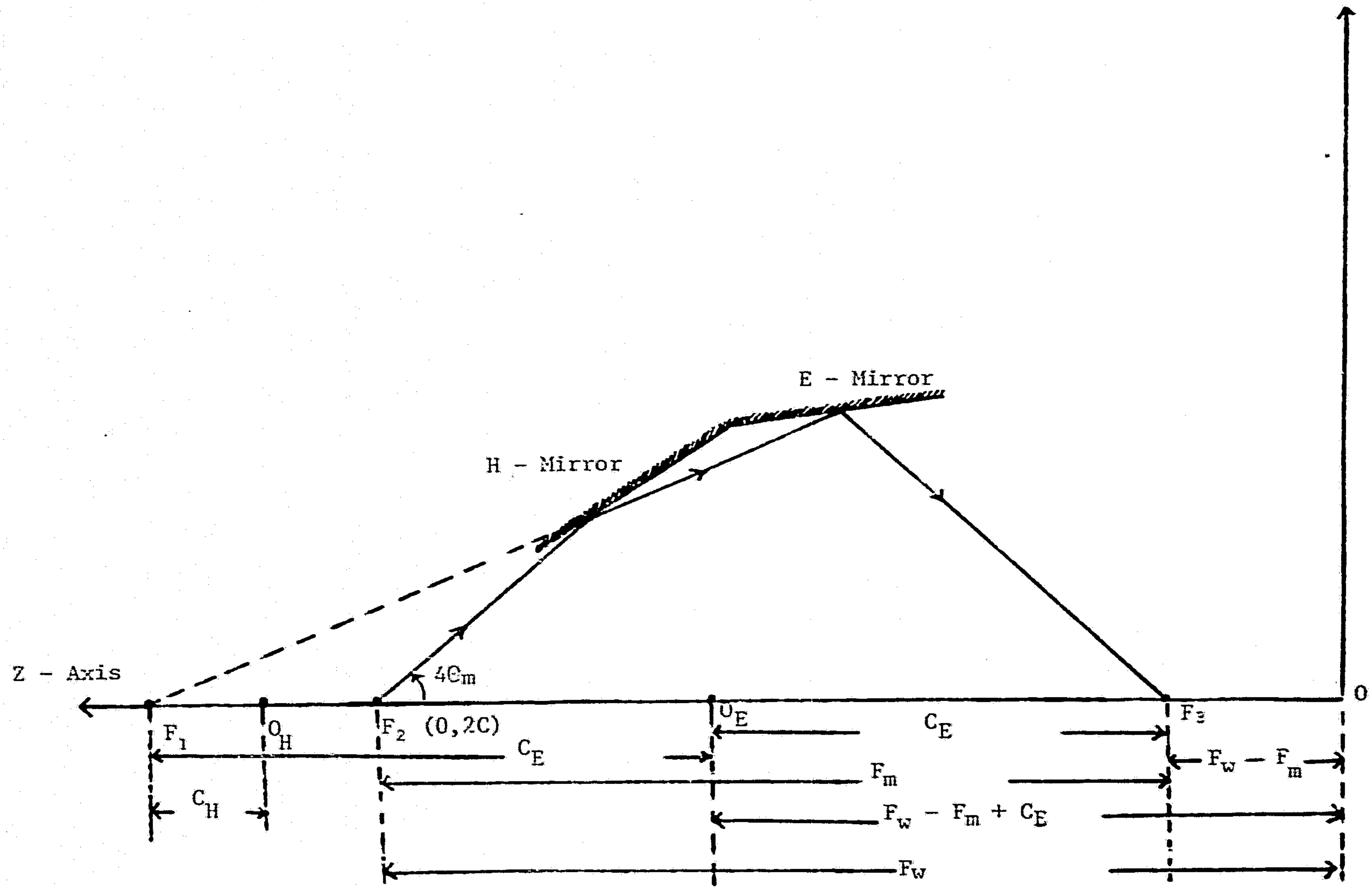

Figure A-1 Cross Sectional Diagram of X-Ray Microscope

where $B_E^2 = A_E^2 - C_E^2$, and for the hyperboloid,

$$\frac{(Z - Z_{oH})^2}{A_H^2} - \frac{X^2}{B_H^2} = 1 \qquad \text{(A-2)}$$

where $B_H^2 = C_H^2 - A_H^2$.

If F_w, F_m are specified, one can solve for A_E, B_E, A_H, and B_H.

Referring to Fig.A-2, define the magnification of the x-ray microscope (M) as the ratio of the image distance divided by the object distance:

$$M = L_I/L_o \qquad \text{(A-3)}$$

where the object is located at F_2 and the image location at F_3. The object distance is measured from the object to the intersection point of H- and E-mirrors. It is desirable to obtain expression for the microscope parameters in terms of M, F_m, and θ_m (glancing angle at intersection point of telescope). The first step is to solve for θ_m', the glancing incidence angle intersection point of the rays with H-mirror surface. Using the assumption that reflected

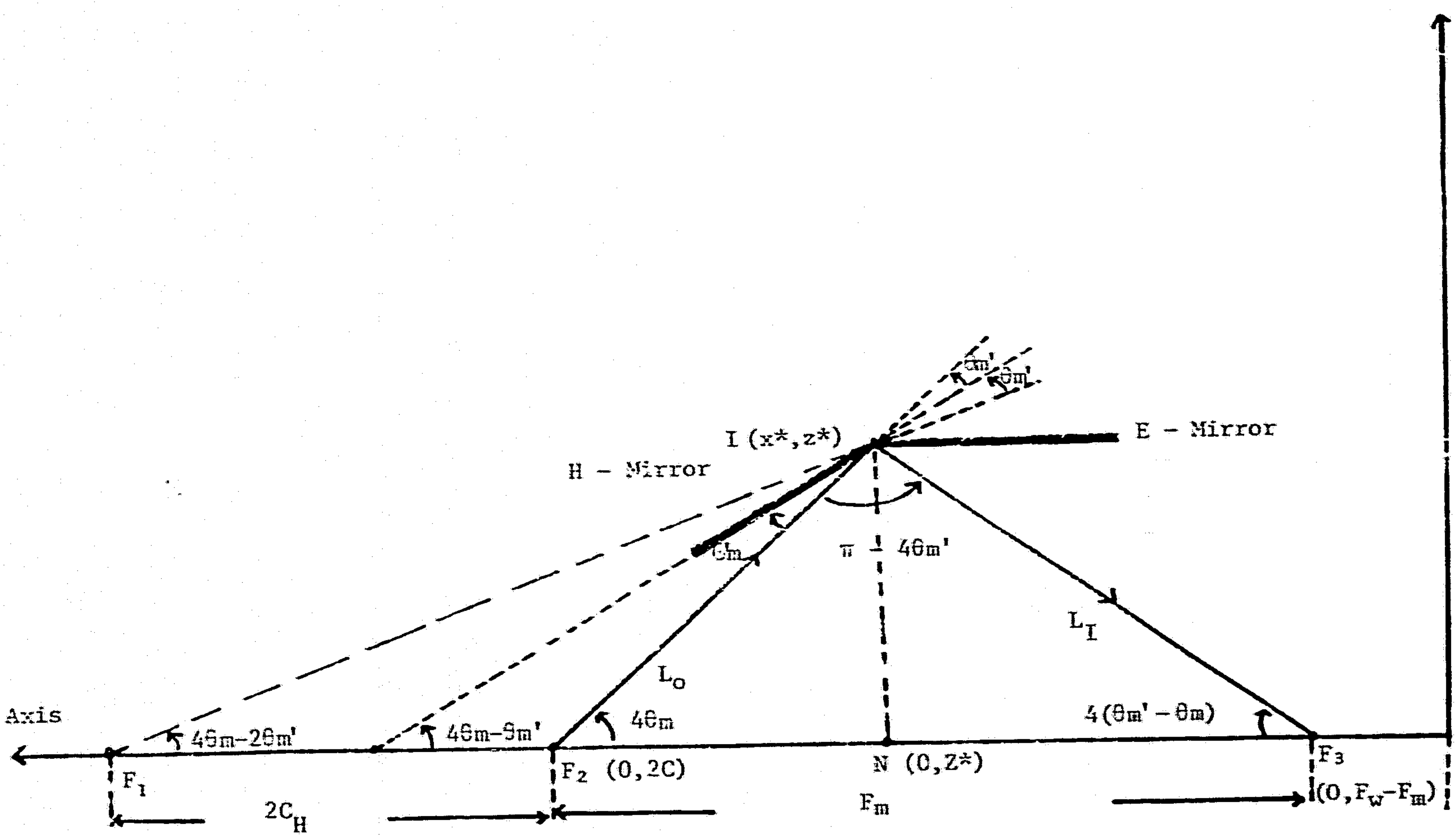

Figure A-2. Ray Tracing Through The X-Ray Microscope.

rays from the H-mirror makes θ_m' angle with the E-mirror and the extension of this ray, passes through F_1, one can derive the following relations:

Considering the ΔF_2IF_3, and using the law of sines gives

$$\frac{L_I}{\sin(4\theta_m)} = \frac{L_o}{\sin 4(\theta_m' - \theta_m)}$$

Therefore, from Eq.A-3

$$M = \frac{L_I}{L_o} = \frac{\sin(4\theta_m)}{\sin[4(\theta_m' - \theta_m)]}$$

or

$$\sin[4(\theta_m' - \theta_m)] = \sin(4\theta_m)/M \qquad \text{(A-4)}$$

$$\theta_m' = \theta_m + \frac{1}{4}\sin^{-1}\left[\frac{\sin(4\theta_m)}{M}\right].$$

Equation A-4 gives θ_m' as function of M.

Using the law of sines to the ΔF_2IF_3 gives

$$\frac{L_I}{\sin(4\theta_m)} = \frac{F_m}{\sin(\pi - 4\theta_m')} = \frac{F_m}{\sin(4\theta_m')}$$

ORIGINAL PAGE
OF POOR QUALITY

$$L_I = F_m \frac{\sin(4\theta_m)}{\sin(4\theta_m')} \quad . \tag{A-5}$$

The intersection point coordinates can be written as

$$X^* = L_I \sin [4(\theta_m'-\theta_m)].$$

Using Eq.A-5, then

$$X^* = F_m \frac{\sin[4\theta_m]}{\sin[4\theta_m']} \sin [4(\theta_m'-\theta_m)]$$

Using Eq.A-4 gives

$$X^* = \frac{F_m}{M} \frac{\sin^2(4\theta_m)}{\sin(4\theta_m')} \quad . \tag{A-6}$$

Equation A-6 gives X*, radius at intersection point of the microscope, as a function of magnification M where F_m, θ_m are fixed.

Using the law of sines for ΔF_2IF_3 gives

$$\frac{L_o}{\sin[4(\theta_m'-\theta_m)]} = \frac{F_m}{\sin(\pi-4\theta_m')} = \frac{F_m}{\sin(4\theta_m')}$$

Using Eq.A-4

$$L_o = \frac{F_m}{M} \frac{\sin(4\theta_m)}{\sin(4\theta_m')} \qquad \text{(A-7)}$$

The Z coordinates of the intersection point of H and E mirror can be written as

$$\begin{aligned} Z^* &= F_w - L_o \cos(4\theta_m) \\ &= F_w - \frac{F_m}{2M} \frac{\sin(8\theta_m)}{\sin(4\theta_m')} \end{aligned} \qquad \text{(A-8)}$$

where Eq.A-7 has been used.

From the properties of the ellipsoid, one can write

$$\overline{F_1 I} + \overline{I F_3} = 2A_E \qquad \text{(A-9)}$$

where $\overline{IF_3} = L_I$, which is given by Eq.A-5. Since the extension of the reflected ray from the H-mirror passes through F_1, then the angle $\angle F_2 F_1 I = 4\theta_m - 2\theta_m'$.

Therefore,

$$\overline{F_1 I} = \frac{X^*}{\sin(4\theta_m - 2\theta_m')} = \frac{L_o \sin(4\theta_m)}{\sin(4\theta_m - 2\theta_m')} . \qquad \text{(A-10)}$$

Then Eq.A-9 becomes

$$A_E = \frac{1}{2} \left[\frac{L_o \sin(4\theta_m)}{\sin(4\theta_m - 2\theta_m')} + L_I \right] .$$

Using Eqs.A-4,5,7,

$$A_E = \frac{F_m}{2} \frac{\sin(4\theta_m)}{\sin(4\theta_m')} \left[\frac{\sin(4\theta_m)}{M \sin(4\theta_m - 2\theta_m')} + 1 \right] . \qquad \text{(A-11)}$$

From the properties of an ellipse

$$\overline{F_1 F_3} = 2C_E . \qquad \text{(A-12)}$$

Considering the Δ $F_1 F_3 I$, one can write

$$\frac{2C_E}{\sin(2\theta_m')} = \frac{L_I}{\sin(4\theta_m - 2\theta_m')} .$$

or

$$C_E = \frac{L_I}{2} \; \frac{\sin\,(2\theta_m')}{\sin\,(4\theta_m - 2\;{}_m')} \quad .$$

Using Eq.A-5 gives

$$C_E = \frac{F_m}{2} \; \frac{\sin\,(4\theta_m)\;\;\sin\,(2\theta_m')}{\sin\,(4\theta_m')\;\;\sin\,(4\theta_m - 2\theta_m')} \tag{A-13}$$

Also,

$$B_E{}^2 = A_E{}^2 - C_E{}^2.$$

The H-mirror parameters are derived as the following from the properties of the hyperboloid. One can write

$$\overline{F_1F_2} = 2C_H \; . \tag{A-14}$$

Using the law of sines for the ΔF_1F_2I gives

$$\frac{\overline{F_1F_2}}{\sin\,(2\theta_m')} = \frac{L_o}{\sin\,(4\theta_m - 2\theta_m')}$$

ORIGINAL PAGE IS OF POOR QUALITY

so

$$C_H = \frac{1}{2} L_o \frac{\sin(2\theta_m')}{\sin(4\theta_m - 2\theta_m')}.$$

Using Eq.A-7 gives

$$C_H = \frac{F_m}{2M} \frac{\sin(4\theta_m)}{\sin(4\theta_m')} \frac{\sin(2\theta_m')}{\sin(4\theta_m - 2\theta_m')}. \tag{A-15}$$

Using the properties of the hyperbola gives

$$\overline{F_1 I} - \overline{F_2 I} = 2A_H \tag{A-16}$$

where $\overline{F_2 I} = L_o$ and $\overline{F_1 I}$ is given by Eq.A-10.

Then,

$$A_H = \frac{F_m}{2M} \frac{\sin(4\theta_m)}{\sin(4\theta_m')} \left\{ \frac{\sin(4\theta_m)}{\sin(4\theta_m - 2\theta_m')} - 1 \right\}. \tag{A-17}$$

Also,

$$B_H^2 = C_H^2 - A_H^2.$$

SUMMARY:

H-mirror Parameters:

$$\frac{(Z-Z_{oH})^2}{A_H^2} - \frac{X^2}{B_H^2} = 1$$

$$Z_{oH} = F_w + C_H$$

$$C_H = \frac{F_m}{2M} \frac{\sin(4\theta_m)}{\sin(4\theta_m')} \frac{\sin(2\theta_m')}{\sin(4\theta_m - 2\theta_m')}$$

$$A_H = \frac{F_m}{2M} \frac{\sin(4\theta_m)}{\sin(4\theta_m')} \left[\frac{\sin(4\theta_m)}{\sin(4\theta_m - 2\theta_m')} - 1 \right]$$

$$B_H^2 = C_H^2 - A_H^2$$

$$\theta_m' = \theta_m + \frac{1}{4} \sin^{-1} \left[\frac{\sin(4\theta_m)}{M} \right]$$

ORIGINAL PAGE IS
OF POOR QUALITY

E-mirror Parameters:

$$\frac{(Z-Z_{oE})^2}{A_E^2} + \frac{X^2}{B_E^2} = 1$$

$$Z_{oE} = F_w - F_m + C_E$$

$$A_E = \frac{F_m}{2} \frac{\sin(4\theta_m)}{\sin(4\theta_m')} \left[1 + \frac{\sin(4\theta_m)}{M \sin(4\theta_m - 2\theta_m')} \right]$$

$$C_E = \frac{F_m}{2} \frac{\sin(4\theta_m)}{\sin(4\theta_m')} \frac{\sin(2\theta_m')}{\sin(4\theta_m - 2\theta_m')}$$

$$B_E^2 = A_E^2 - C_E^2$$

Mid-Point Parameters:

$$L_I = F_m \frac{\sin(4\theta_m)}{\sin(4\theta_m')} \quad ; \quad L_o = \frac{F_m}{M} \frac{\sin(4\theta_m)}{\sin(4\theta_m')}$$

$$X^* = \frac{F_m}{M} \frac{\sin^2(4\theta_m)}{\sin(4\theta_m')}$$

$$Z^* = F_w - \frac{F_m}{2M} \frac{\sin(8\theta_m)}{\sin(4\theta_m')}$$

REFERENCES

1. J.D.Mangus, J.H.Underwood, APPLIED OPTICS 8.1, 95 (1969).

2. J.W.Forman,Jr., G.W.Hunt, E.K.Lawson, "Analytical Study of The Imaging Characteristics of The Goddard ATM X-Ray Telescope," Technical publication #SP-505-0270, Space Support Division, Sperry Rand Corporation, Huntsville, Alabama, September, 1969.

3. H.Wolter, Ann. Phys 10, 94 (1952).

4. J.K.Silk, Annals of NY Academy of Sciences 342, 116 (1980).

5. OPTICAL DESIGN, MILITARY STANDARDIZATION HANDBOOK, #MIL-HDBK-141, U.S. Government Printing Office, WASHINGTON, D.C., 1962.

6. O.N.Stavroudis, "The Optics of Rays, Wavefronts, and Caustics" (Academic Press, New York, 1972).

7. R.J.Gagnon, JOSA 58.8 (1968).

8. R.C.Chase, J.K.Silk, APPLIED OPTICS 14.9, 2096 (1975).

9. M.J.Boyles, H.G.Ahlstrom, Rev. Sci. Instrum. 49.6, 746 (1978).

10. A.Franks, et.al., Annals of NY Academy of Sciences 342, 167 (1980).

11. J.M.Davis, A.S.Krieger, J.K.Silk, R.C.Chase, Proc. SPIE 184, 96 (1979).

12. D.L.Shealy, "Analysis of NOAA-MSFC GOES X-Ray Telescope," Final Report under contract #H-34373B, Marshall Space Flight Center, Huntsville, Alabama (1979).

13. W.Werner, APPLIED OPTICS 16.3, 764 (1977).

14. D.G.Burkhard, D.L.Shealy, APPLIED OPTICS 20.5, 897 (1981).

15. C.E.Winkler, D.Korsch, NASA Technical Paper #1088 (1977). APPLIED OPTICS 16.9, 2464 (1977).

16. H.Wolter, OPTICA ACTA 18.6, 425 (1971).

17. R.Giacconi, W.P.Reidy, T.Zehnpfennig, J.C.Lindsay, and W.S.Muney, J.ASTROPHYS 142, 1274 (1965).

18. J.H.Underwood, Am. Scientist, 66.4, 476 (1978).

19. R.Giacconi, et.al., J.ASTROPHYS 230, 540 (79).

20. M.V.Zombeck, C.C.Wyman, M.C.Weisskopf, Opt. Eng. 21.1, 63 (1982).

21. M.V.Zombeck, Proc. AIP Topical Conference on Low Energy X-Ray Diagnostics, Monterey, California, June 8-10, 1981.

22. R.C.Chase, J.M.Davis, A.S.Krieger, J.H.Underwood, Proc. SPIE 316, 74 (1981).

23. J.M.Davis, "STARPROBE: An Interim Report," contract #955928, Jet Propulsion Laboratory, Pasadena, California, July 2, 1981.

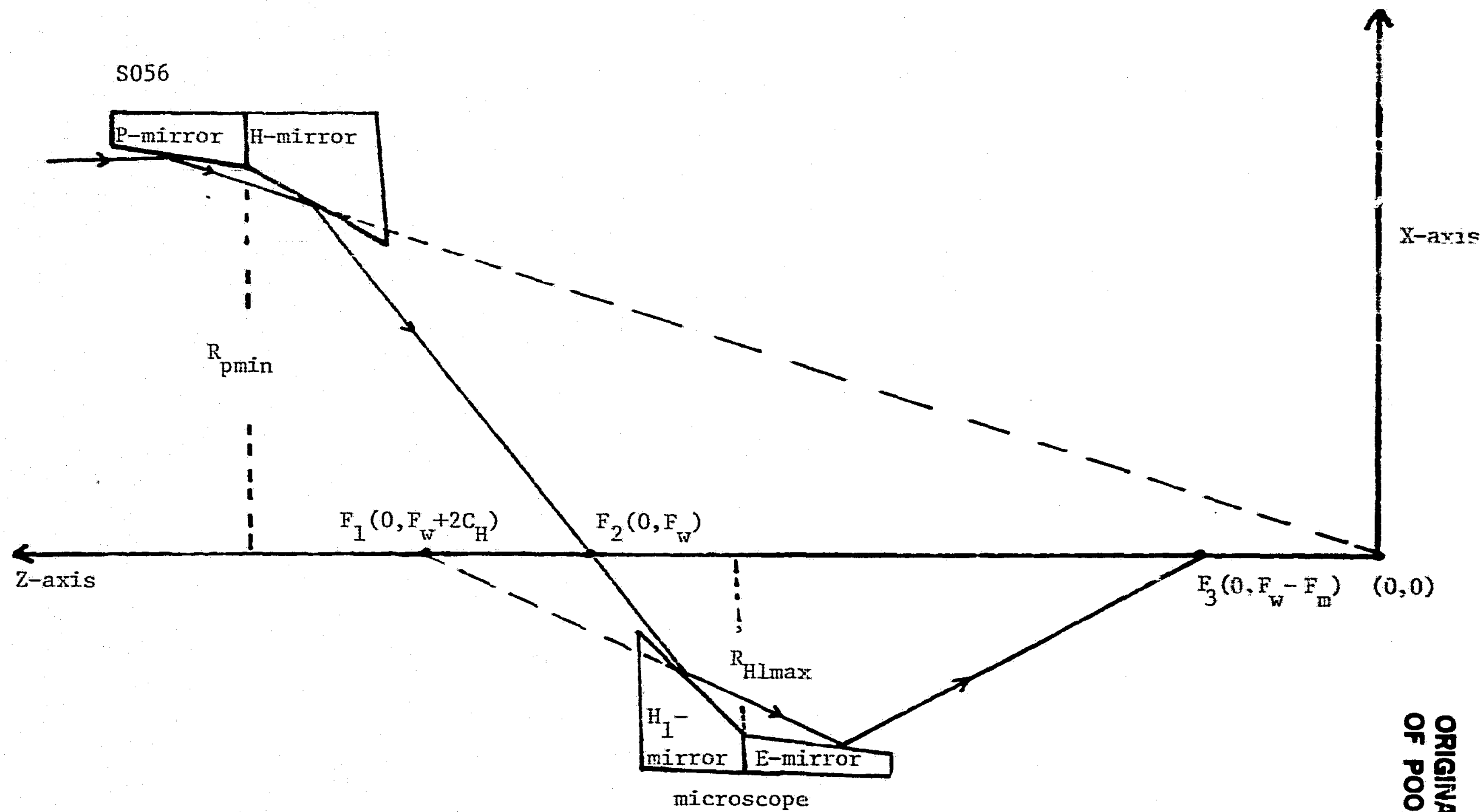

Fig. 1: Symbolic View of the ERXRT System.

ORIGINAL PAGE IS
OF POOR QUALITY

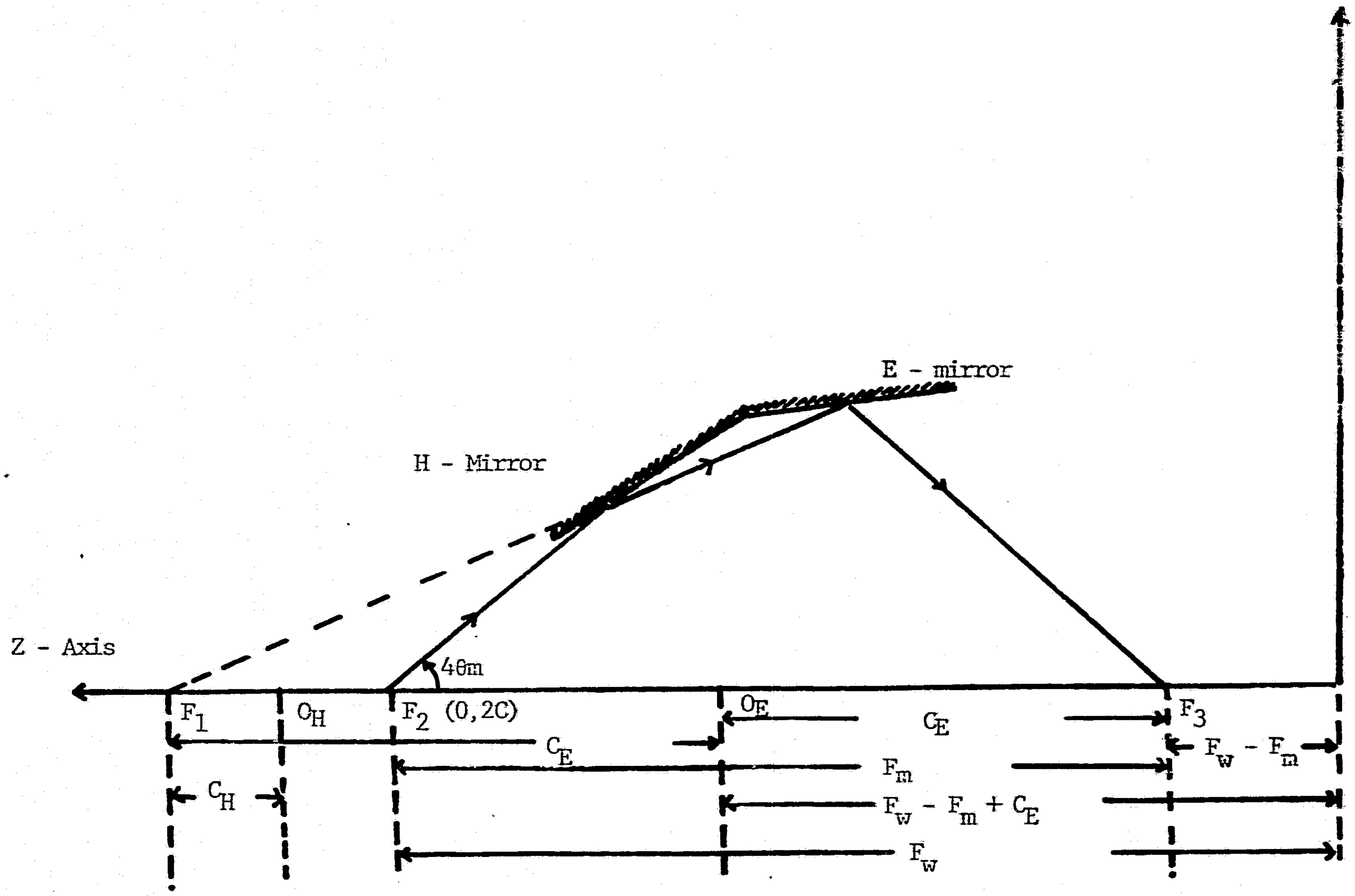

FIGURE 2: Cross Sectional Diagram of X-Ray Microscope

**ORIGINAL PAGE IS
OF POOR QUALITY**

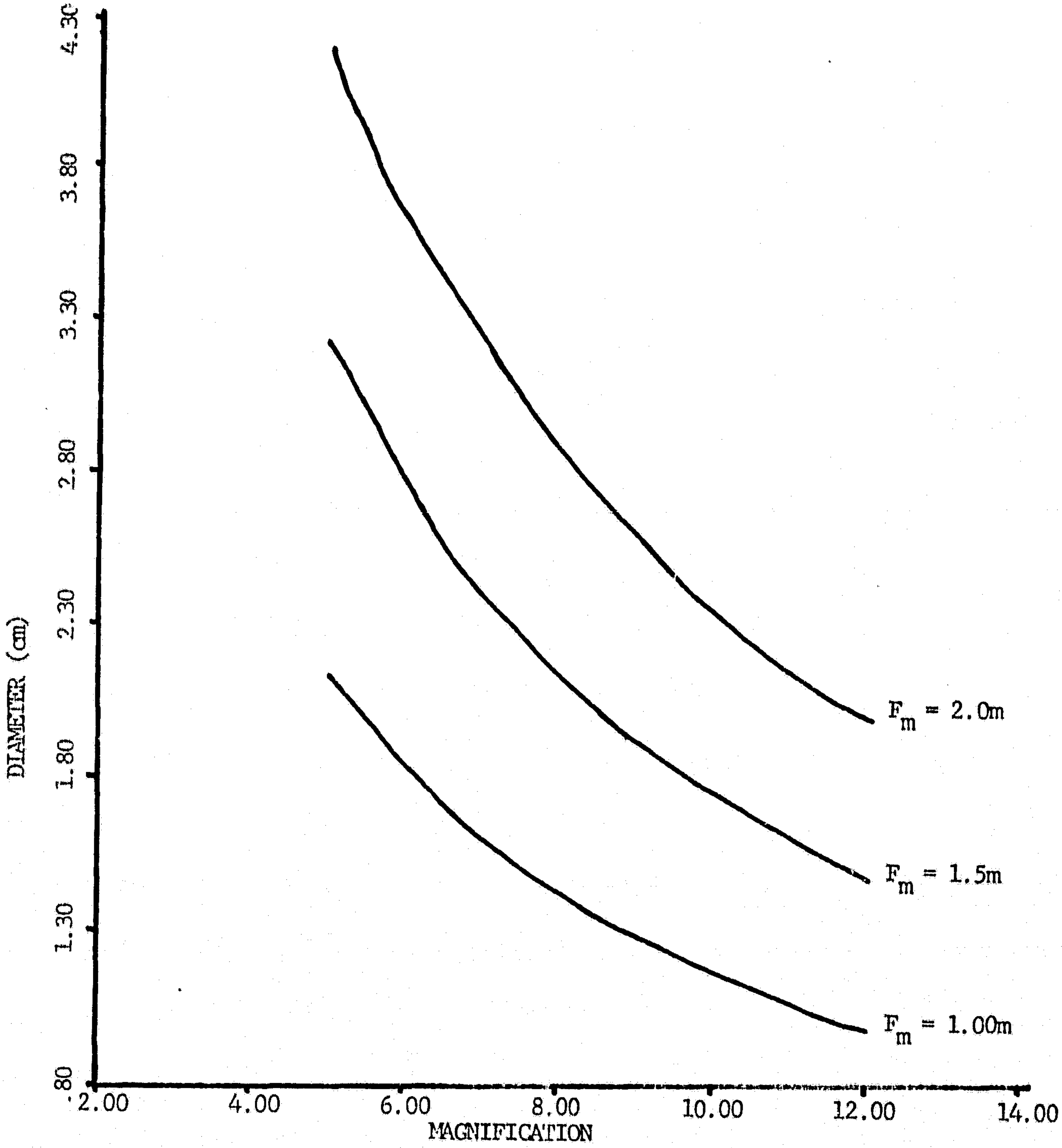

FIG. 3: Microscope intersection diameter versus the magnification.

ORIGINAL PAGE IS
OF POOR QUALITY

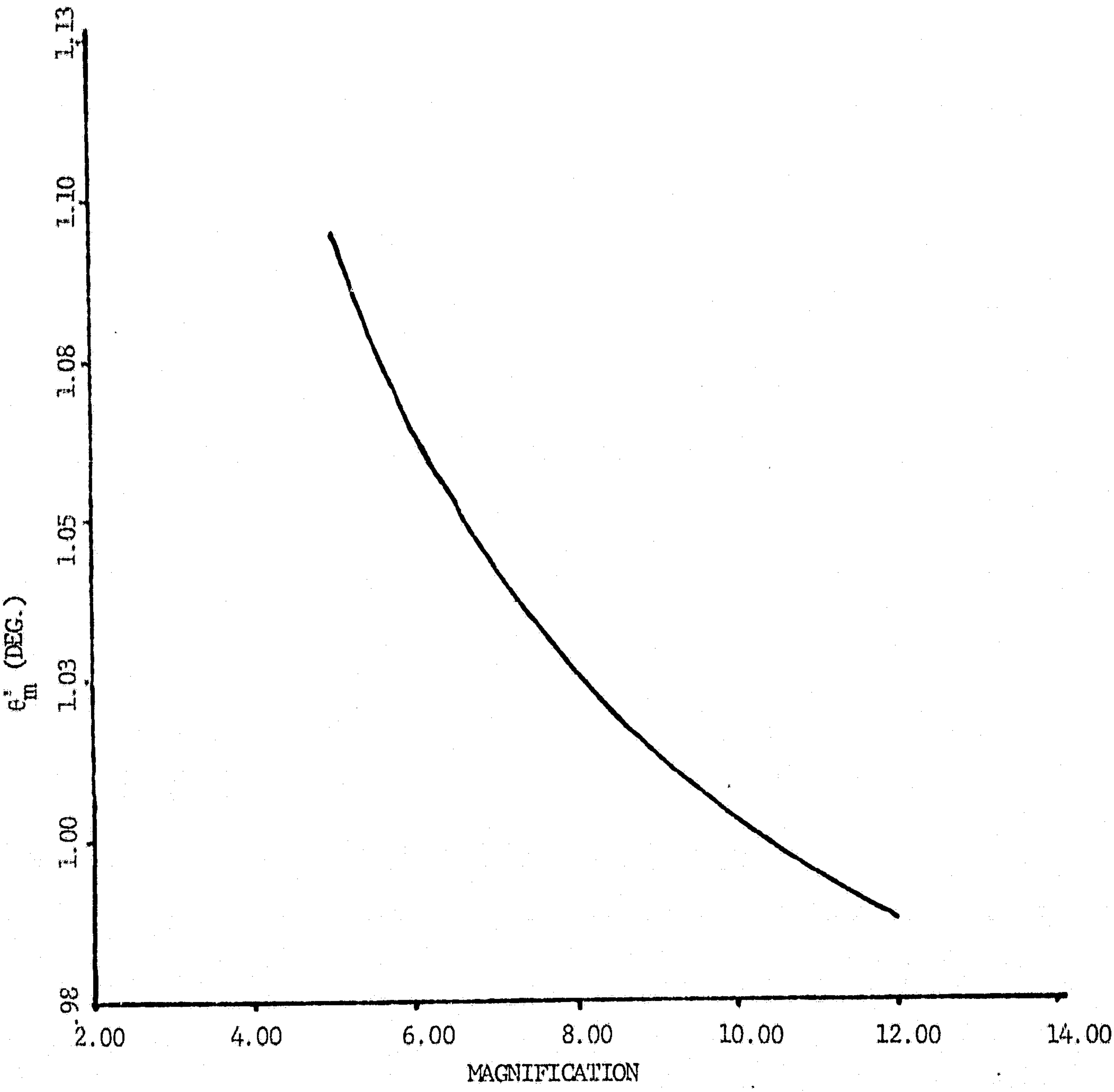

FIG. 4: Glancing angle at the intersection point of microscope versus the magnification for $\alpha = 0$.

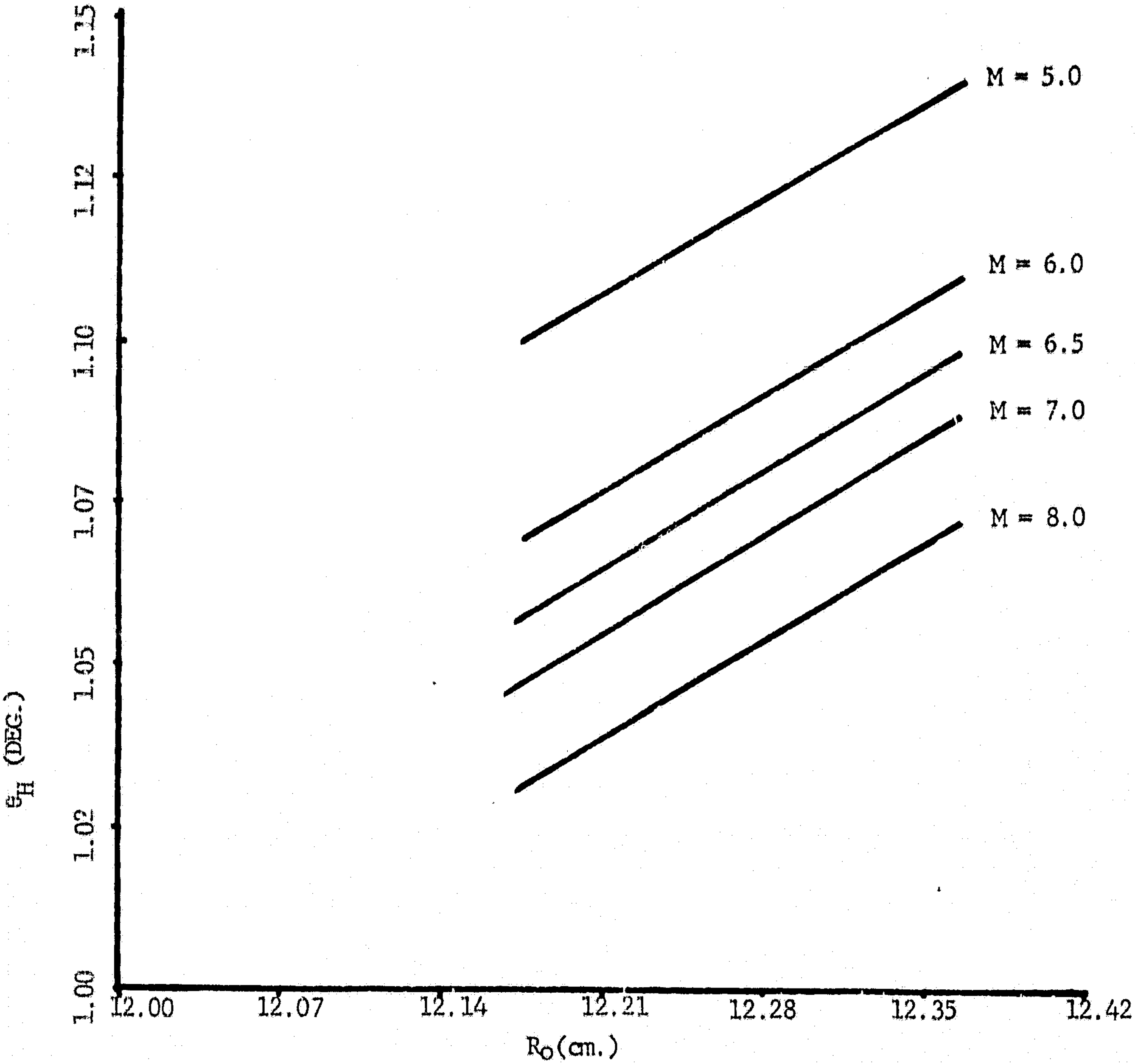

FIG. 5: Glancing angle over the microscope hyperboloid surface versus the entrance pupil radius, R_0 for $\alpha = 0$.

ORIGINAL PAGE IS
OF POOR QUALITY

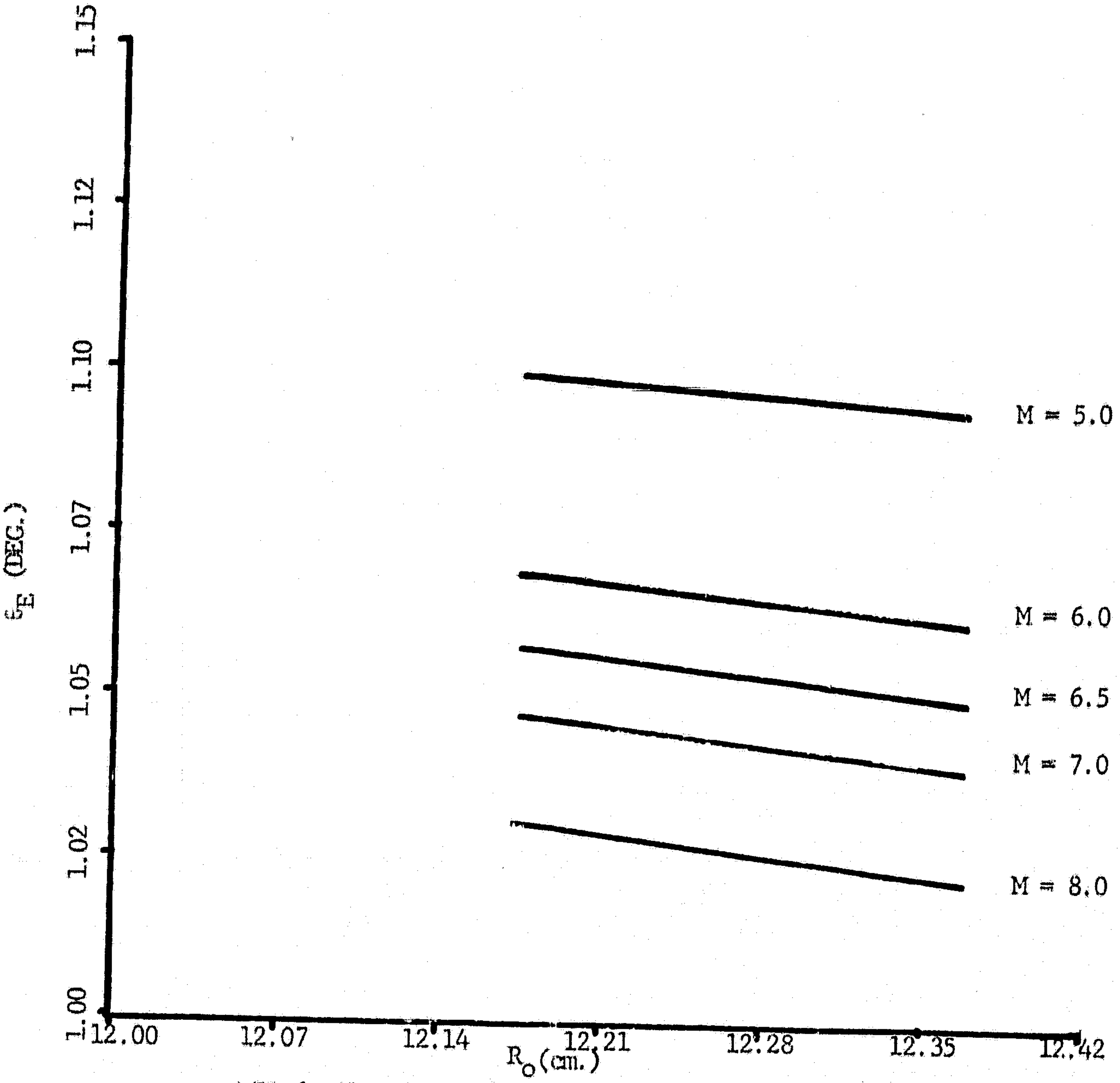

FIG. 6: Glancing angle over the microscope ellipsoid surface versus the entrance pupil radius, R_o, for $\alpha = 0$.

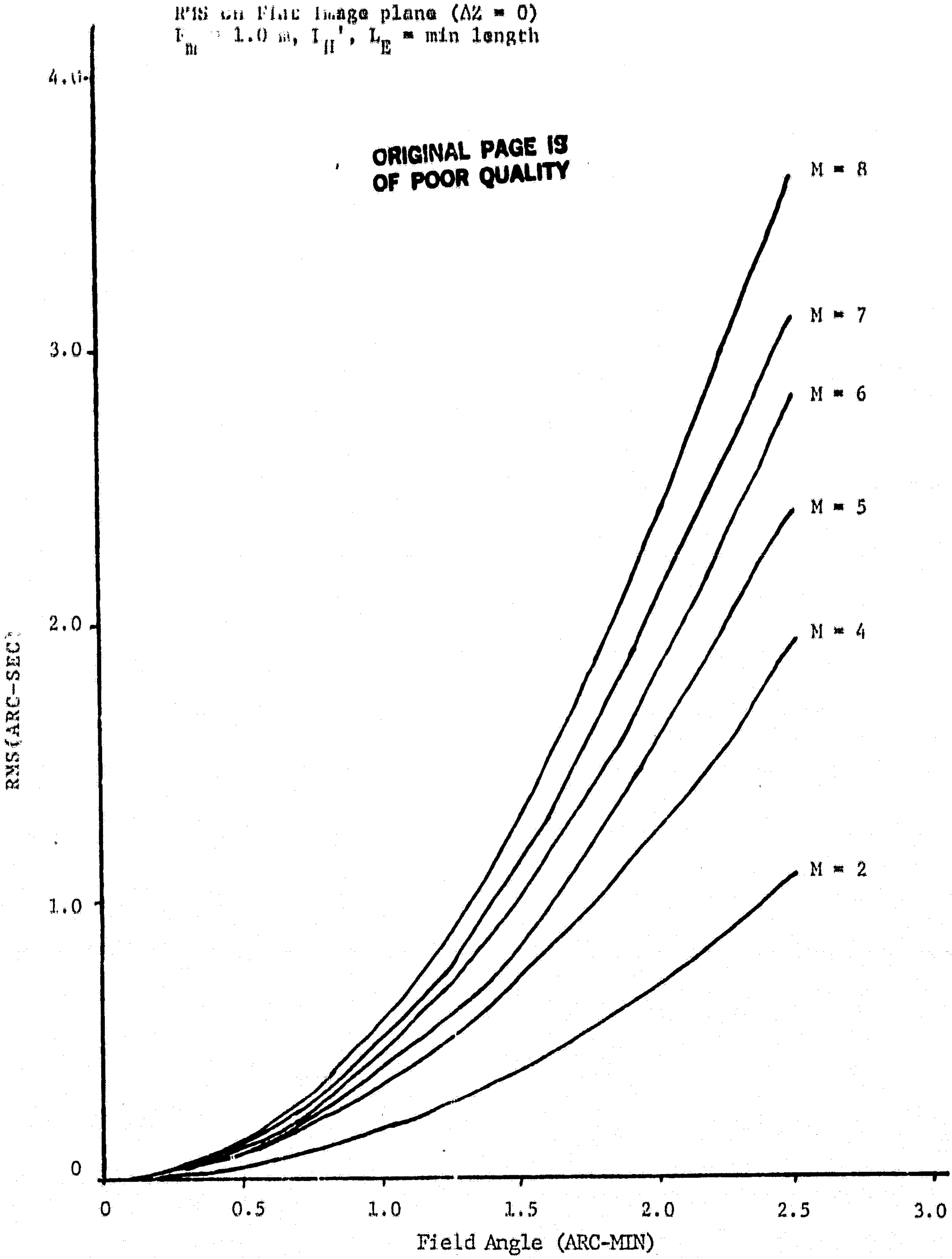

FIG. 7: RMS Spot Radius vs Field Angle

ORIGINAL PAGE IS
OF POOR QUALITY

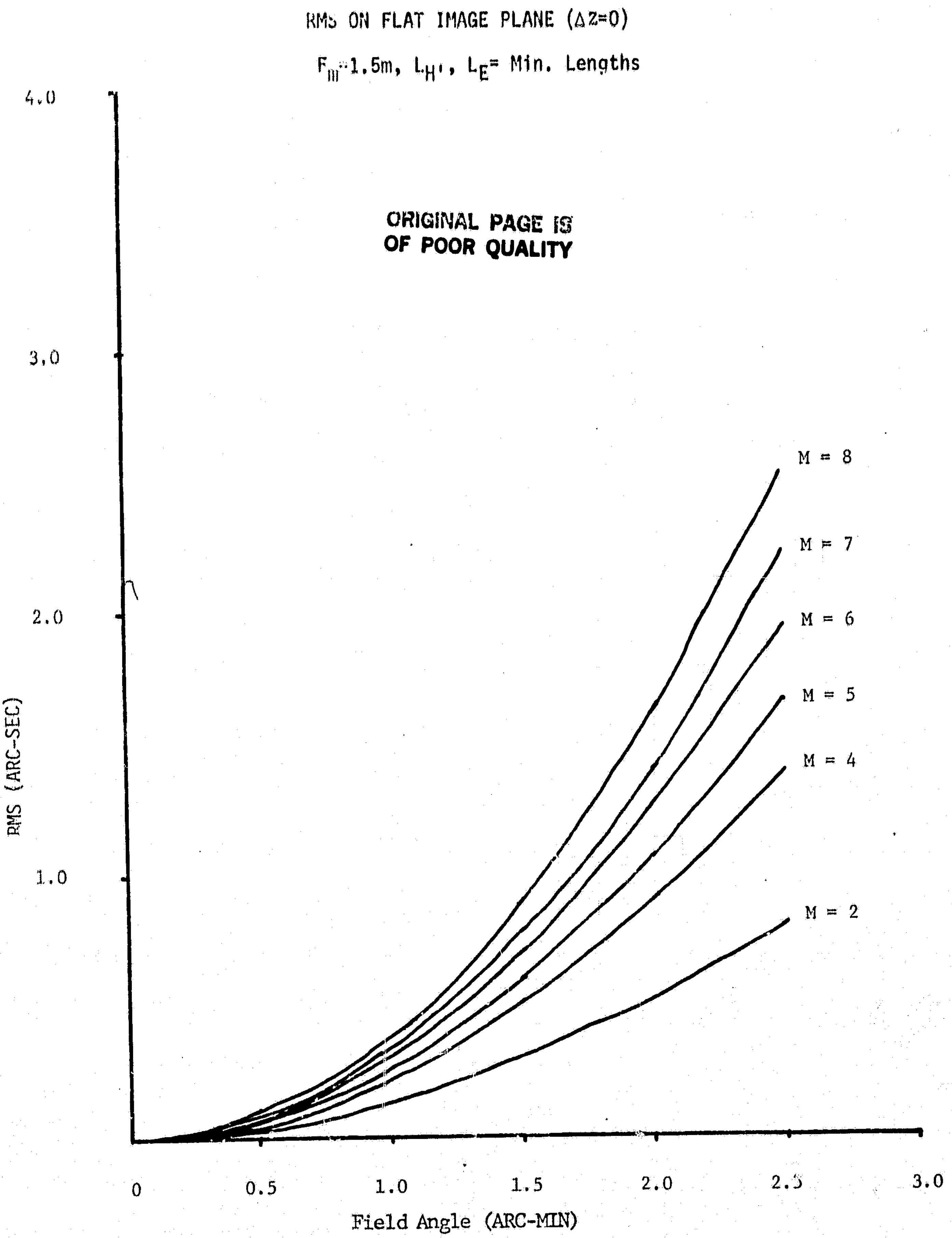

FIG. 8: RMS Spot Radius vs Field Angle

ORIGINAL PAGE IS
OF POOR QUALITY

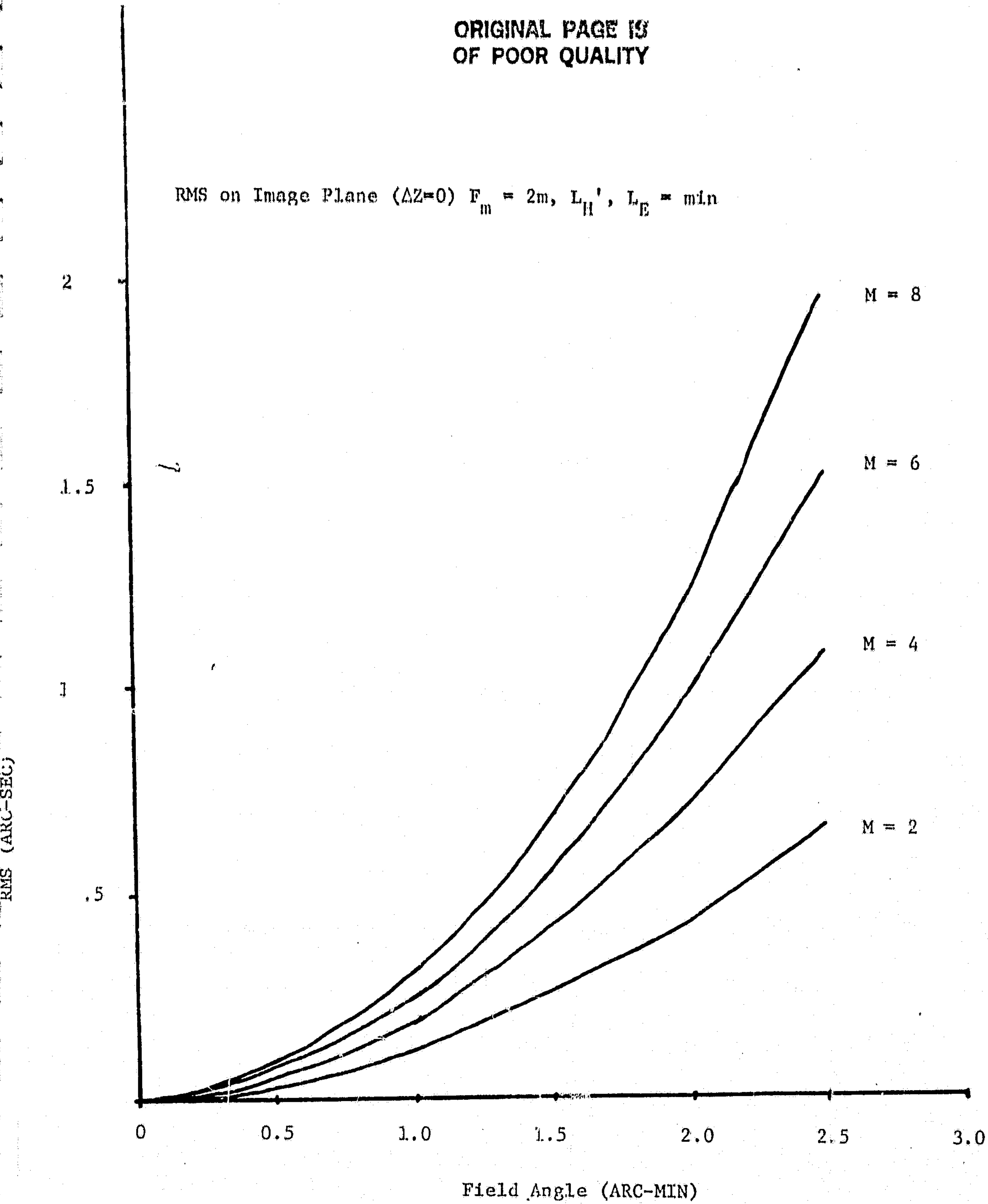

Fig. 9: RMS Spot Radius vs Out Field Angle

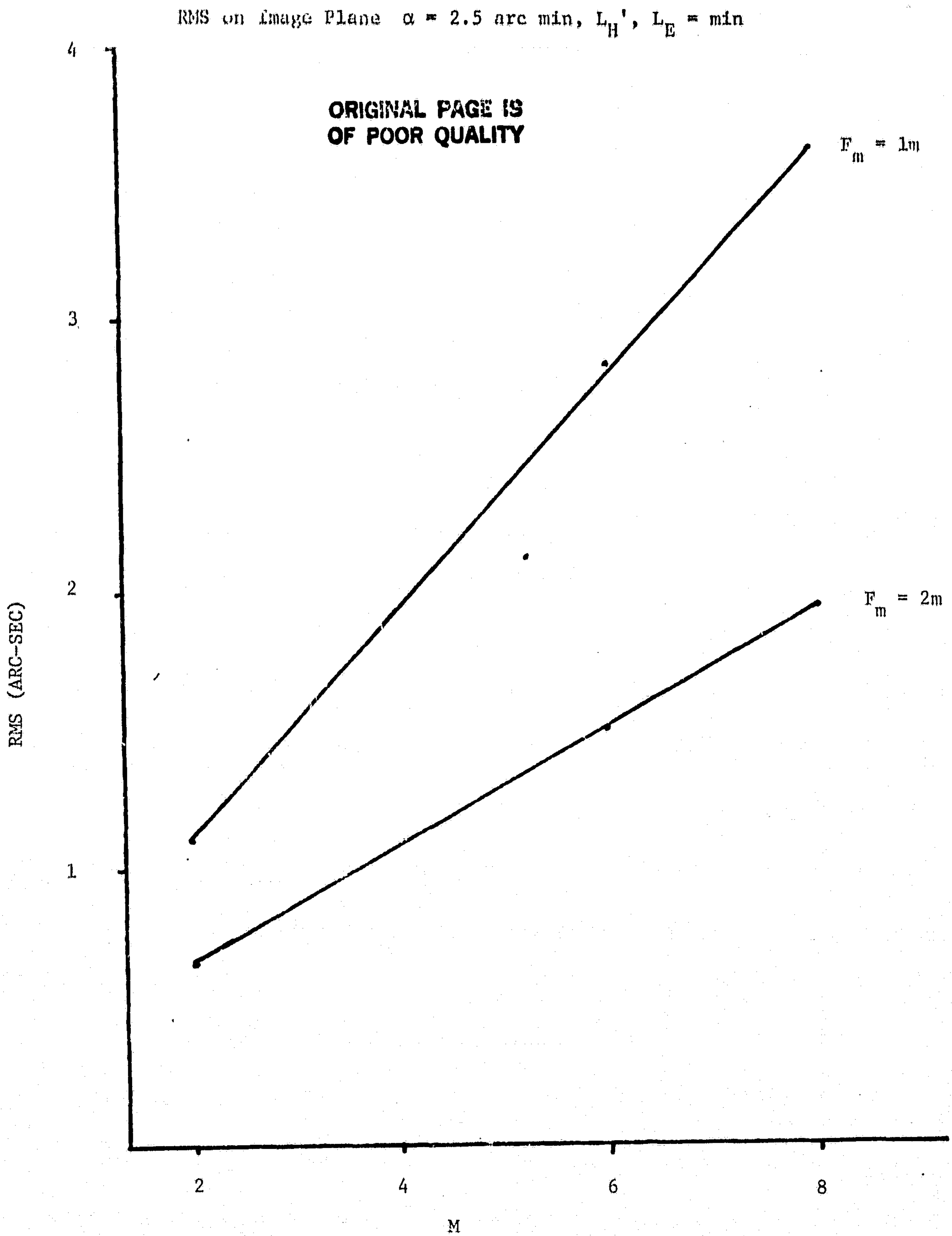

Fig. 10: RMS Spot Radius vs Magnification

ORIGINAL PAGE IS
OF POOR QUALITY

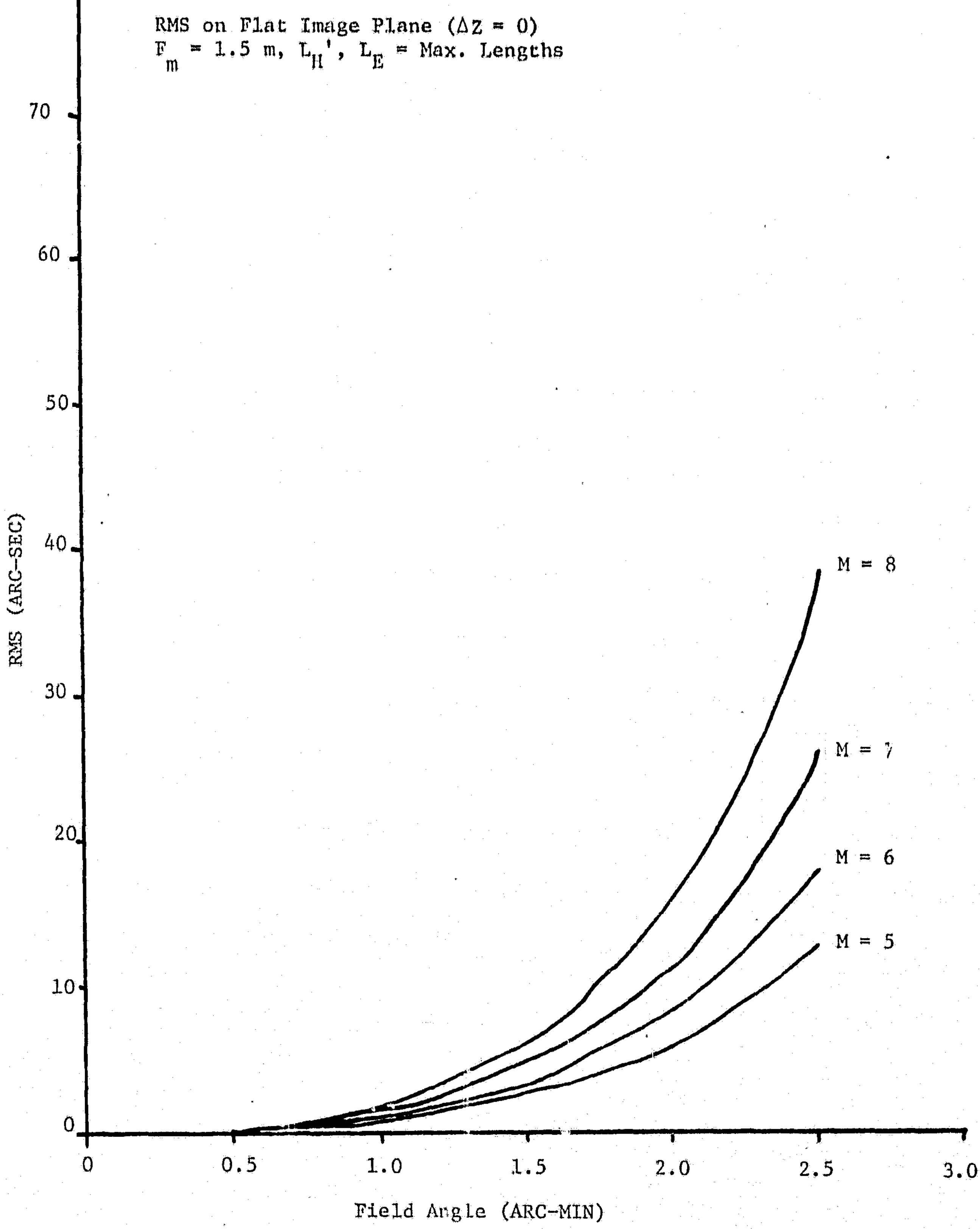

Fig. 11: RMS Spot Radius vs Field Angle

ORIGINAL PAGE IS
OF POOR QUALITY

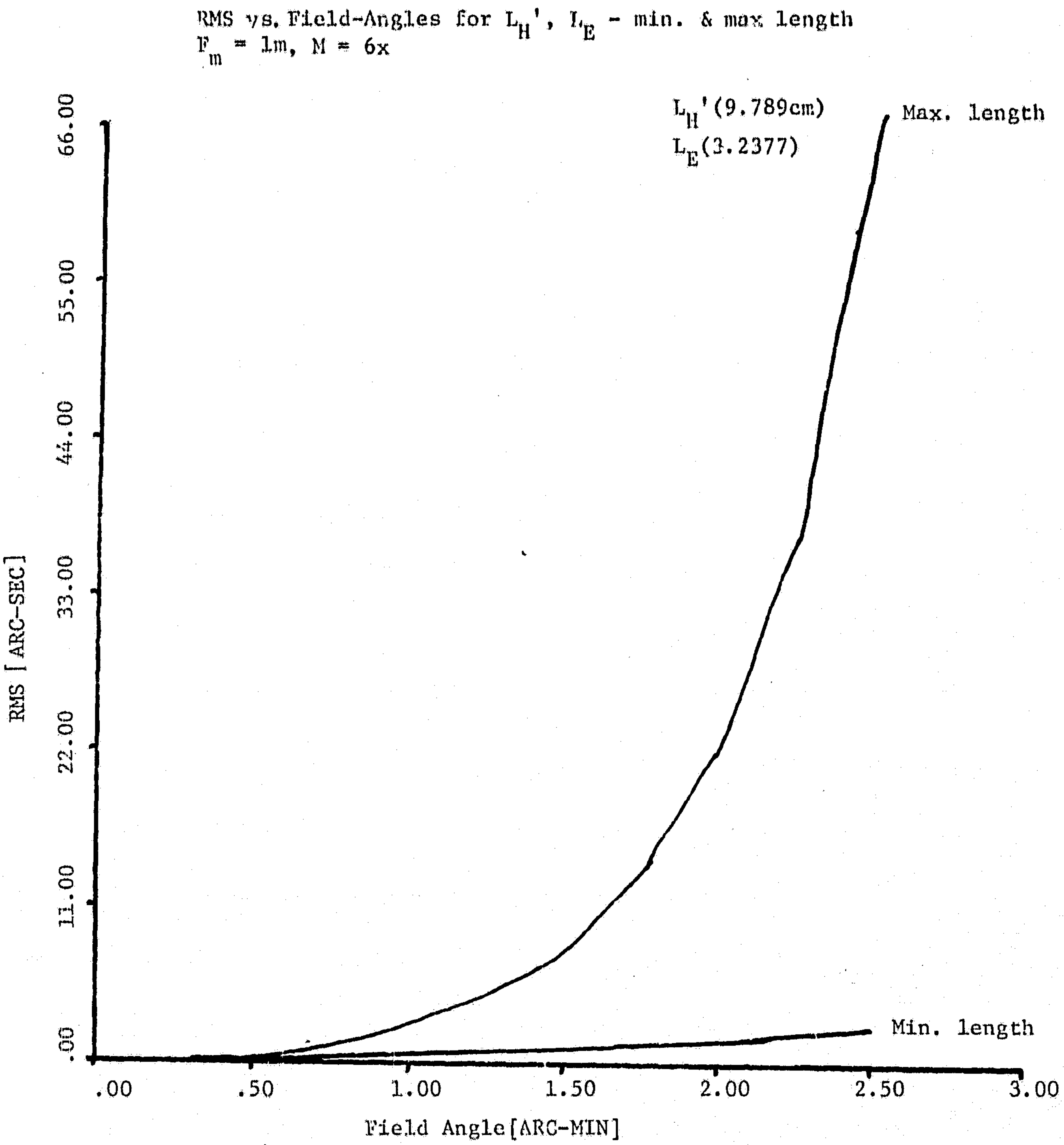

Fig. 12: RMS Spot Radius vs Field Angle

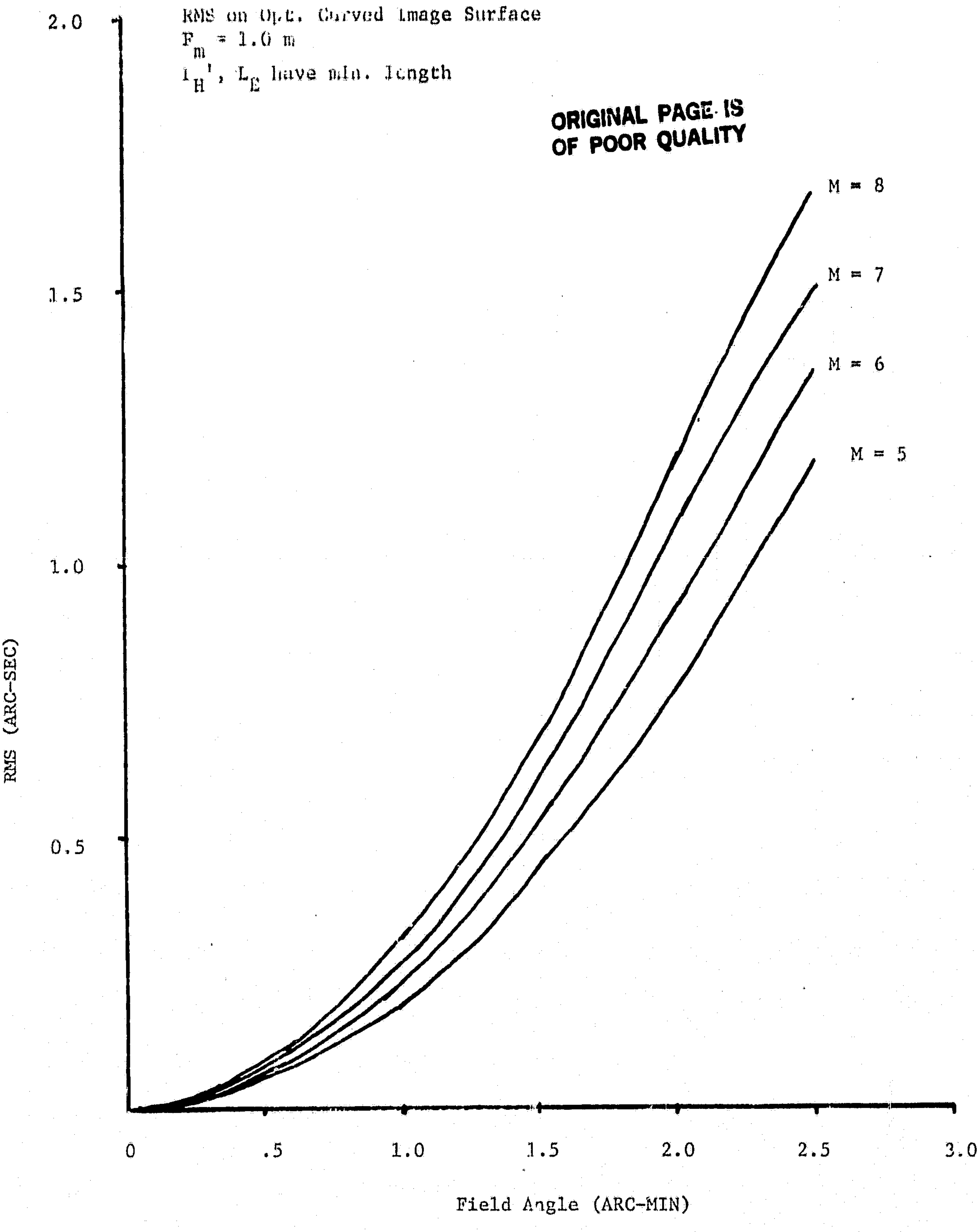

Fig. 13: RMS Spot Radius vs Field Angle

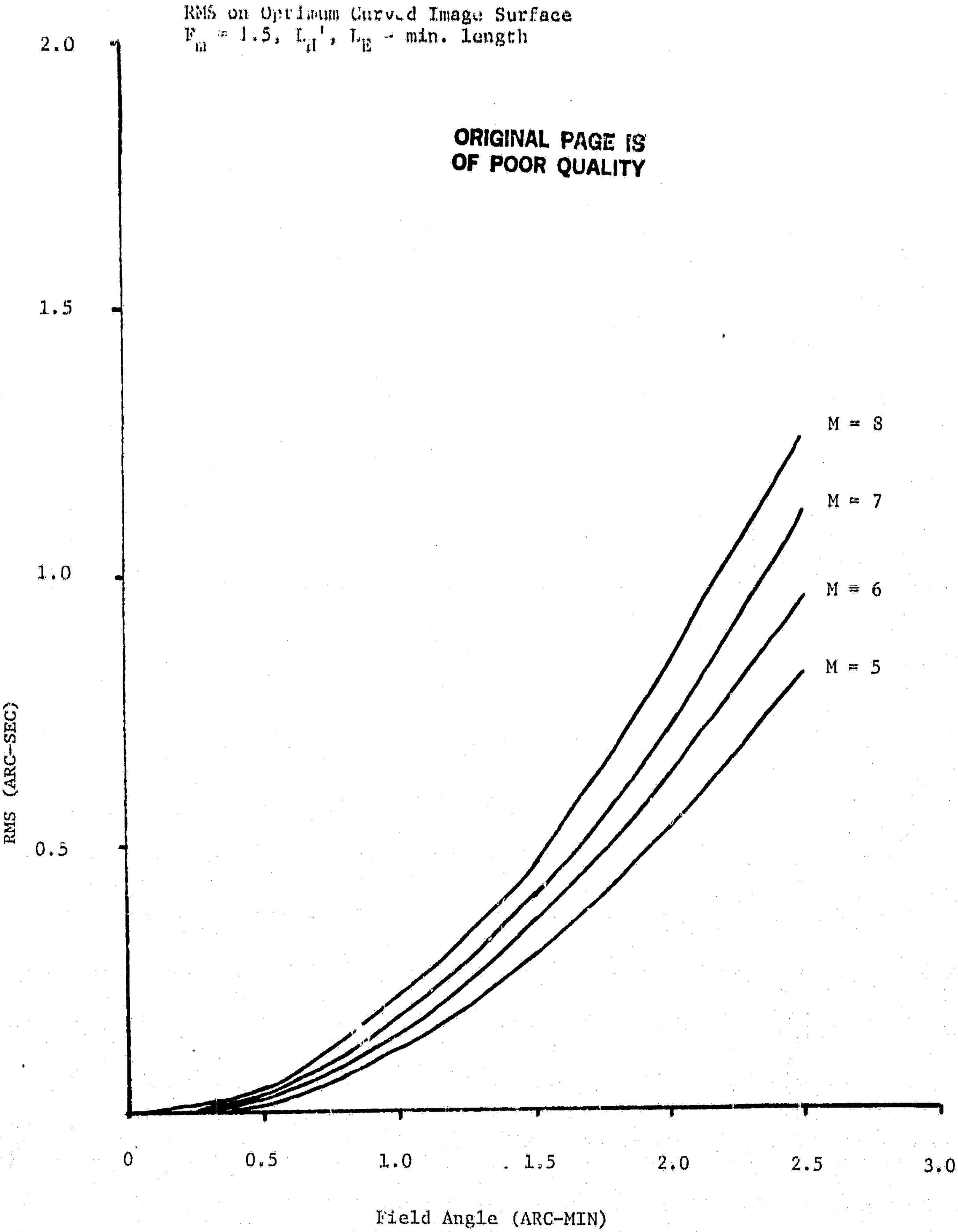

Fig. 14: RMS Spot Radius vs Field Angle

ORIGINAL PAGE IS
OF POOR QUALITY

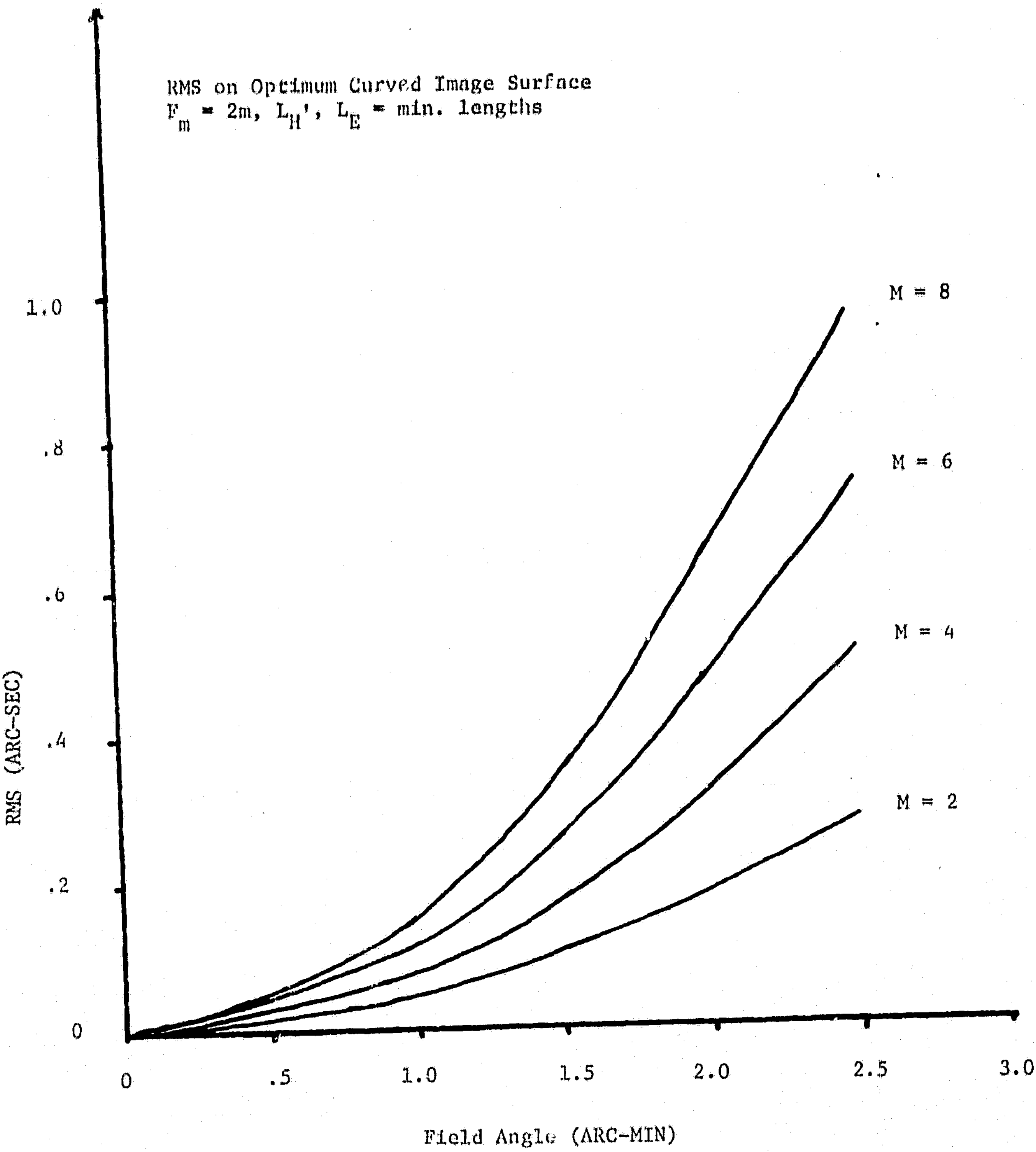

Fig. 15. RMS Spot Radius vs Field Angle

ORIGINAL PAGE IS
OF POOR QUALITY

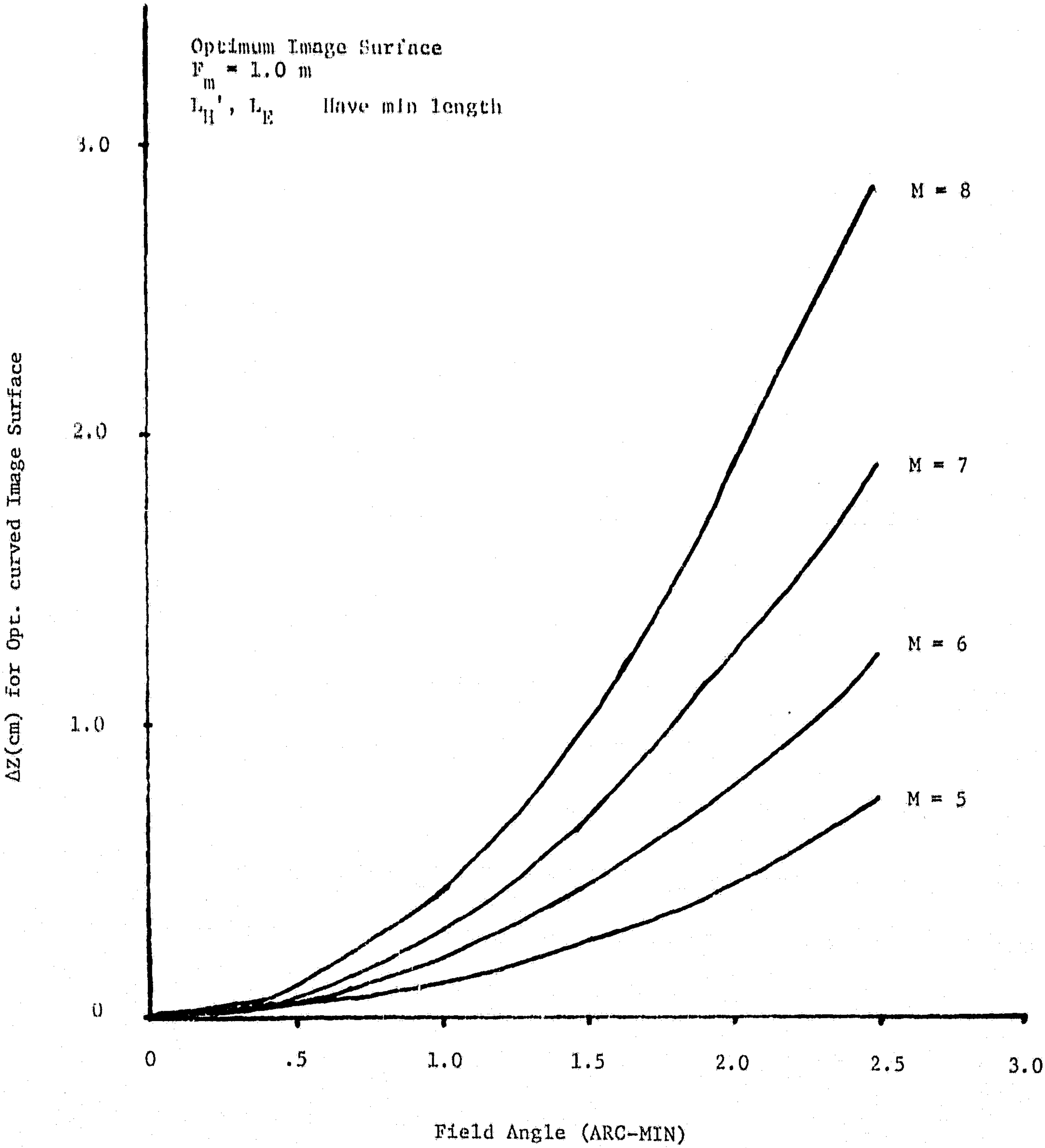

Fig. 16: Optimum Image Surface

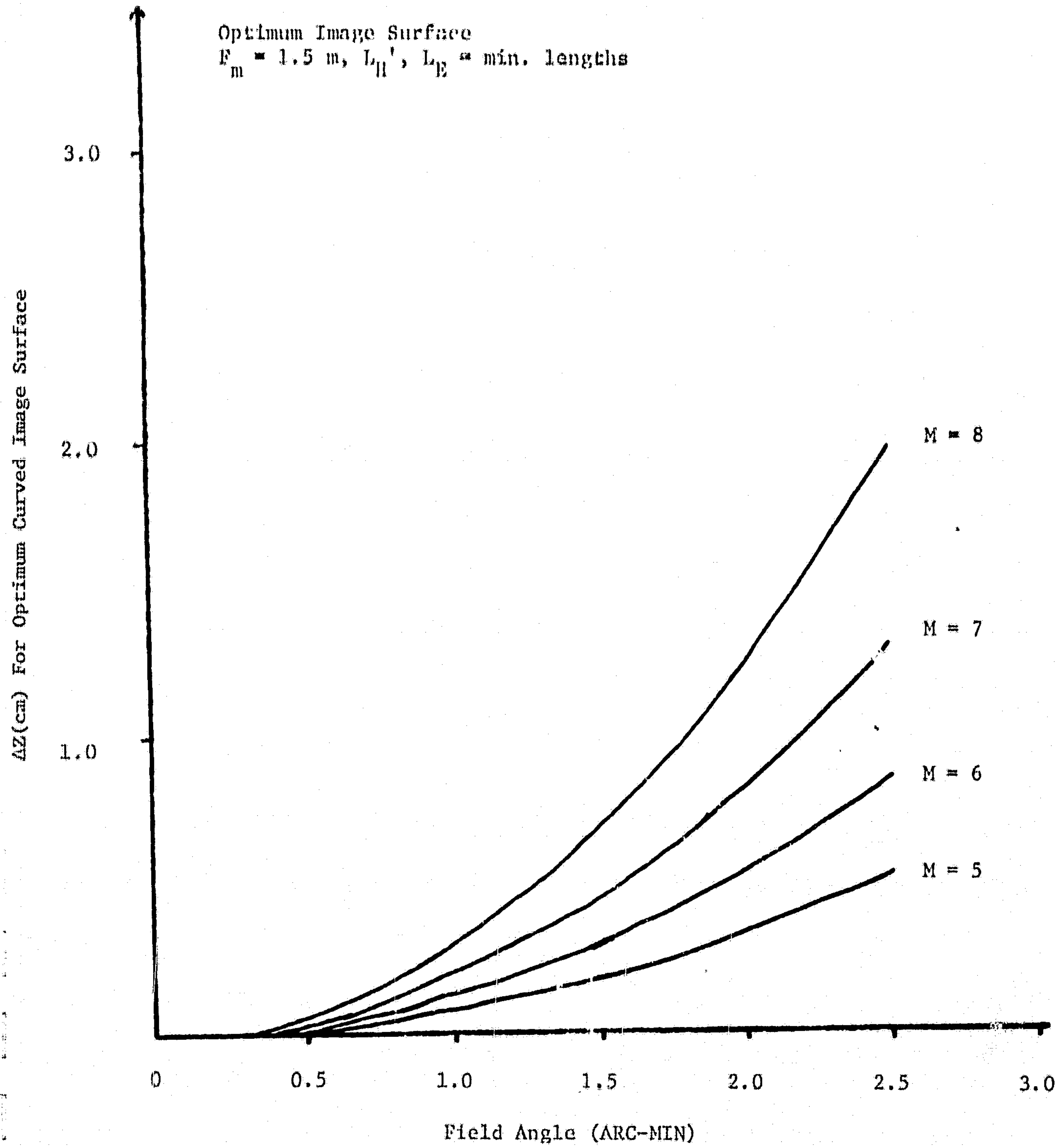

Fig. 17: Optimum Image Surface

ORIGINAL PAGE IS OF POOR QUALITY

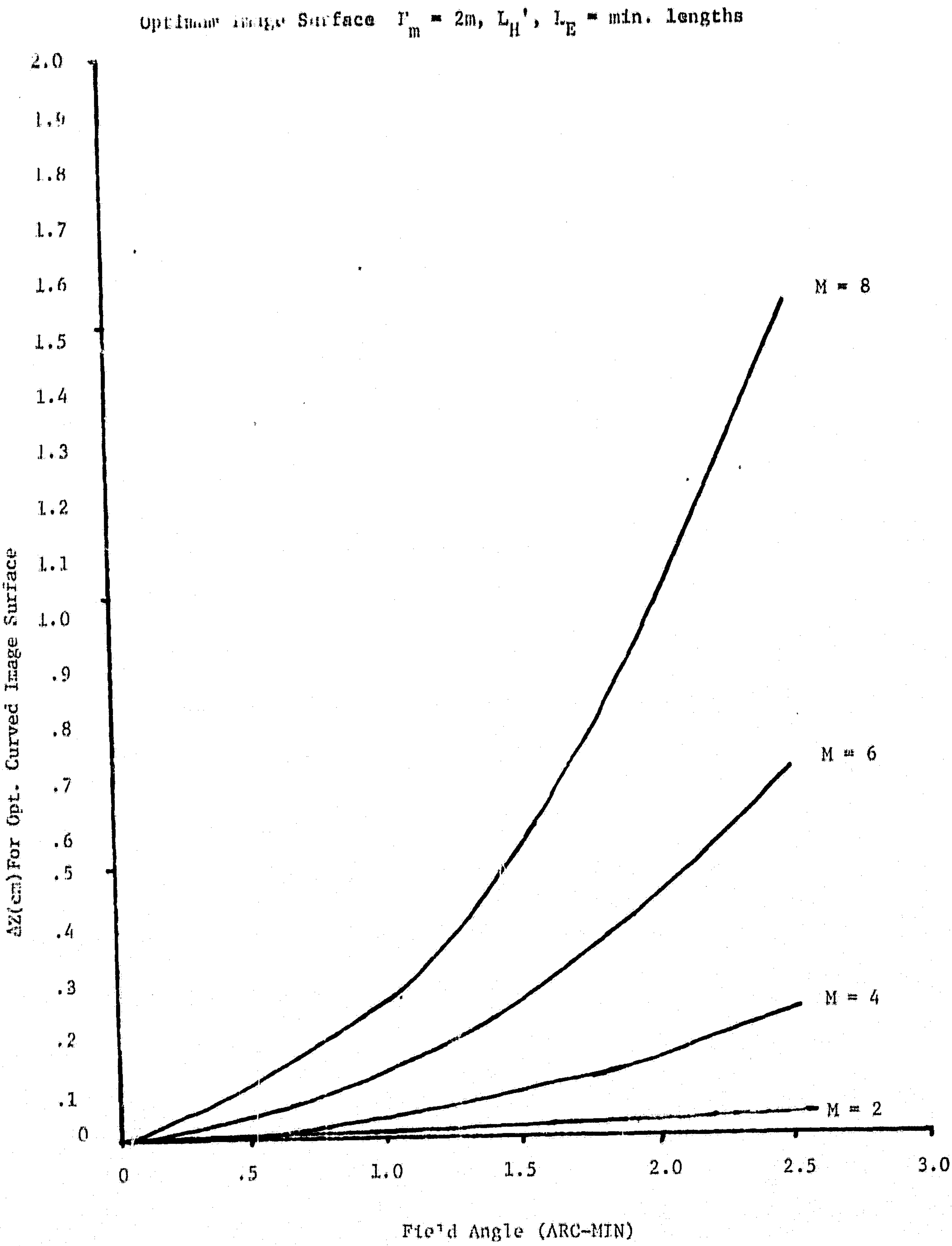

Fig. 18: Optimum Image Surface

ORIGINAL PAGE IS
OF POOR QUALITY

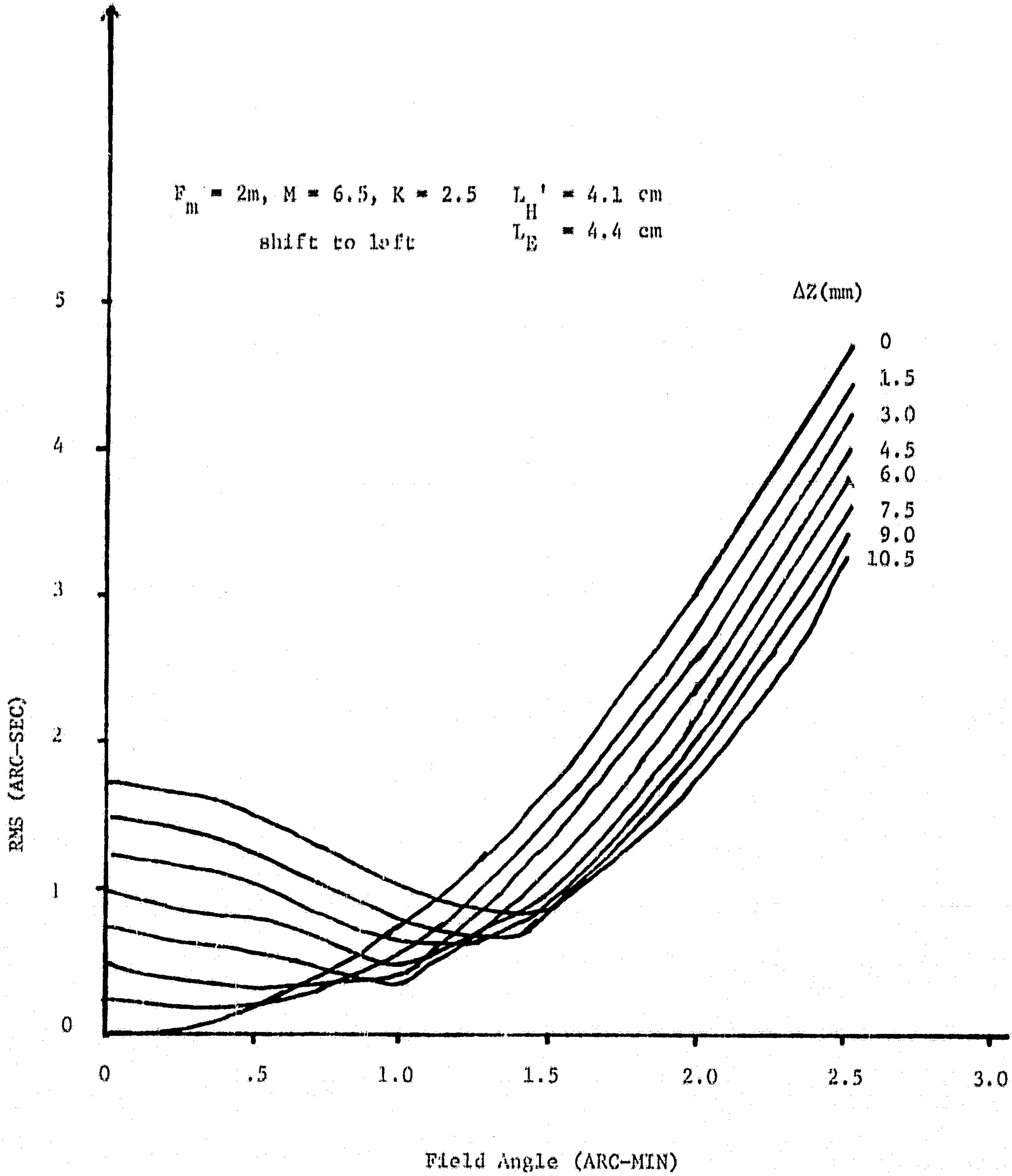

Fig. 19: RMS Spot Radius vs Field Angle

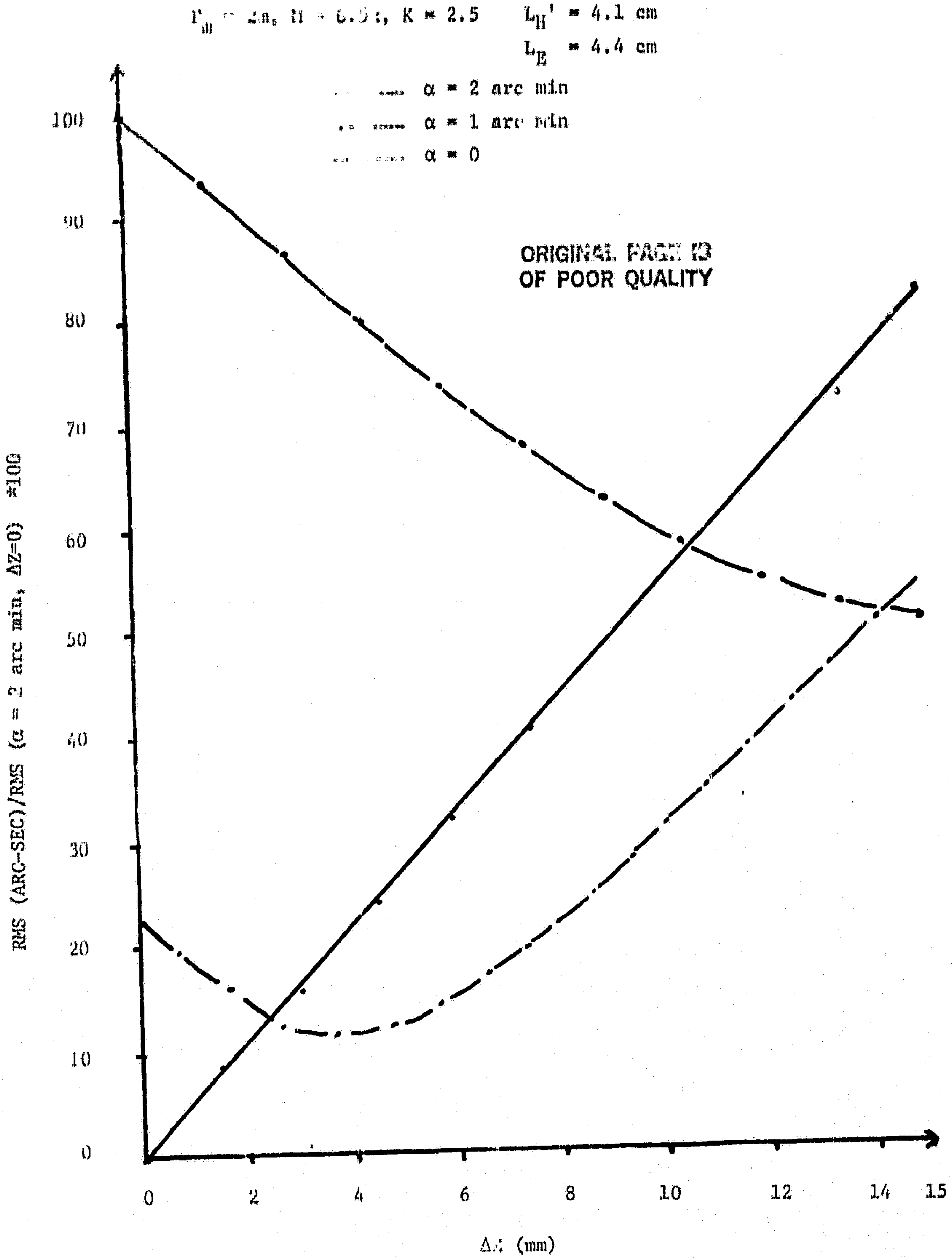

Fig. 20: Normalized RMS Spot Radius vs Image Plane Displacement

ORIGINAL PAGE IS
OF POOR QUALITY

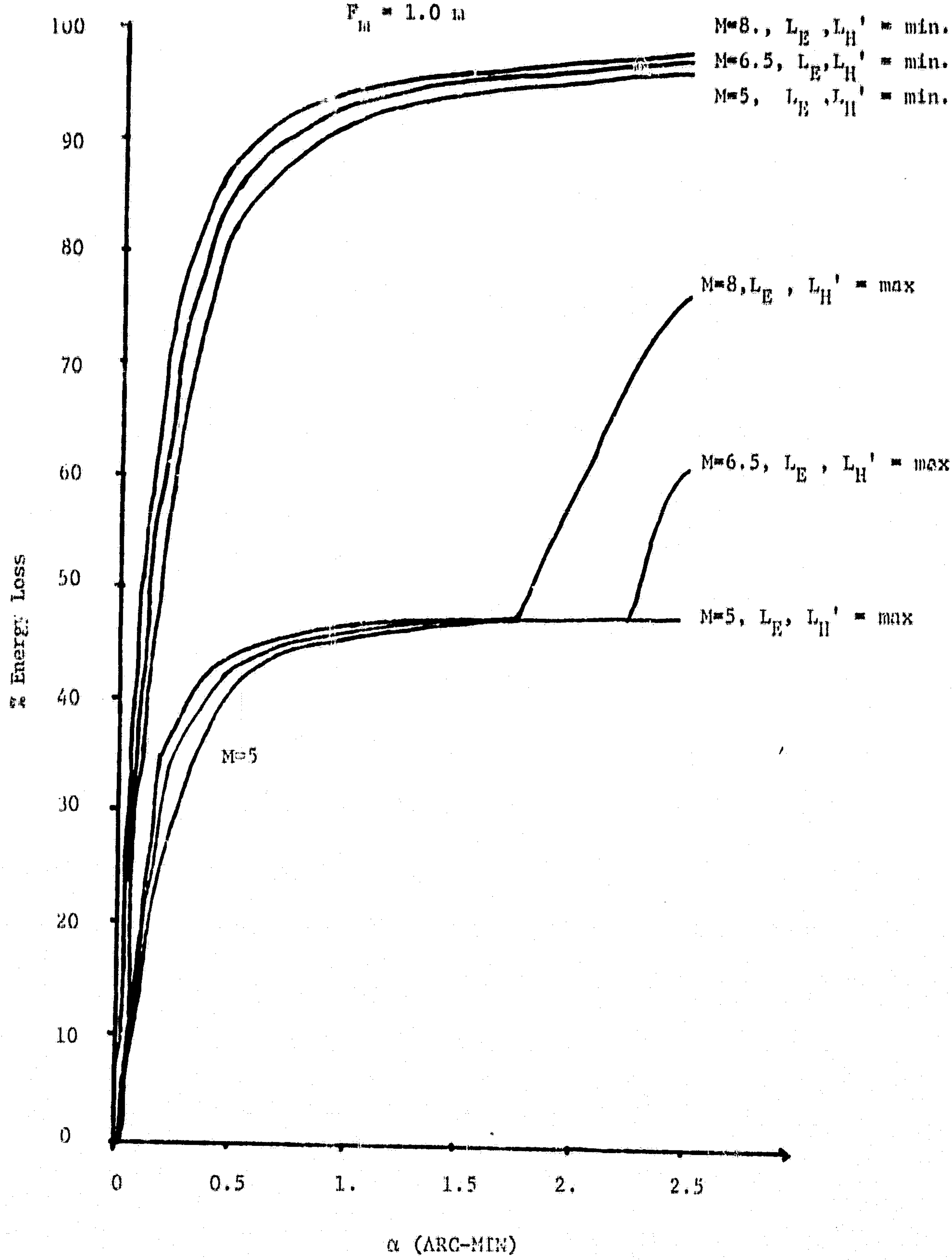

Fig. 21: Percent Energy Loss vs Field Angle

% Energy Loss vs H' - mirror's length for α = 1.0 and L_E is max.
F_m = 1m

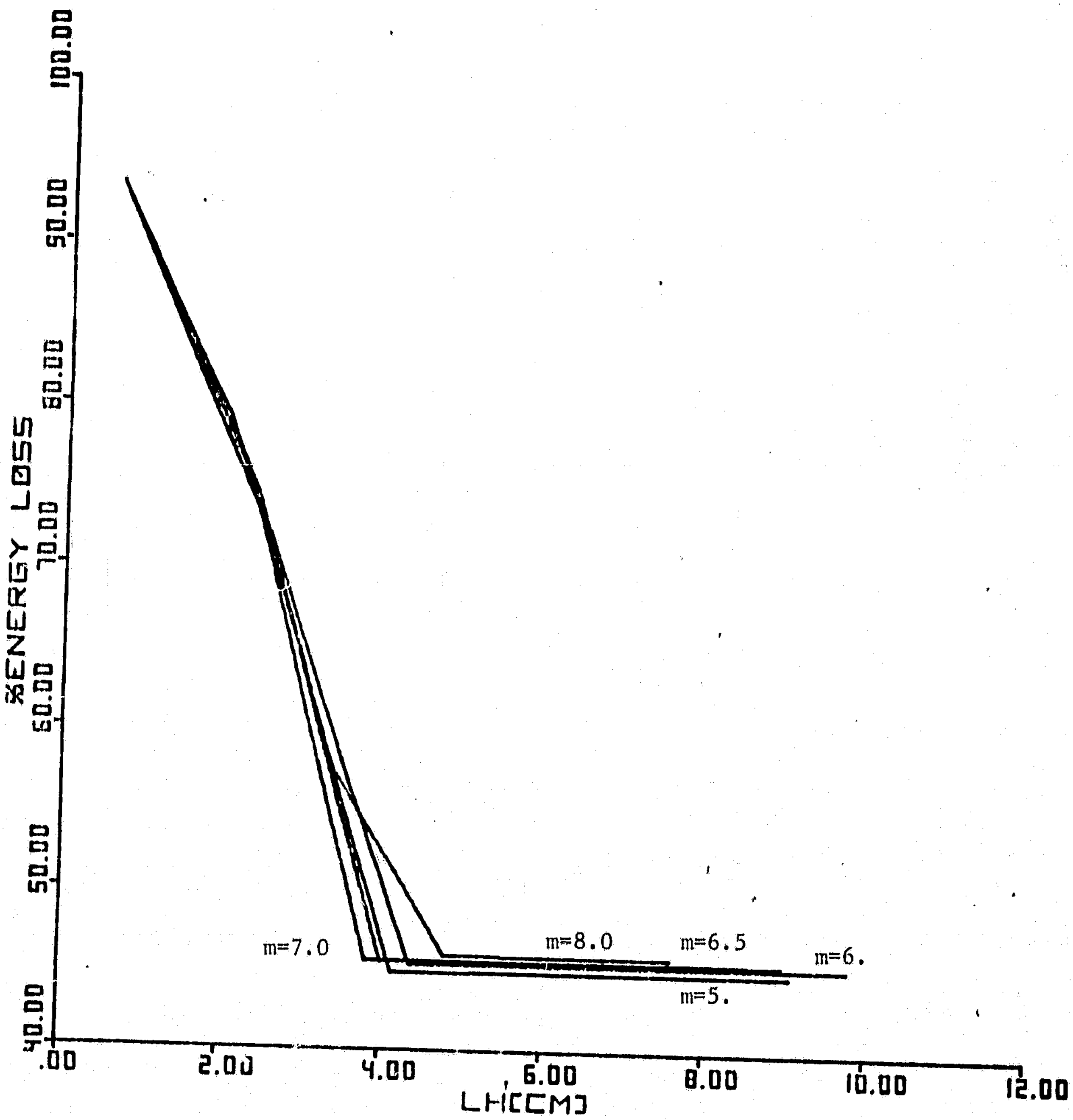

Fig. 22a: Percent Energy Loss vs $L_{H'}$

C-2

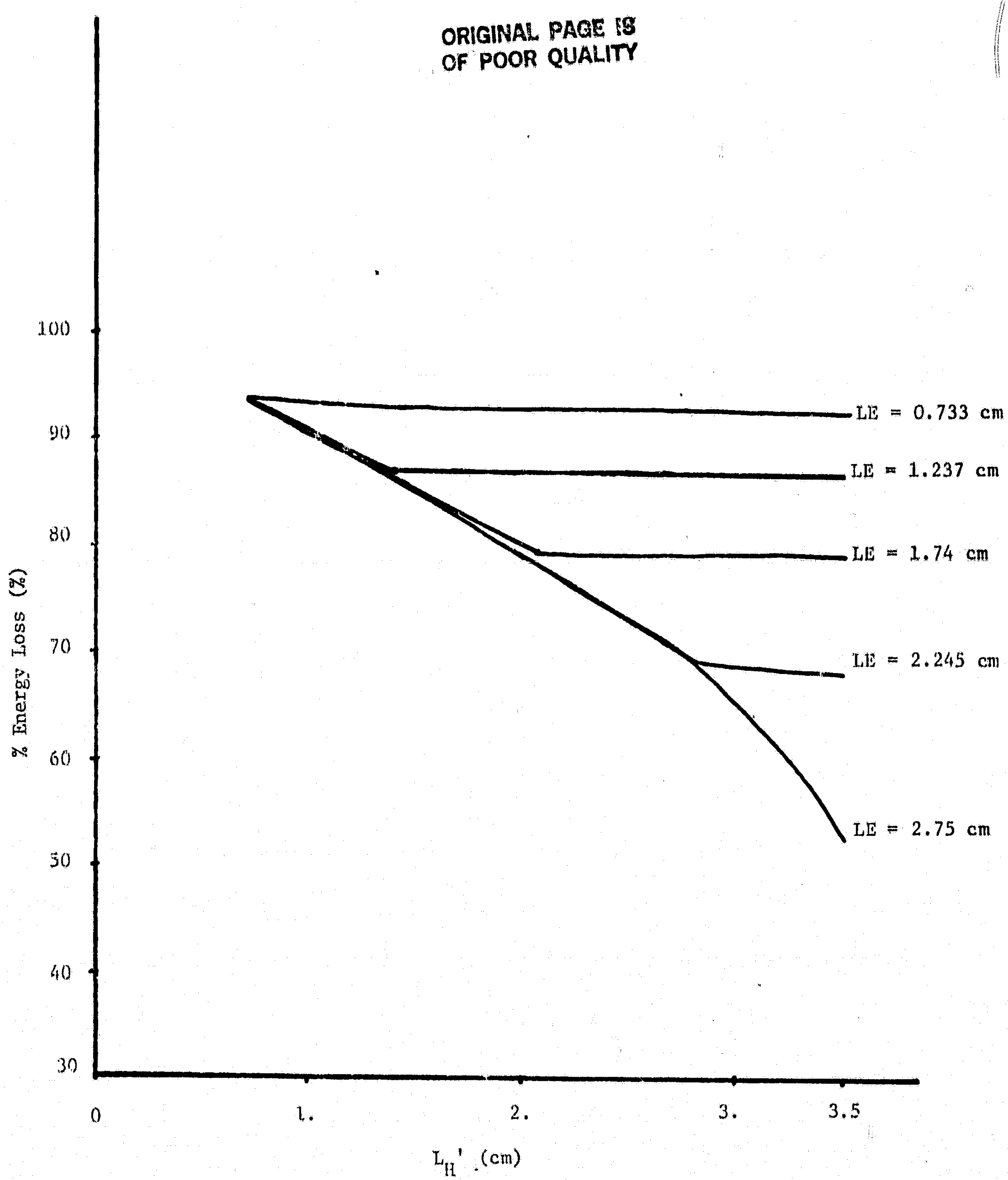

$F_m = 1.0$ m, $\alpha = 1.0'$, $M = 6.5$

Fig. 22b: Percent Energy Loss vs $L_{H'}$

ORIGINAL PAGE IS OF POOR QUALITY

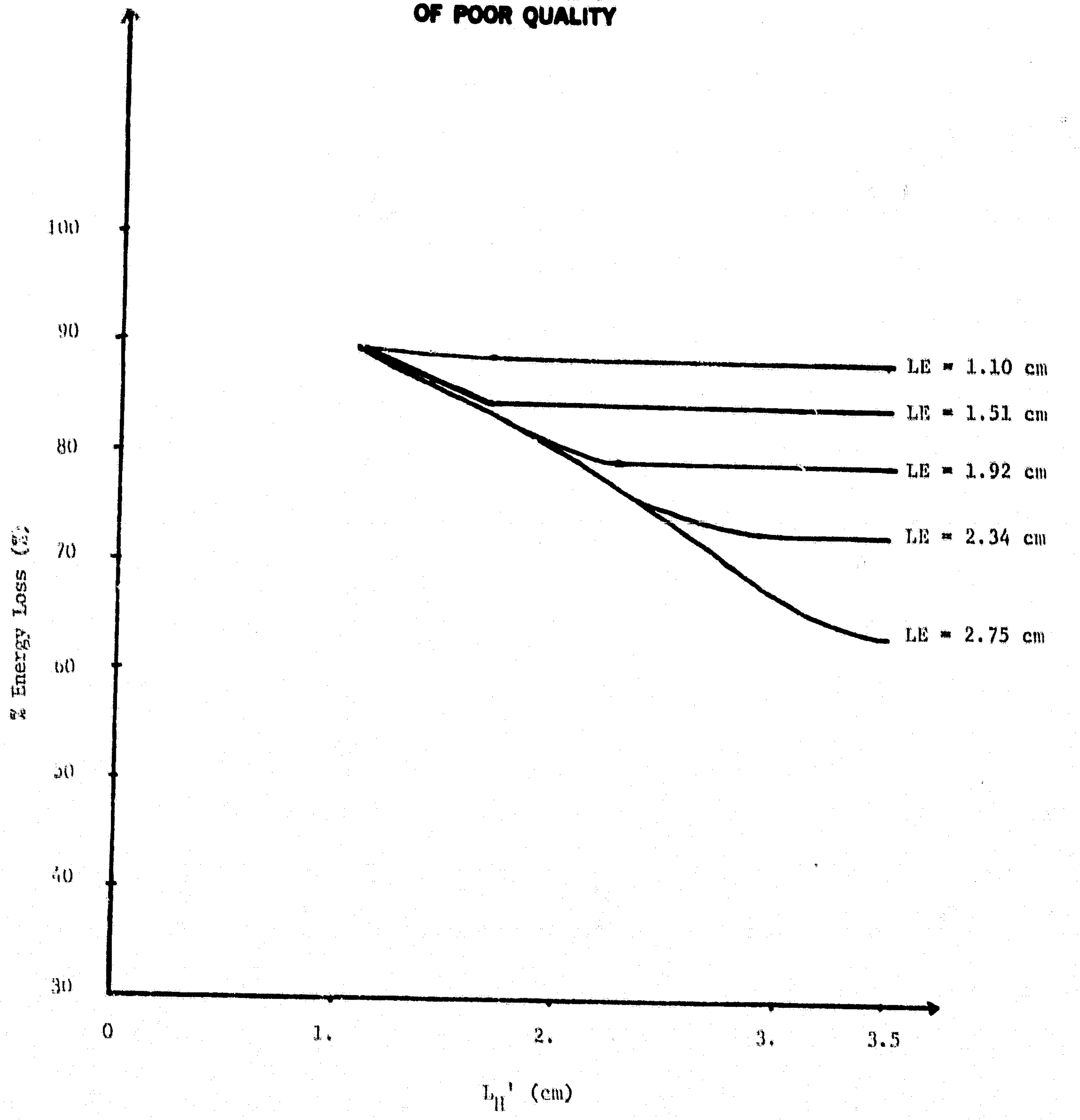

$F_m = 1.5$ m, $\alpha = 1.0'$, $M = 6.5$

Fig. 22c: Percent Energy Loss vs $L_{H'}$

% Energy Loss vs. L_E - mirror length for α = 1.00, and
Max. length of H- mirror and different magnification
F_m = 1m

ORIGINAL PAGE IS
OF POOR QUALITY

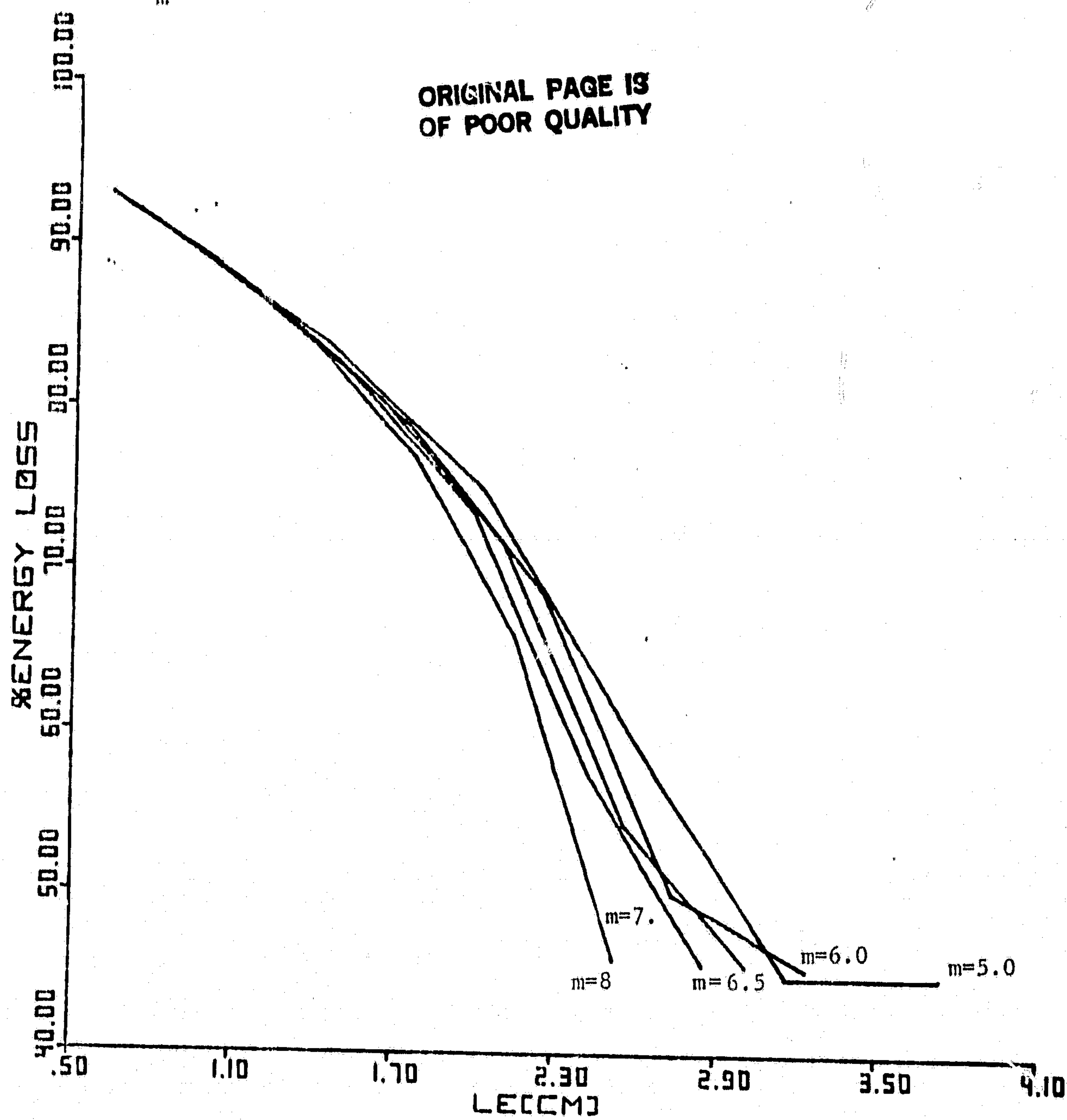

Fig. 23a: Percent Energy Loss vs L_E

ORIGINAL PAGE IS
OF POOR QUALITY

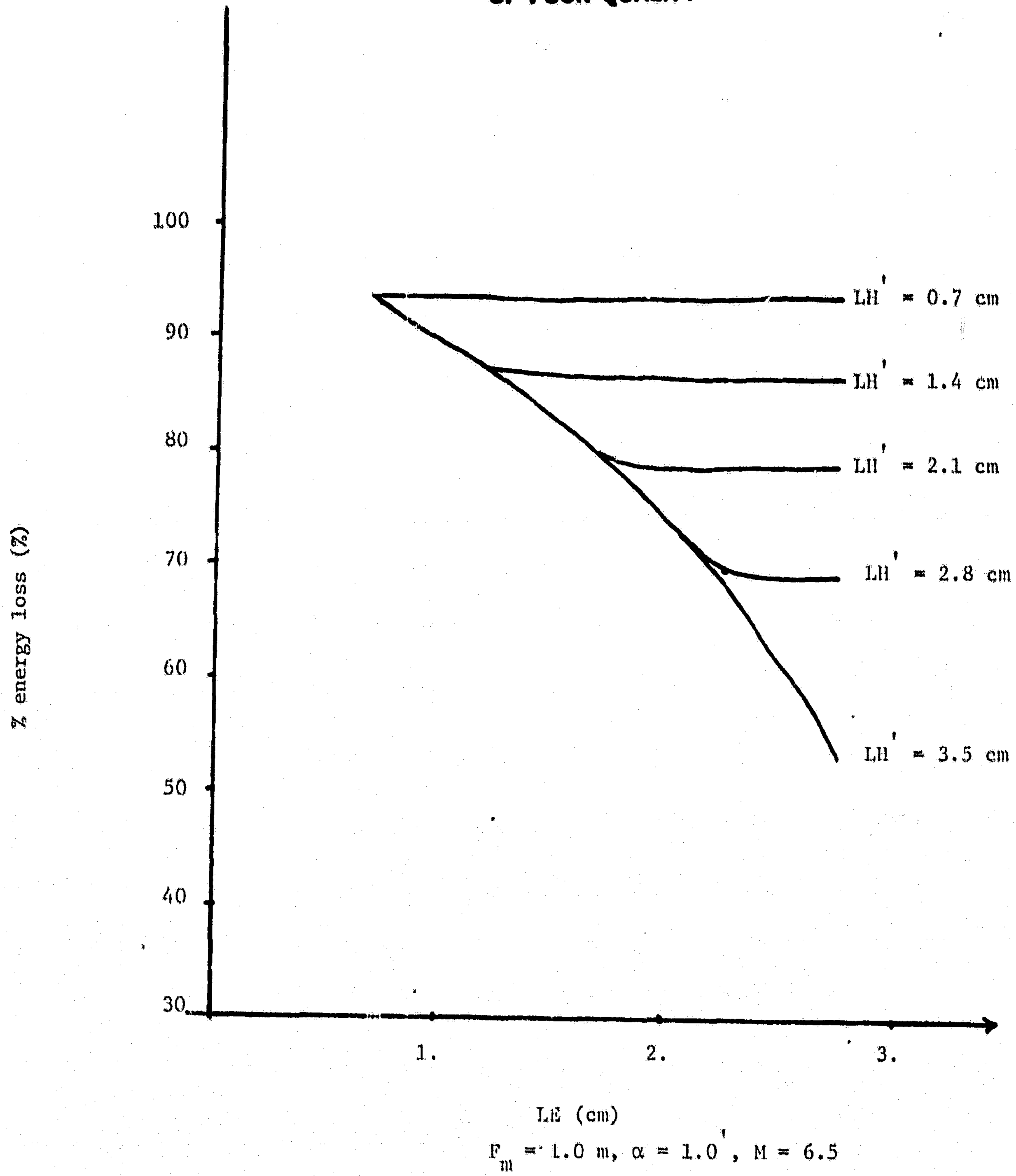

Fig. 23b: Percent Energy Loss vs L_E

ORIGINAL PAGE IS
OF POOR QUALITY

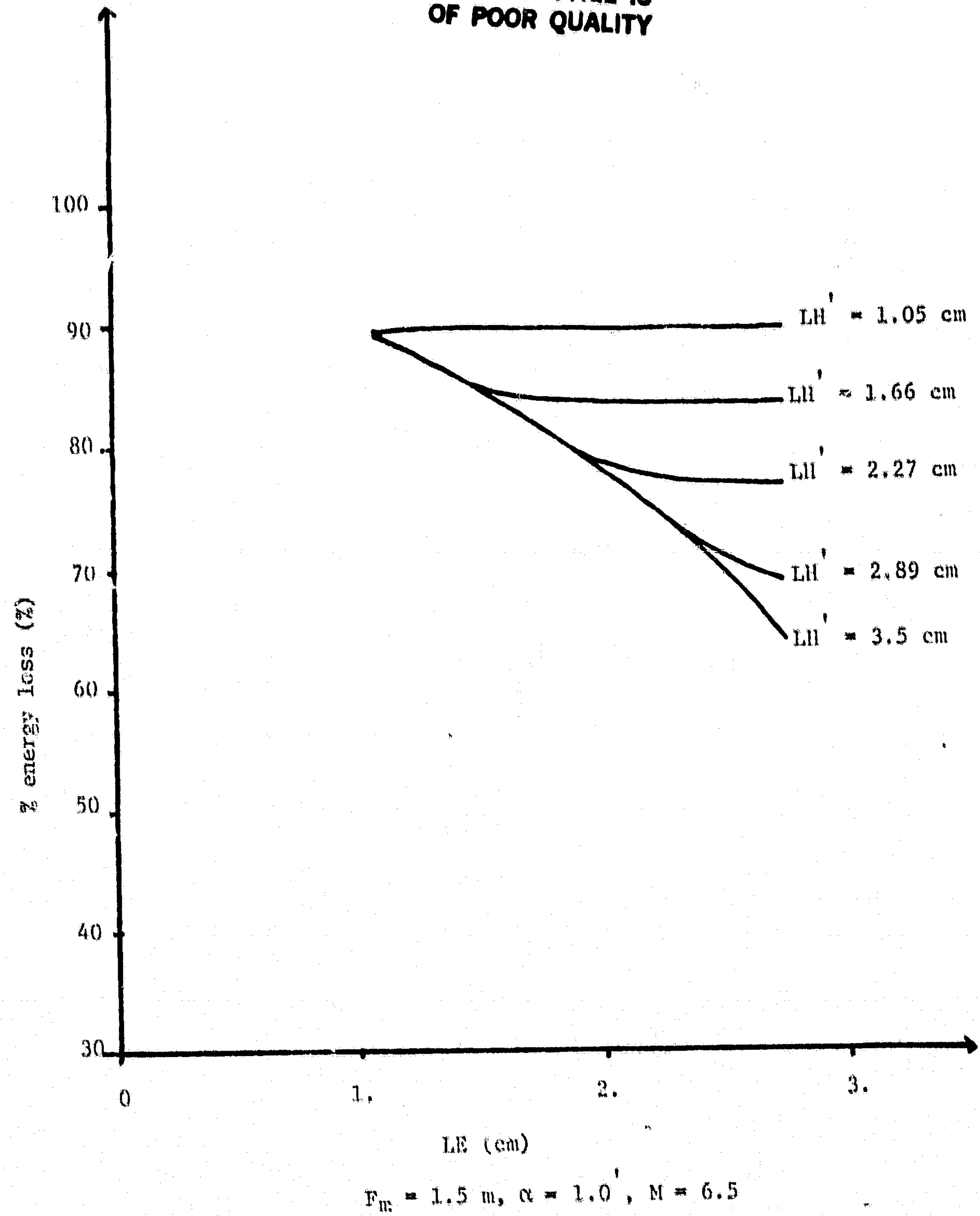

Fig. 23c: Percent Energy Loss vs L_E

ORIGINAL PAGE IS
OF POOR QUALITY

$M = 5.0$

L_E is max. length

$F_m = 1m$

$\alpha = 1$ arc min

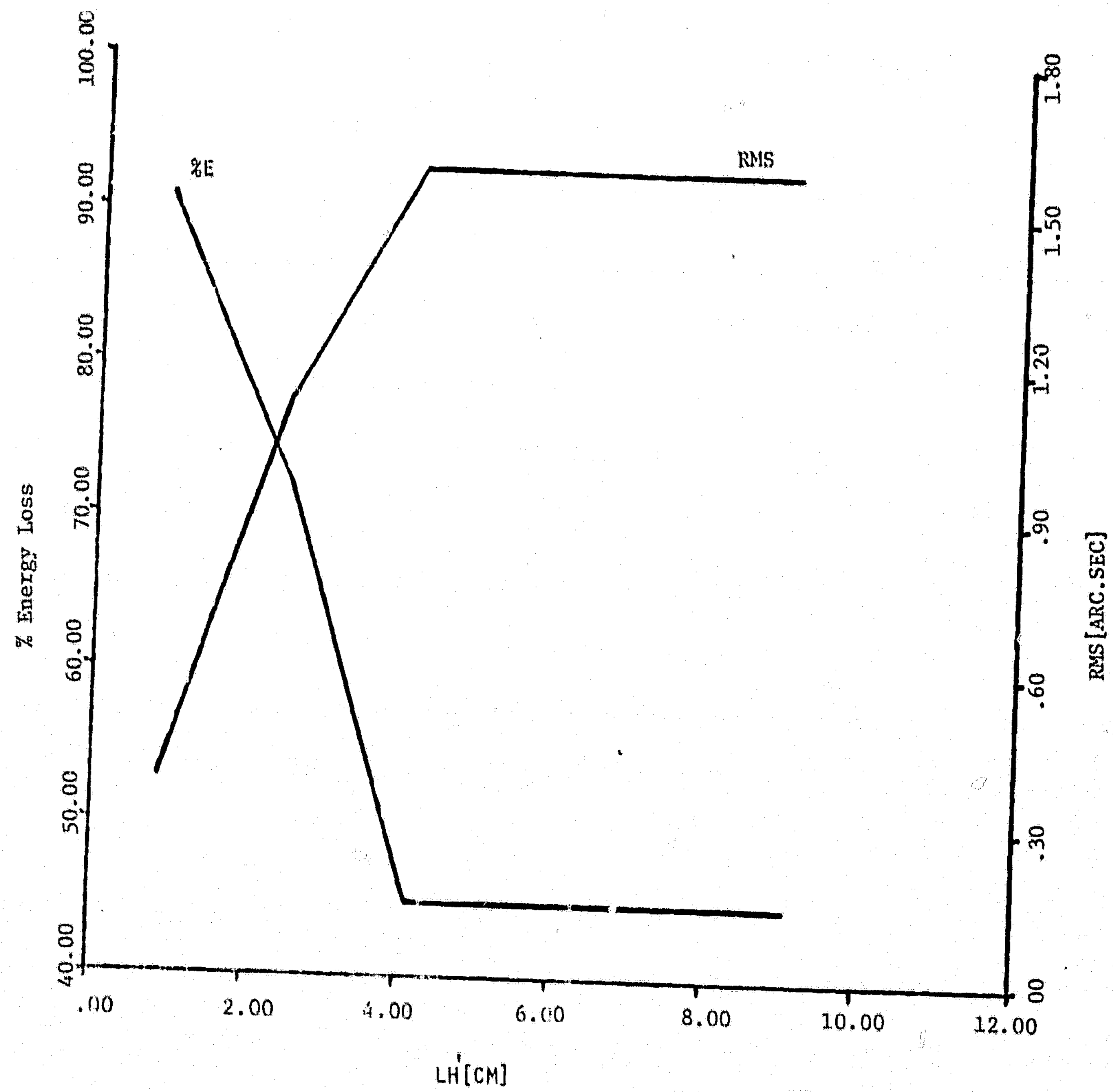

Fig.24: Percent Energy Loss and RMS Spot Radius vs $L_{H'}$

M = 5.0

L_H' is max.

F_m = 1m, α = 1 arc-min

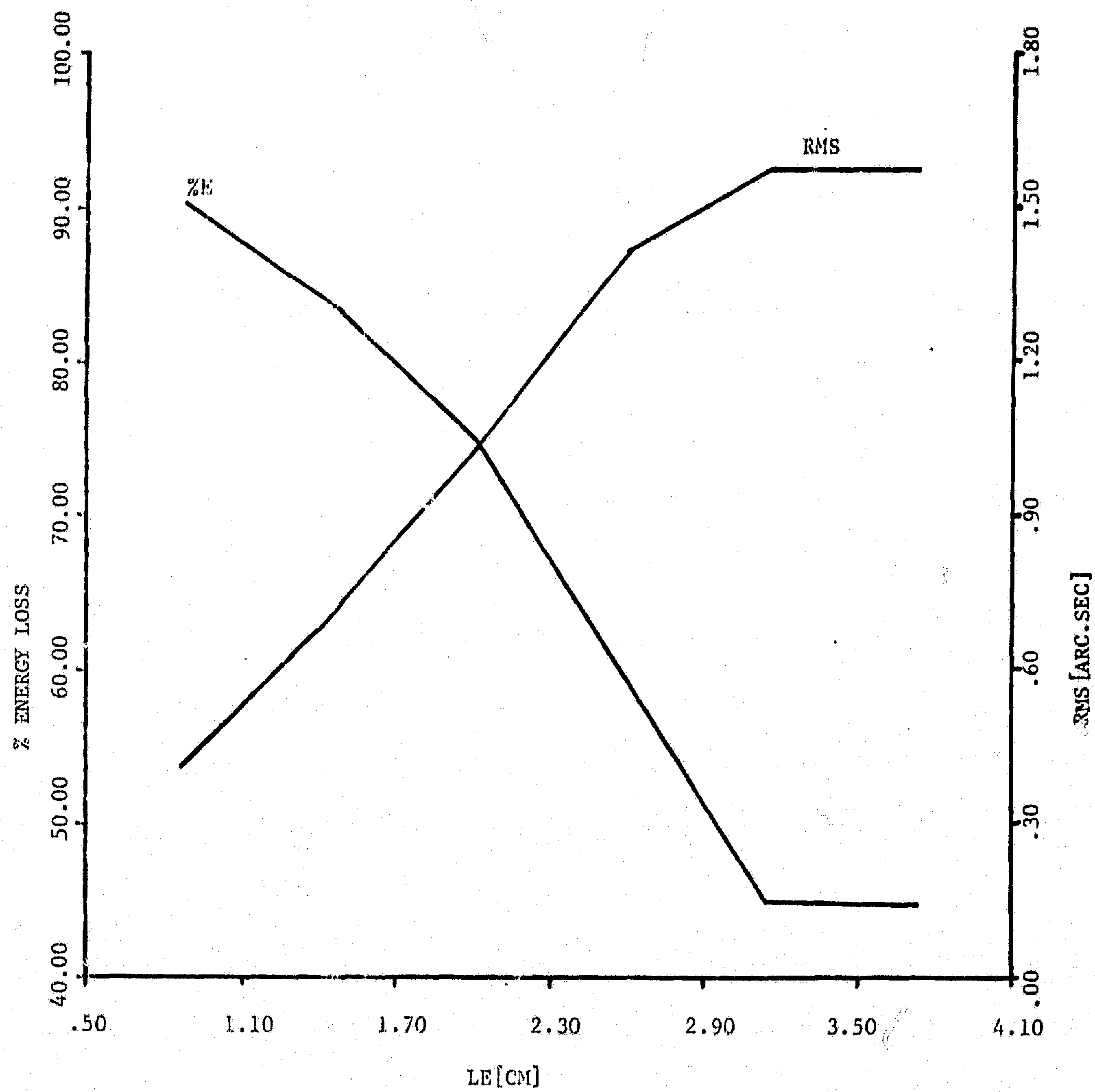

Fig. 25: Percent Energy Loss and RMS Spot Radius vs L_E

ORIGINAL PAGE IS
OF POOR QUALITY

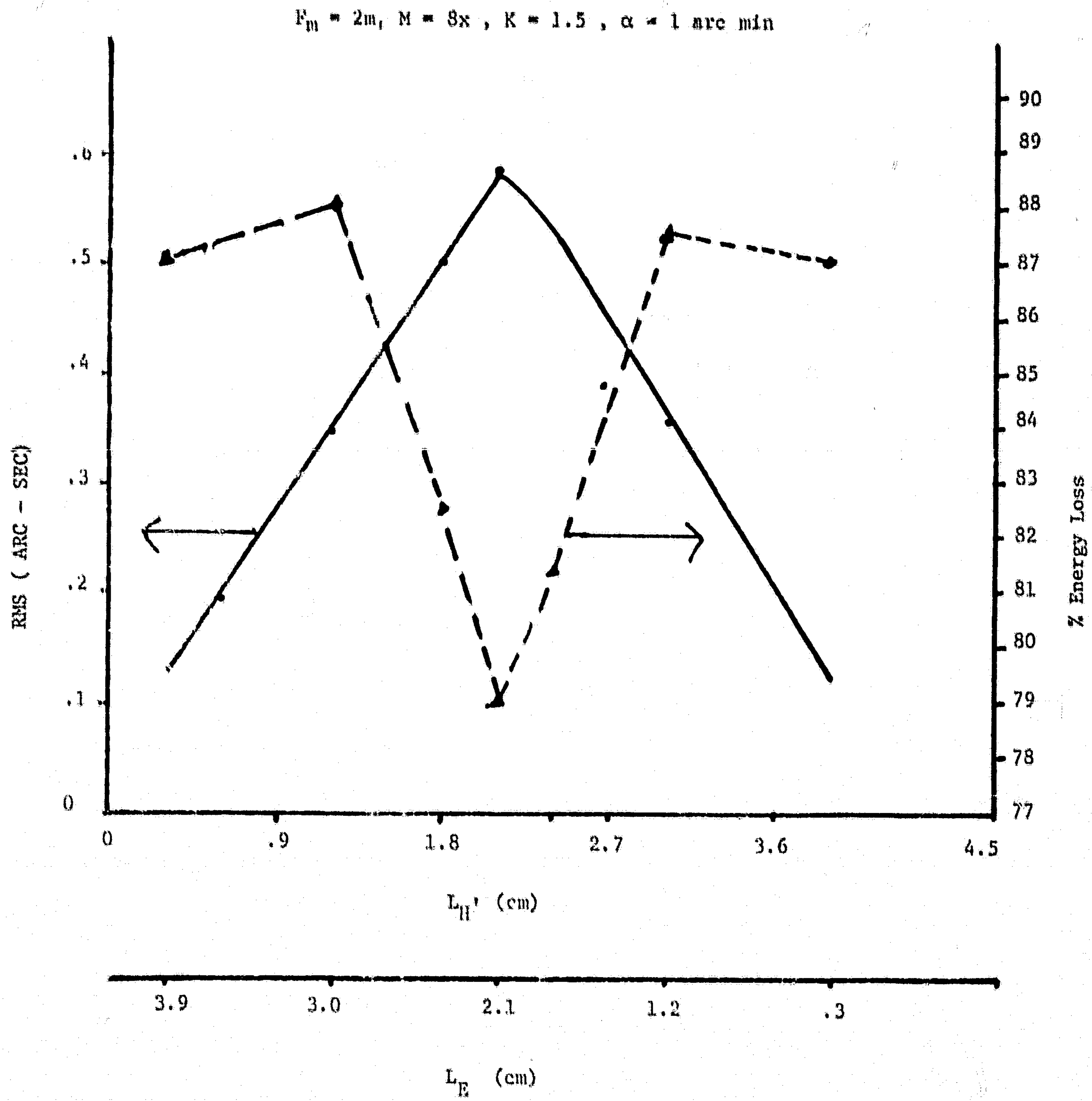

Fig. 26: RMS Spot Radius and Percent Energy Loss vs $L_{H'}$ and L_E

ORIGINAL PAGE IS OF POOR QUALITY

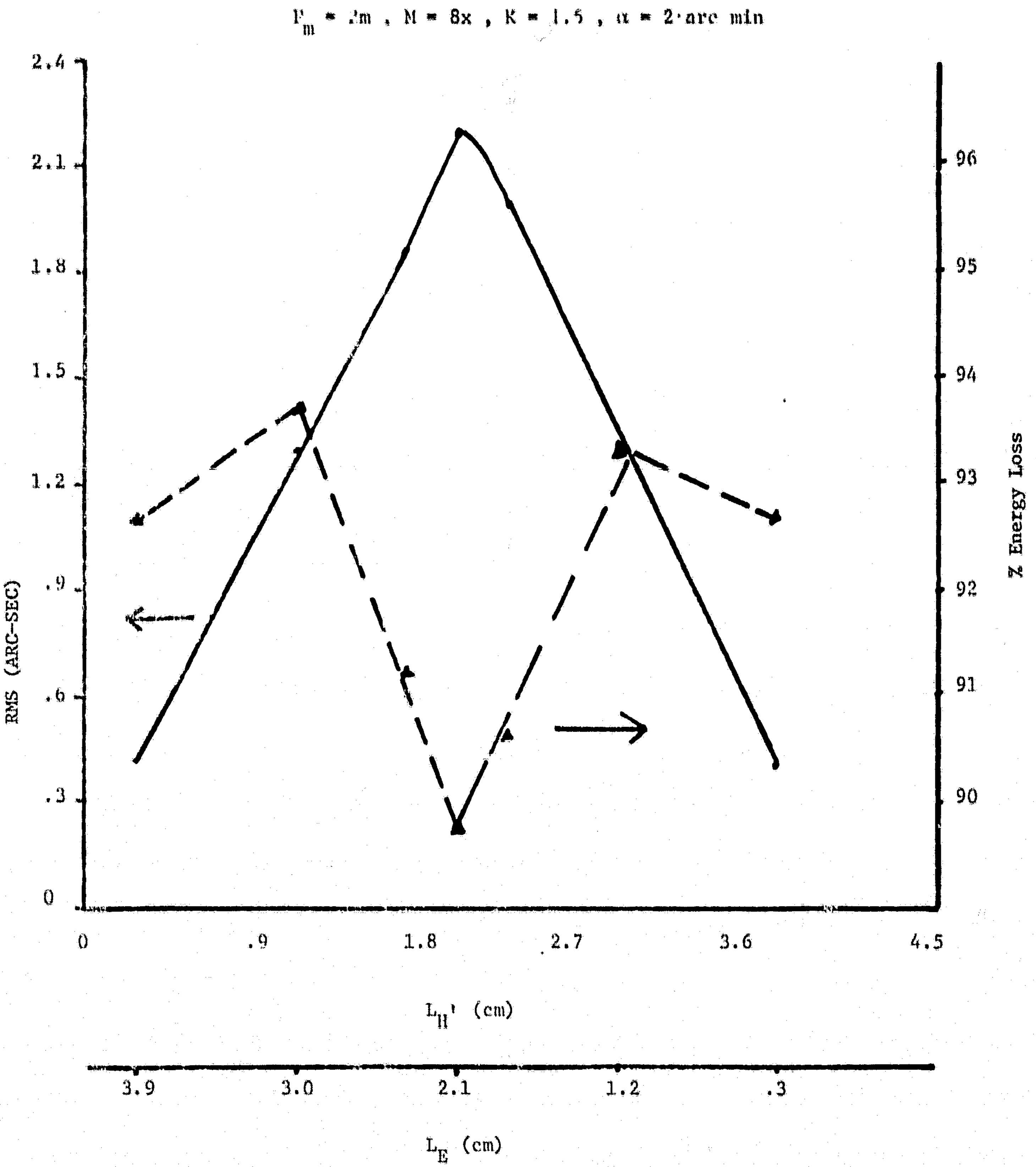

Fig. 27: RMS Spot Radius and Percent Energy Loss vs $L_{H'}$ and L_E

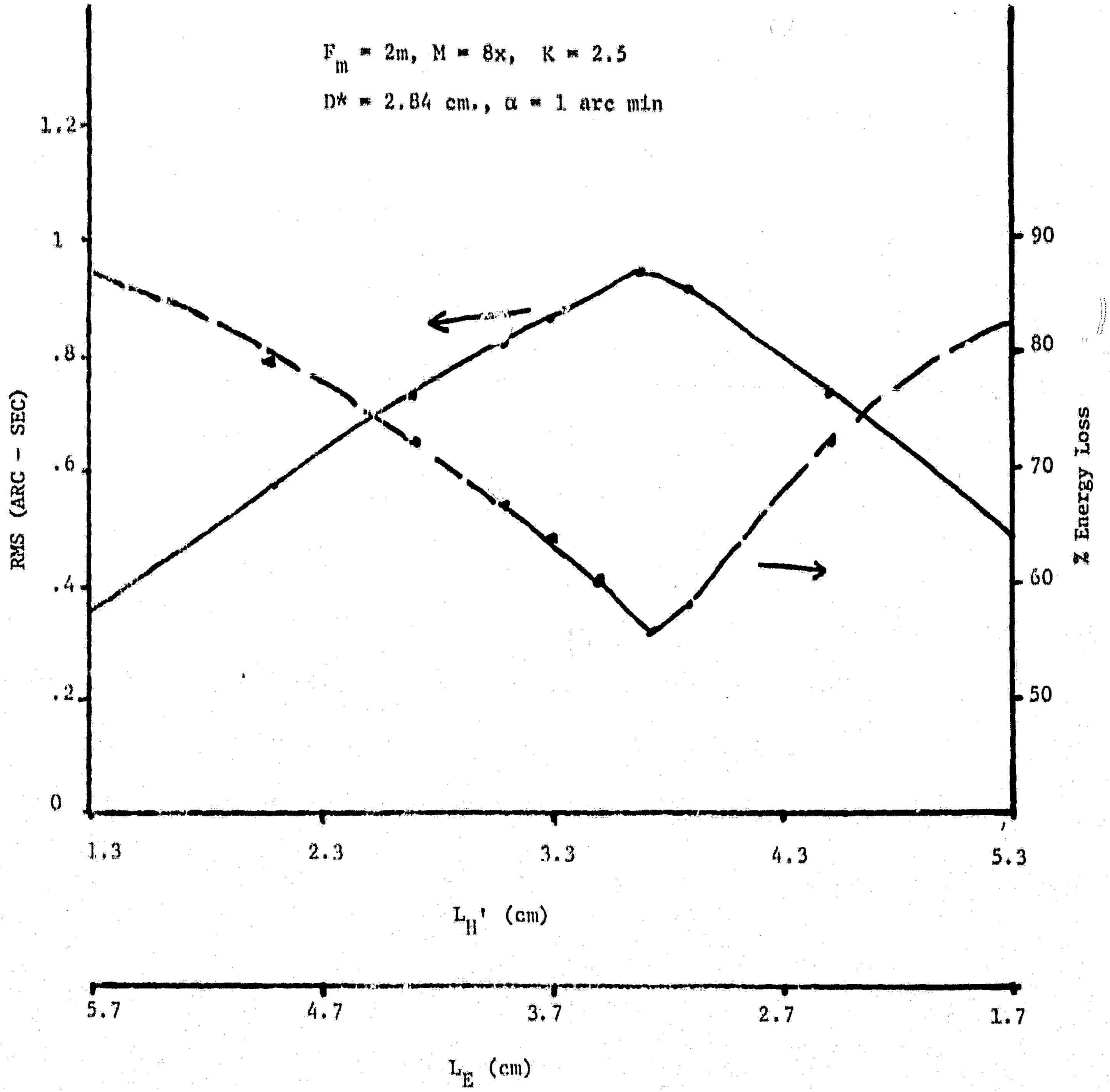

Fig. 28: RMS Spot Radius and Percent Energy Loss vs $L_{H'}$ and L_E

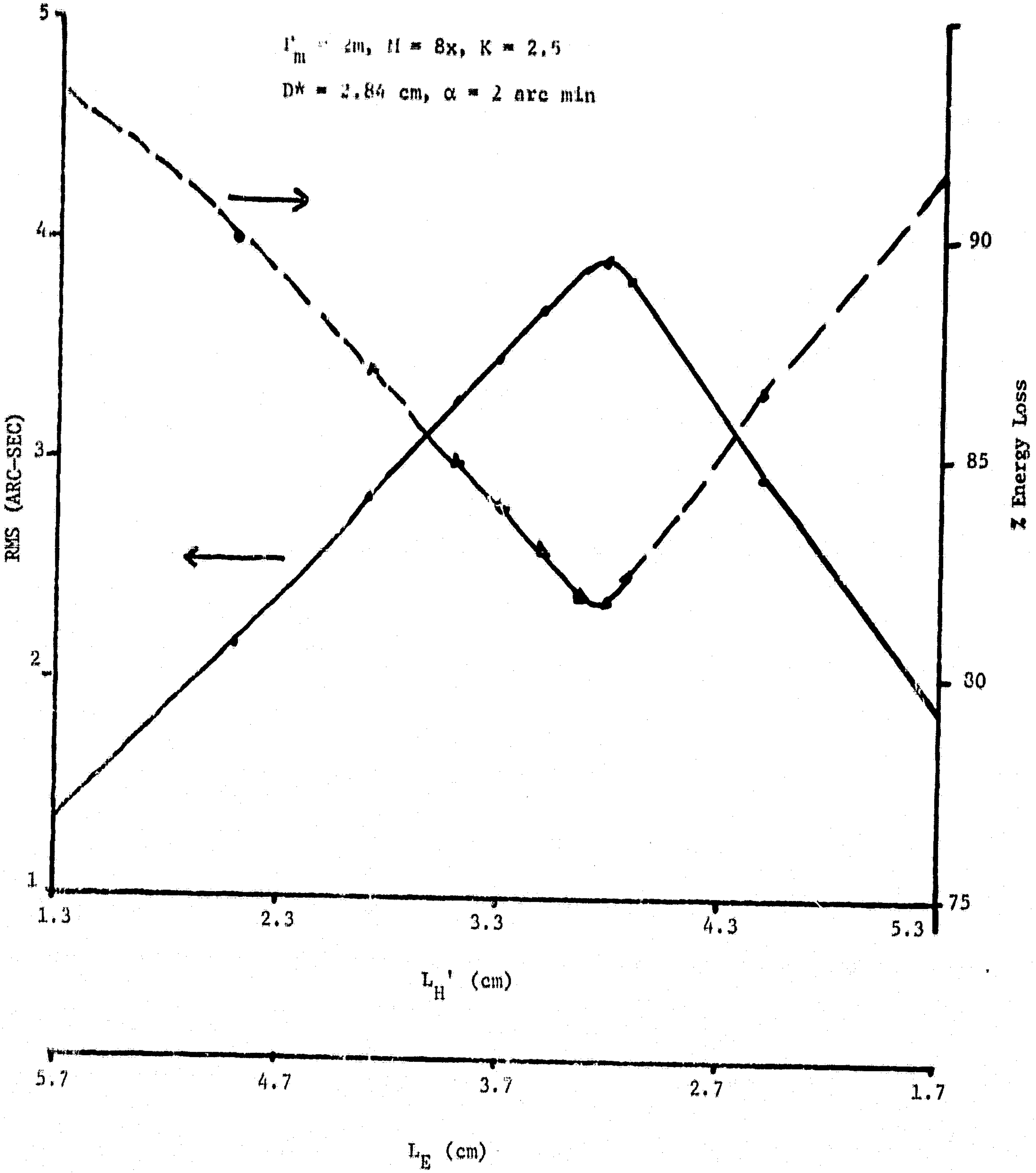

Fig. 29: RMS Spot Radius and Percent Energy Loss vs $L_{H'}$ and L_E

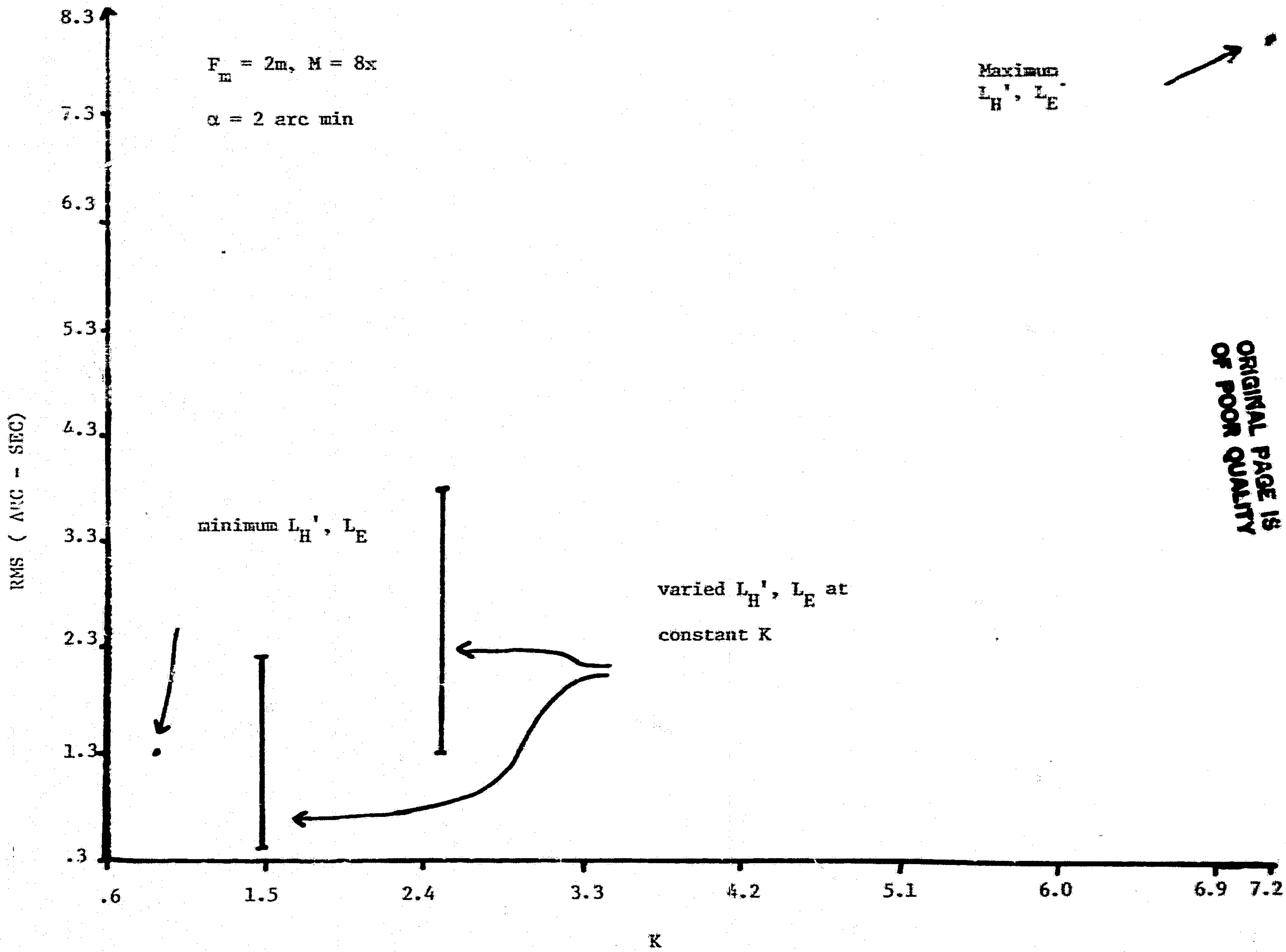

Fig. 30: RMS Spot Radius vs K

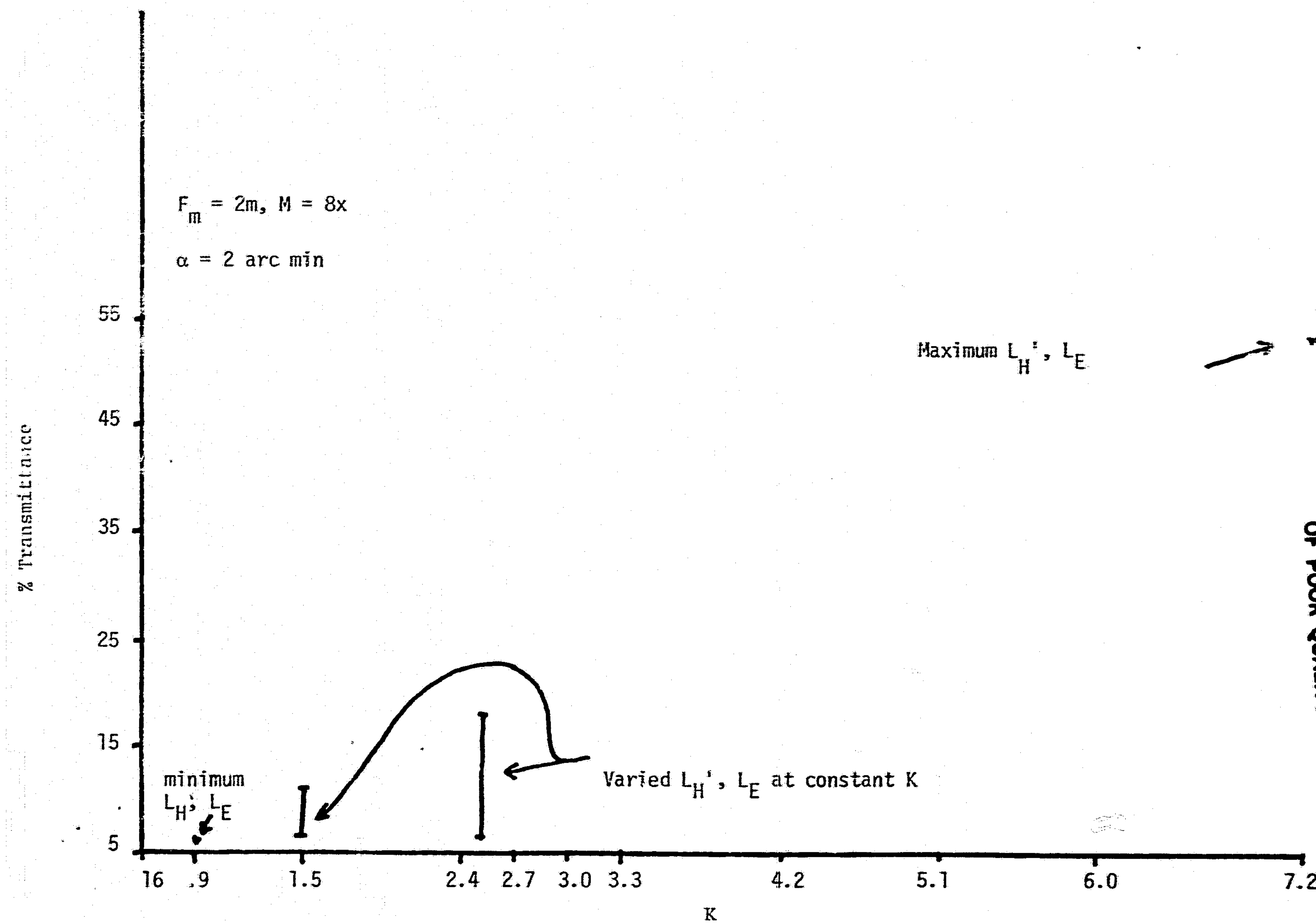

Fig. 31: RMS Spot Radius vs K

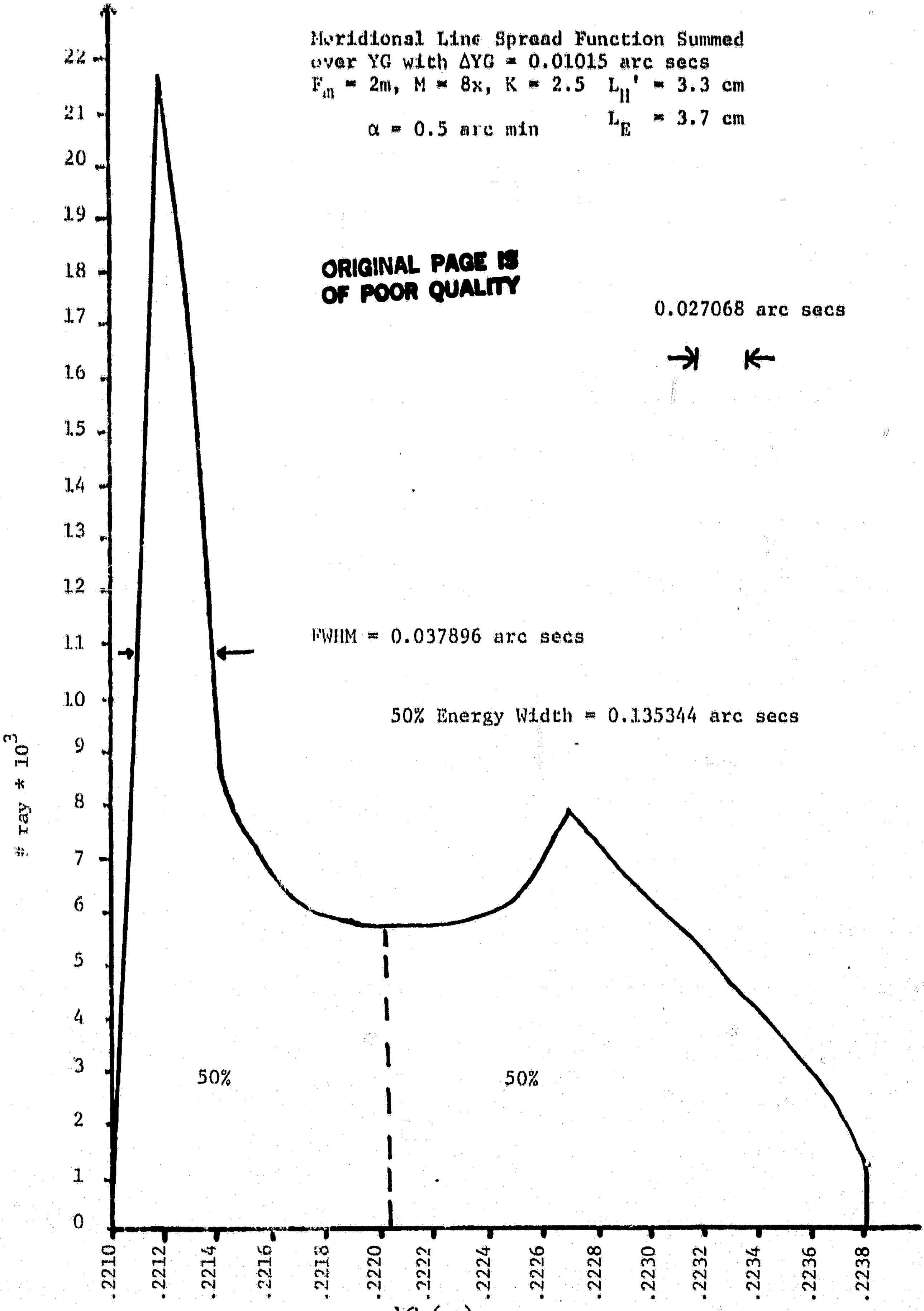

Fig. 33: Meridional Line Spread Function

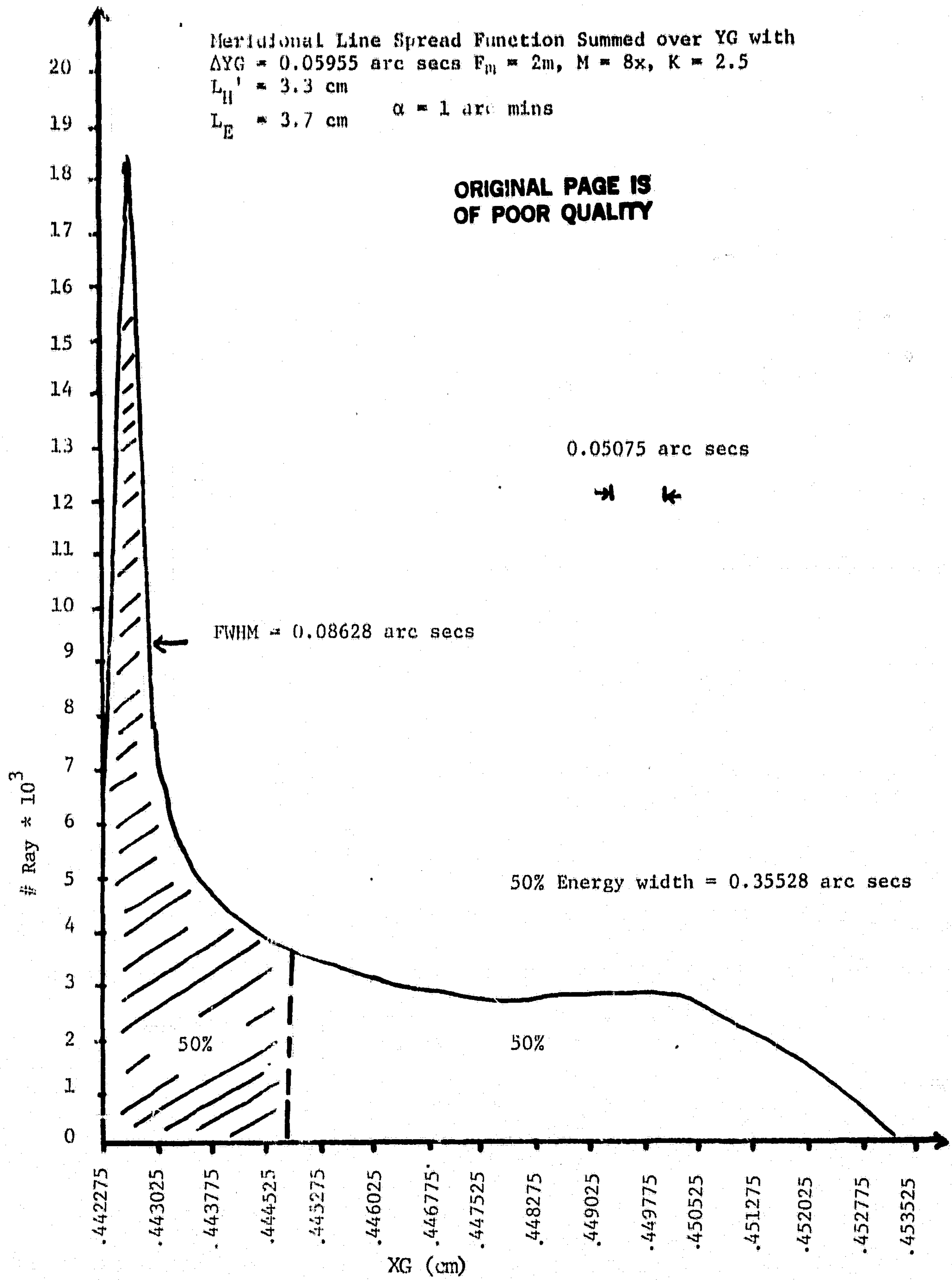

Fig. 33: Meridional Line Spread Function

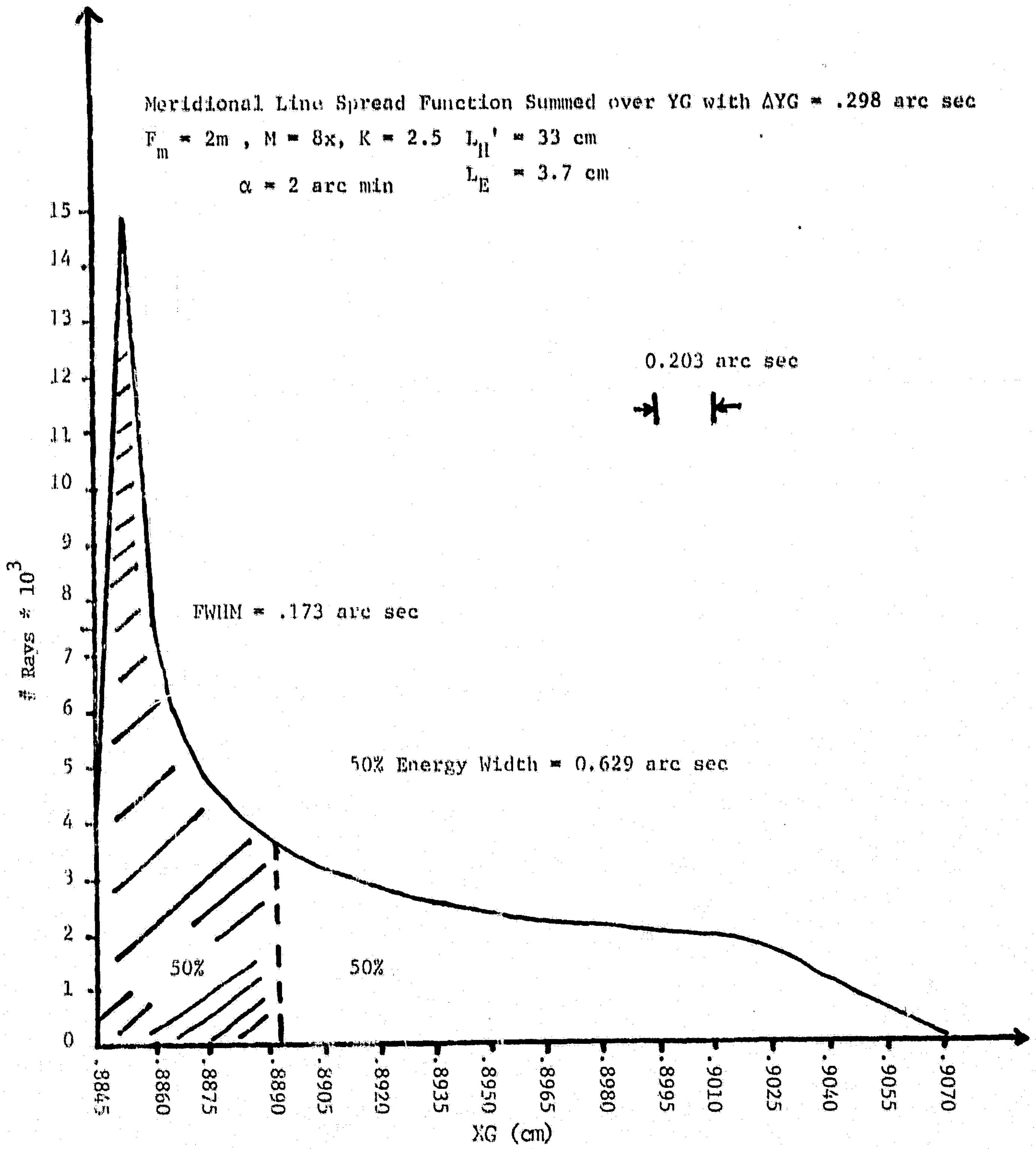

Fig. 34: Meridional Line Spread Function

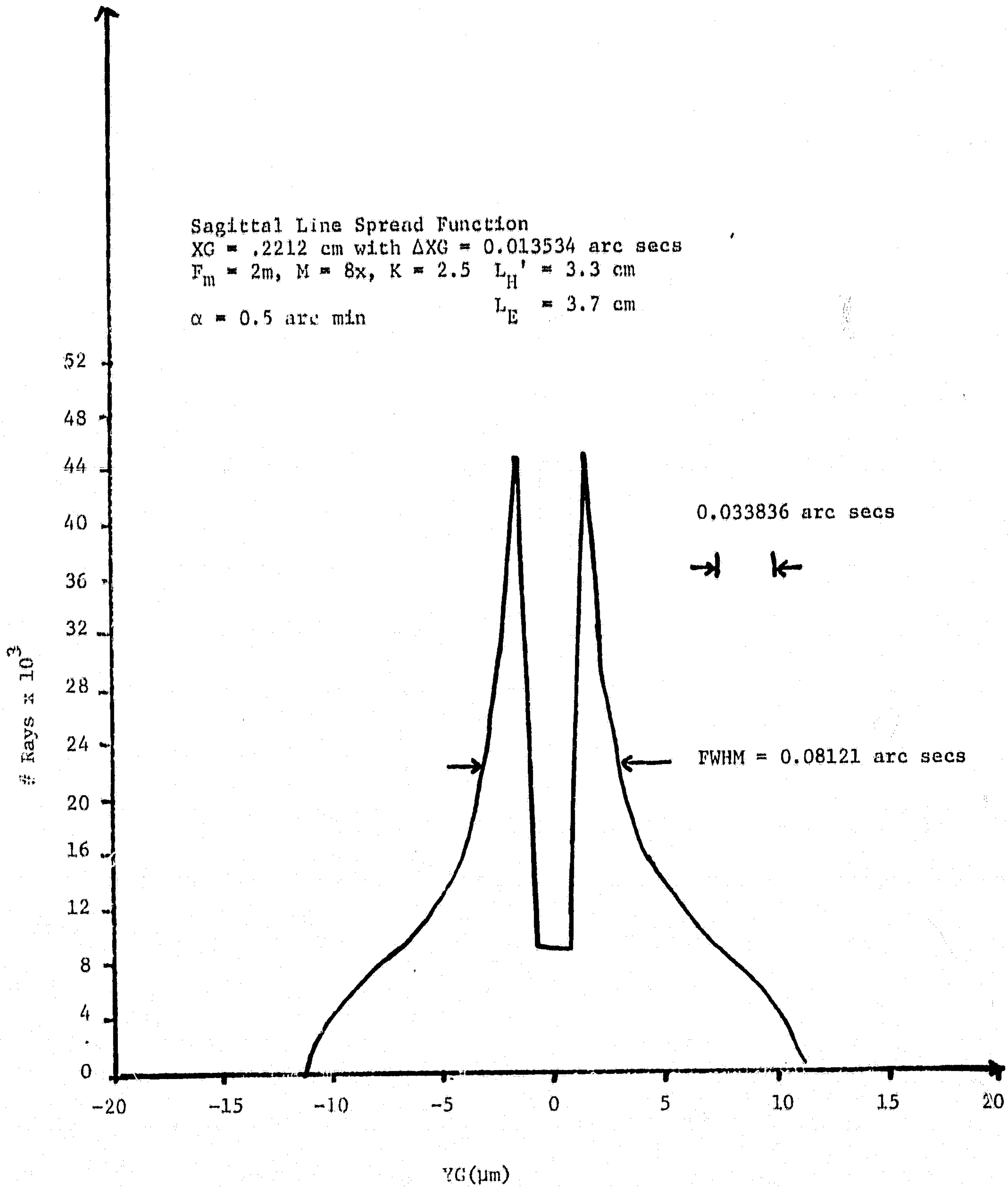

Fig. 35: Sagittal Slice of Point Spread Function

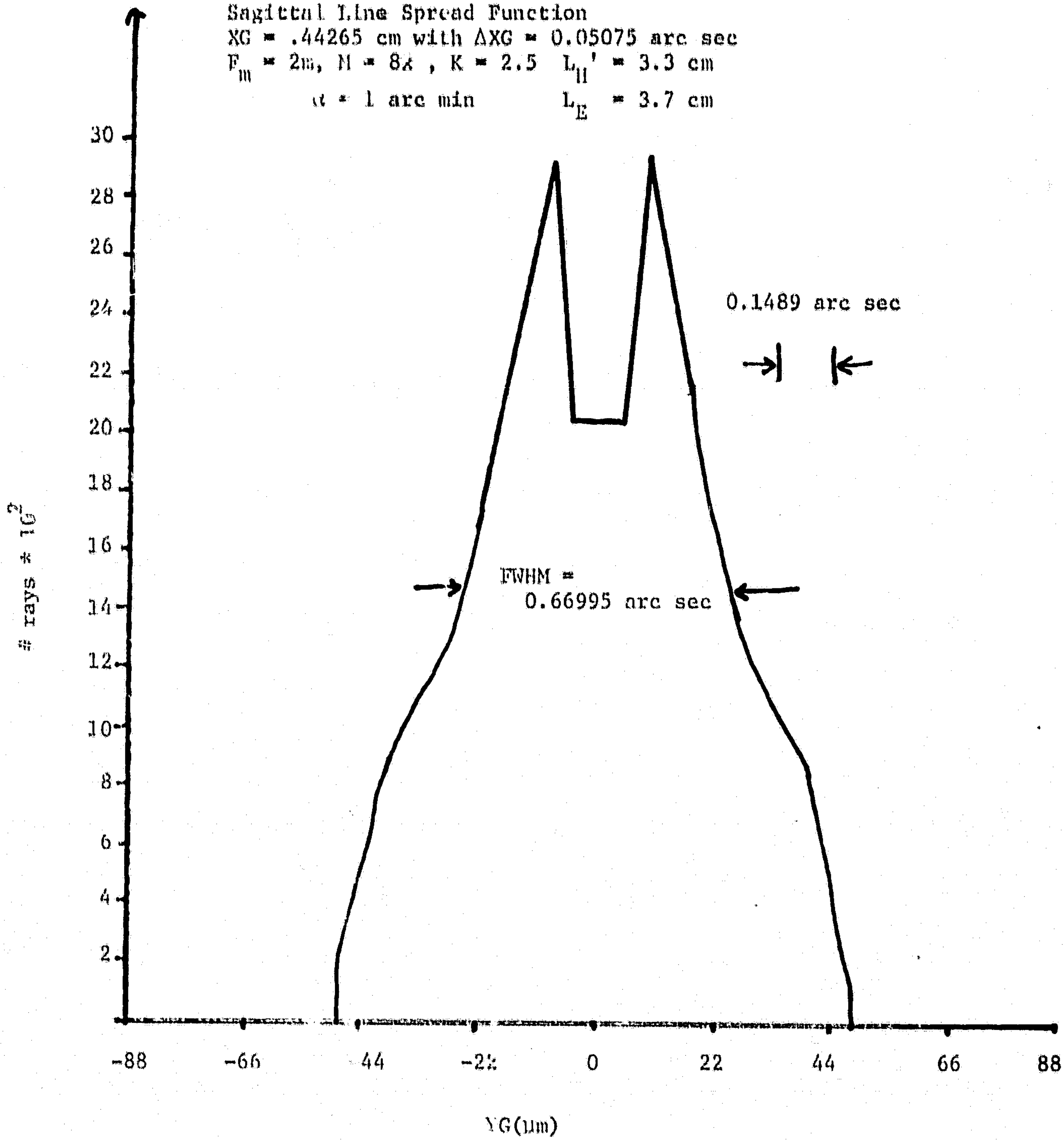

Fig. 36: Sagittal Slice of Point Spread Function

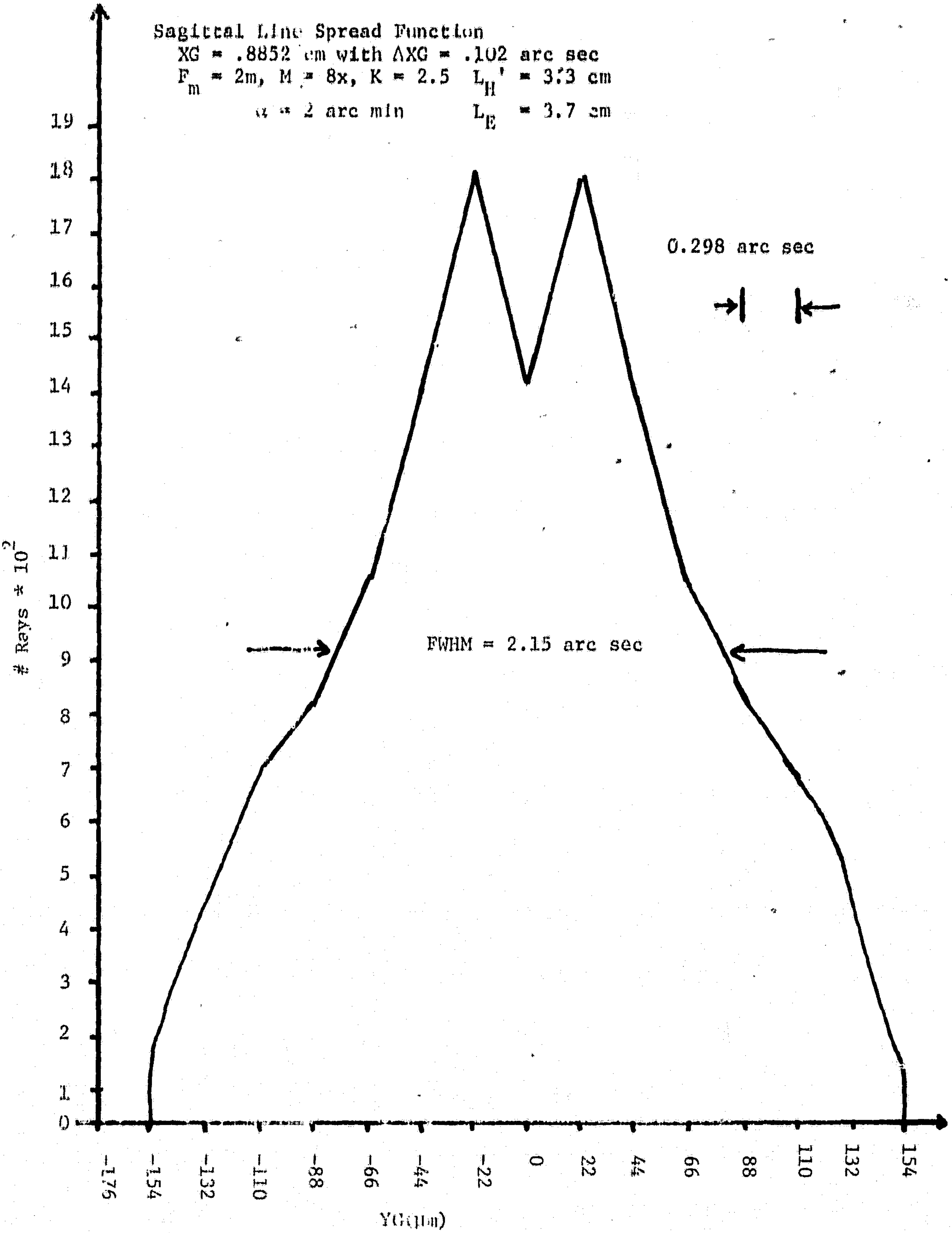

Fig. 37: Sagittal Slice of Point Spread Function

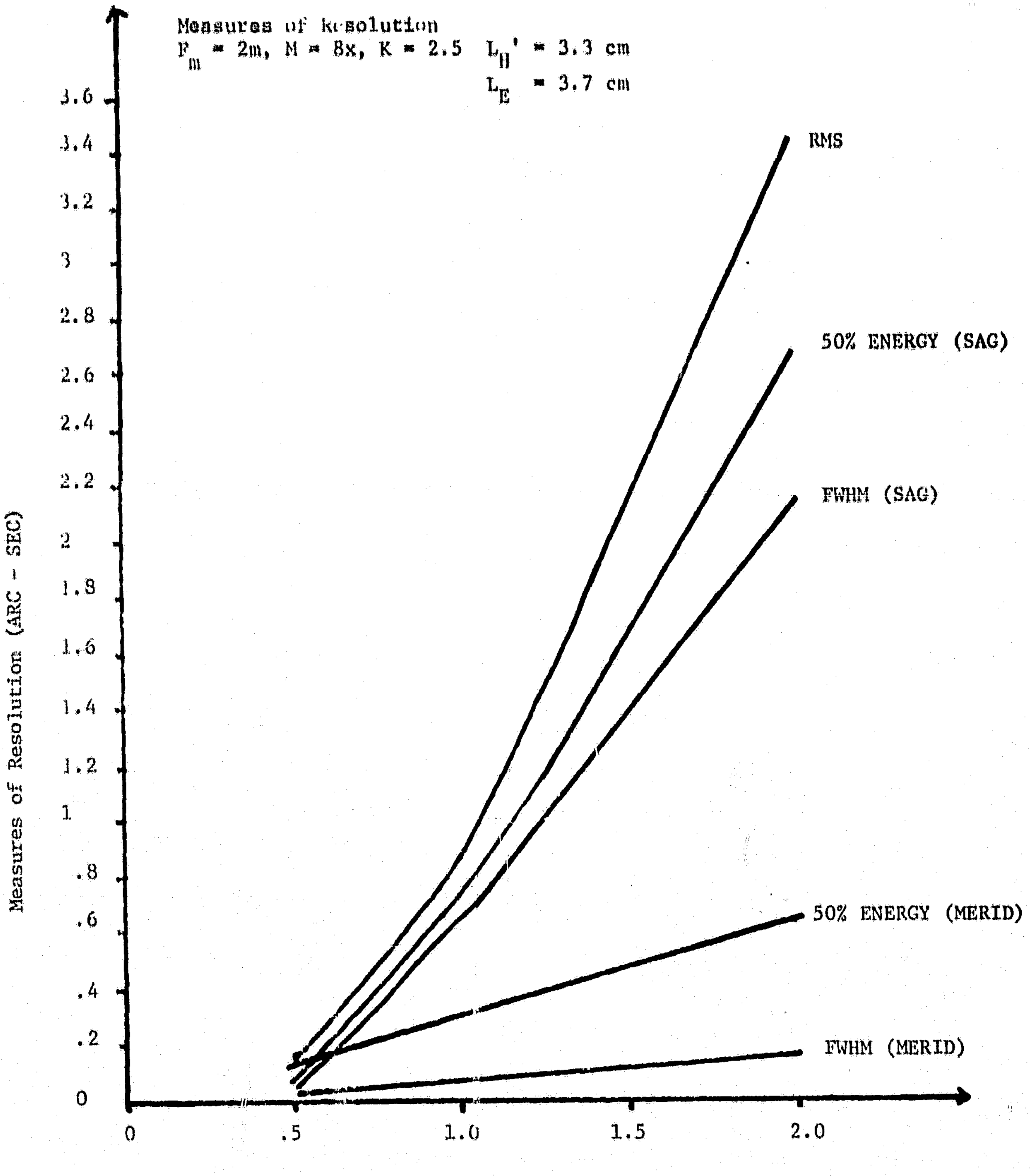

Fig. 38: Resolution vs Field Angle

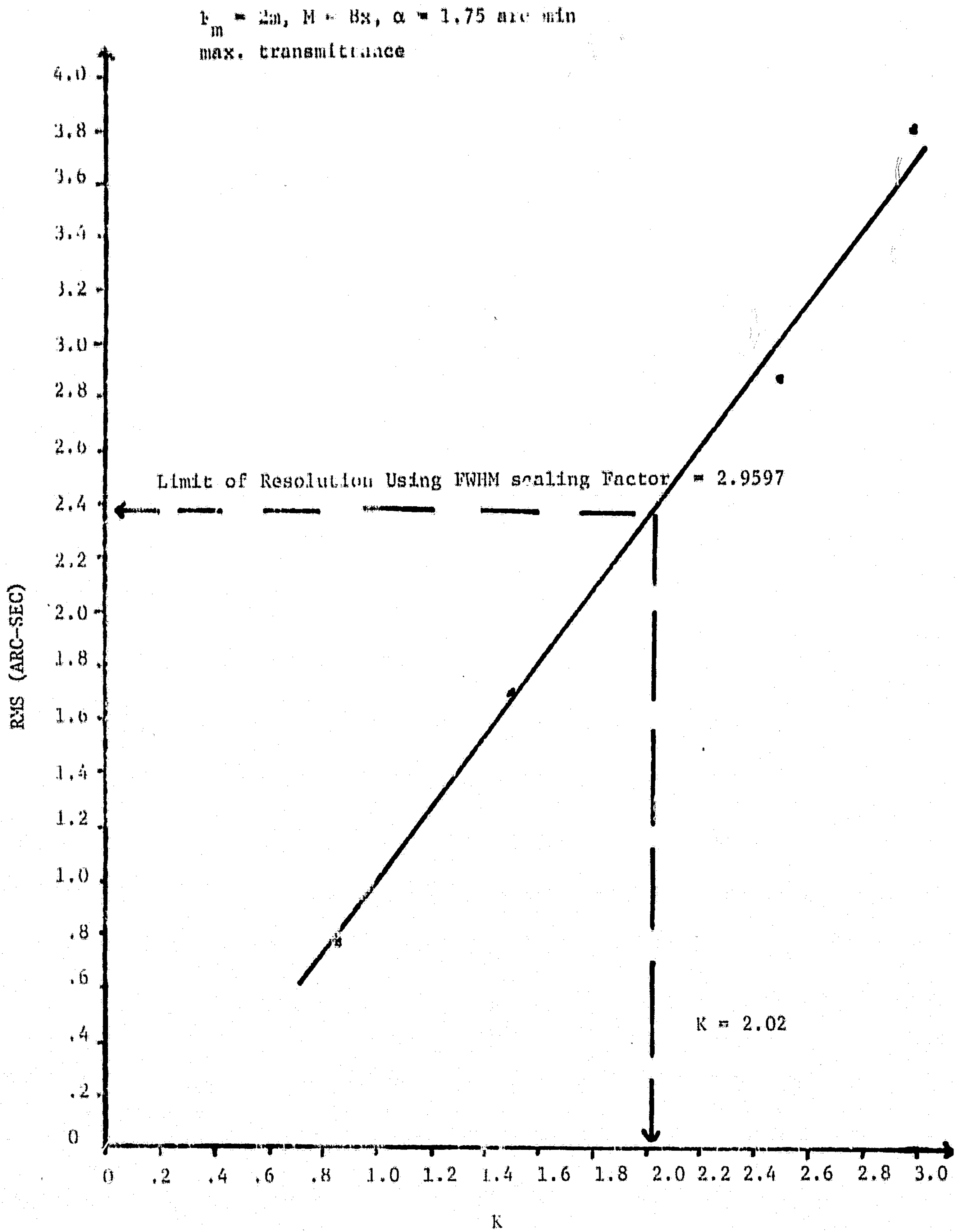

Fig. 39: RMS Spot Radius vs K

ORIGINAL PAGE IS
OF POOR QUALITY

F_m = 2m, M = 8x, α = 1.75 arc min

Max Transmittance

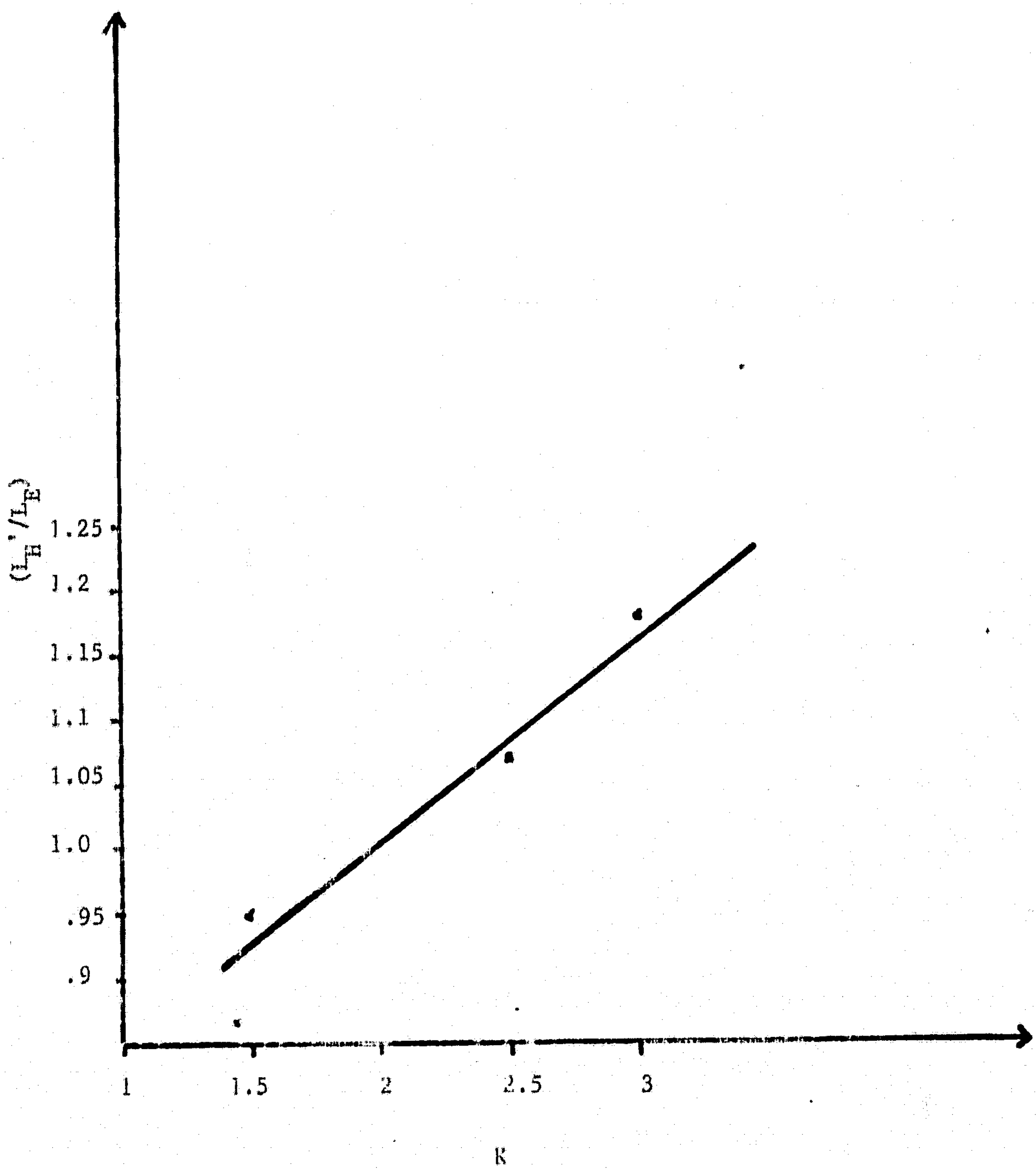

Fig. 40: Ratio of $L_{H'}$ to L_E vs K

Front (R_{15}) and REAR (R_{25}) microscope aperture radii versus Field angle.

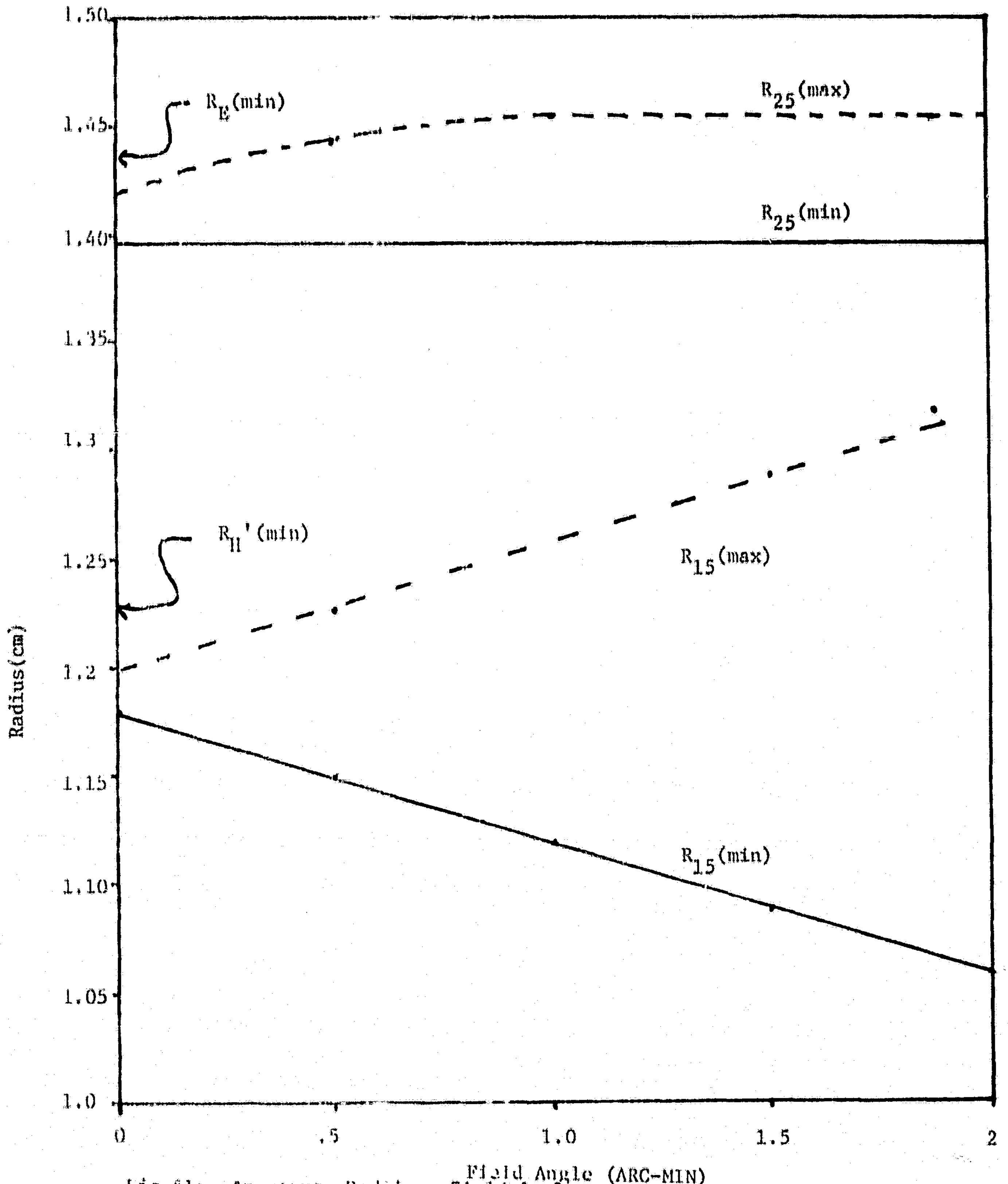

Fig.41: Aperture Radii vs Field Angle